THE UNIVERSITY OF CHICAGO

COMPETITIVE AND COOPERATIVE INTERACTIONS BETWEEN ACTIN BINDING PROTEINS DRIVE THEIR SORTING TO DIFFERENT ACTIN CYTOSKELETON NETWORKS

A DISSERTATION SUBMITTED TO
THE FACULTY OF THE DIVISION OF THE BIOLOGICAL SCIENCES
AND THE PRITZKER SCHOOL OF MEDICINE
IN CANDIDACY FOR THE DEGREE OF
DOCTOR OF PHILOSOPHY

DEPARTMENT OF MOLECULAR GENETICS AND CELL BIOLOGY

BY

JENNA RENEE CHRISTENSEN

CHICAGO, ILLINOIS

DECEMBER 2016

TABLE OF CONTENTS

LIST OF FIGURES

LIST OF TABLES

ACKNOWLEDGEMENTS

I would like to thank past and present Kovar lab members for all of their assistance with my research and for making every day in lab a lot of fun. Thanks to Caitlin Anderson, Andy Bestul, Tom Burke, Alyssa Harker, Katie Homa, Glen Hocky, Yujie Li, Patrick McCall, Alisha Morganthaler, Kate Proudfoot, Jen Sees, Cristian Suarez, Jonathan Winkelman, and Dennis Zimmermann. In particular, I want to emphasize the work of two current Kovar lab members—Katie Homa and Alisha Morganthaler—who have helped in innumerable ways on the two actin binding protein sorting projects. I would also like to thank Glen Hocky for being a fantastic collaborator and performing the mathematical modeling present in this dissertation. Additionally, I would like to thank Meghan O'Connell whose rotation project "help Jenna graduate" did exactly that. I would also like to thank Jonathan Winkelman, Cristian Suarez, and Tom Burke and who were my initial instructors in TIRF microscopy and fission yeast biology. I would finally like to thank Dave Kovar who is a terrific mentor and has created a lab environment that is collaborative and productive.

Outside of the lab, I've been lucky to have a great support system. Jen La and David Weinberg in particular have been constant sources of hilarity and support during my time in Chicago. I would finally like to thank my family, Karen and Steve Christensen and Jill Park, who have also provided me with support throughout graduate school.

ABSTRACT

The actin cytoskeleton is a dynamic system involved in a variety of cellular processes, including endocytosis, motility, polarity, and cytokinesis. In a single crowded cytoplasm, the cell assembles multiple different filamentous actin (F-actin) networks at the correct time and place and with the proper architecture and dynamics. How the cell is capable of assembling multiple distinct F-actin networks simultaneously remains an unanswered question. In a cell, actin monomers are assembled into actin filaments, and these actin filaments are organized into defined and distinct networks by the coordinated action of the associated actin binding proteins (ABPs). ABPs are involved in nucleating, bundling, severing, pulling, and capping actin filaments, and therefore, the ABPs associated with an actin network define its specific properties. Therefore, it is crucial that ABPs properly localize to the correct actin network. However, the mechanisms behind how different sets of ABPs sort to different actin networks are unclear. My hypothesis is that competition between ABPs for association with F-actin is a driving factor behind proper ABP sorting.

Fission yeast is an ideal simplified system in which to study the underlying molecular mechanisms behind F-actin network self-organization. Fission yeast has three primary actin cytoskeleton networks, in which all of the actin filaments are assembled by a distinct actin assembly factor: endocytic actin patches (Arp2/3 complex), polarizing actin cables (formin For3), and the cytokinetic contractile ring (formin Cdc12). Moreover, each of these F-actin networks contains a distinct set of ABPs. We hypothesize that ABP competition for association with actin filaments is critical for their proper sorting to distinct F-actin networks. Previous work identified three ABPs (two that localize to endocytic actin patches, fimbrin Fim1 and cofilin Adf1, and one, tropomyosin Cdc8, that localizes to the contractile ring) that have competitive

interactions (Skau and Kovar, 2010). I investigated the molecular mechanisms behind their competitions and determined that fimbrin Fim1 actively displaces tropomyosin Cdc8 specifically from bundled regions. I additionally found that tropomyosin Cdc8 inhibits cofilin Adf1-mediated severing by blocking the initial association of cofilin Adf1 with F-actin. Finally, I found that Fim1 and Adf1 compete for the same binding site on F-actin, but that this competition results in the generation of Adf1 boundaries, facilitating rapid severing by Adf1 and bundling of the F-actin network by Fim1. This dense actin network generated by Fim1 and Adf1 rapidly displaces Cdc8 from the network. I speculate that this mechanism causes Cdc8 to be removed from actin patches and associate instead with the contractile ring.

Additionally, I performed a survey in fission yeast to determine other potential competitive interactions between ABPs. I identified a competitive interaction between fimbrin Fim1 and contractile ring ABP α-actinin Ain1. I found that fimbrin Fim1 outcompetes α-actinin Ain1 for association with F-actin, likely via competition for the same binding site on the actin filament. This competition can occur at both the contractile ring and actin patches. Additionally, I found that contractile ring ABP tropomyosin Cdc8 enhances Ain1-mediated bundling. Finally, I found that Cdc8 synergizes with Ain1 to prevent Fim1 from associating with F-actin.

Though my primary work has been on investigating ABP competition, I also completed a project started by a former graduate student in the lab, Mike Glista, characterizing the formin (CrFor1) and profilin (CrPRF) from *Chlamydomonas reinhardtii*. I found that CrPRF is an unusual profilin that prevents both the nucleation of CrPRF-bound actin monomers as well as F-actin elongation. CrFor1 is capable of overcoming this inhibition of actin polymerization and rapidly assembles CrPRF-bound actin monomers into F-actin. These findings suggest that CrPRF and CrFor1 are tailor-made to rapidly assemble F-actin at the correct time and place.

Additionally, CrPRF inhibits actin assembly by the fission yeast Arp2/3 complex, suggesting that CrPRF favors CrFor1-mediated actin assembly both by directly enhancing CrFor1's ability to assemble F-actin and by inhibiting competing actin assembly factors.

PREFACE

This dissertation is a compilation of manuscripts currently in preparation. Chapters 2, 3, and 4 are each distinct manuscripts. Additional contributors to Chapter 2, "*Chlamydomonas reinhardtii* expresses a formin and profilin that are optimized for rapid actin filament assembly" are Michael J. Glista, David Mueller, Yujie Li, Jennifer A. Sees, Colleen T. Skau, Laurens J. Mets, Prachee Avasthi, and David R. Kovar. Additional contributors to Chapter 3, "Competition between tropomyosin, fimbrin, and cofilin drives their sorting to distinct actin filament networks" are Glen M. Hocky, Alisha N. Morganthaler, Kaitlin E. Homa, Sarah E. Hitchcock-DeGregori, Gregory A. Voth, and David R. Kovar. Additional contributors to Chapter 4, "Tropomyosin and α-actinin cooperate to compete with fimbrin, driving their localization to different actin cytoskeleton networks in fission yeast" are Kaitlin E. Homa, Meghan E. O'Connell, Alisha N. Morganthaler, and David R. Kovar. Prefaces before each chapter denote specific work performed by contributors listed above.

CHAPTER 1: INTRODUCTION

Section 1.1—THE ACTIN CYTOSKELETON AS A MODEL FOR CELLULAR SELF-ORGANIZATION

The self-organization of complex structures from interactions between basic components is a general phenomenon of chemistry and material sciences, as well as more complicated biological systems (Misteli, 2001; Karsenti, 2008). The interior of cell is an extremely complicated milieu, composed of proteins, lipids, nucleic acids, and other molecules that are organized into higher-order structures including membrane-bound compartments, organelles, multi-component droplets, and complex protein assemblies. However, despite its large number of component parts, the cell remains remarkably well-organized. This proper organization is necessary for many processes such as cellular transport, in which cargo must be moved from one defined location in the cell to another, and cell division, in which two daughter cells must equally receive component parts from the previous generation. Therefore, the proper organization of components within a single cell is of extreme importance. A single cell can span anywhere from ~0.3 μm (*Mycoplasma* bacteria (Razin, 1996)) to several inches (*Caulerpa taxifolia* (Ranjan et al., 2015)) in diameter, yet its individual protein components are much smaller—nanometers in scale. This difference in scale between a whole cell and its component parts elicits the question of how interactions at the level of the individual proteins are propagated such that organization is achieved at a whole cell level.

The actin cytoskeleton is an ideal system to study complex cellular self-organization. In a cell, the same basic unit, the actin monomer, is assembled into actin filaments that comprise networks of varying architecture, dynamics, and physical properties. How a single basic unit can

be utilized in such different ways as to generate the correct actin network at the proper time and place is not well understood.

The actin cytoskeleton

The basic unit of the actin cytoskeleton is the globular actin monomer (G-actin). G-actin is a ~40-kD protein composed of four subdomains (Figure 1-1). Each actin monomer contains a single nucleotide binding cleft that binds adenosine triphosphate (ATP), ADP-Pi, or adenosine diphosphate (ADP) (Straub and Feuer, 1950). In the cytoplasm, the majority of G-actin is in an ATP-bound state. G-actin can assemble into filaments, known as filamentous actin or F-actin. Though the name 'cytoskeleton' implies that these filaments create a rigid and stable framework that defines the structure of the cell, the actin cytoskeleton is actually extremely dynamic. G-actin is assembled into F-actin, but F-actin is additionally disassembled back into its monomeric unit, with this cycle of assembly and disassembly occurring continuously and at different rates depending on environmental conditions and associated proteins. In particular, the formation of a stable actin 'nucleus' from three actin monomers is the rate-limiting step of actin filament formation. Once a stable actin trimer has been formed, actin monomers can add to both ends of an actin filament. However, this addition occurs at different rates, with actin monomer addition occurring preferentially at the barbed end of the actin filament (with a rate of $k+=11.6\ \mu M^{-1}s^{-1}$) compared to the pointed end ($k+=1.3\ \mu M^{-1}s^{-1}$) (Pollard, 1986). This difference results in the observed polar growth of an actin filament at one end.

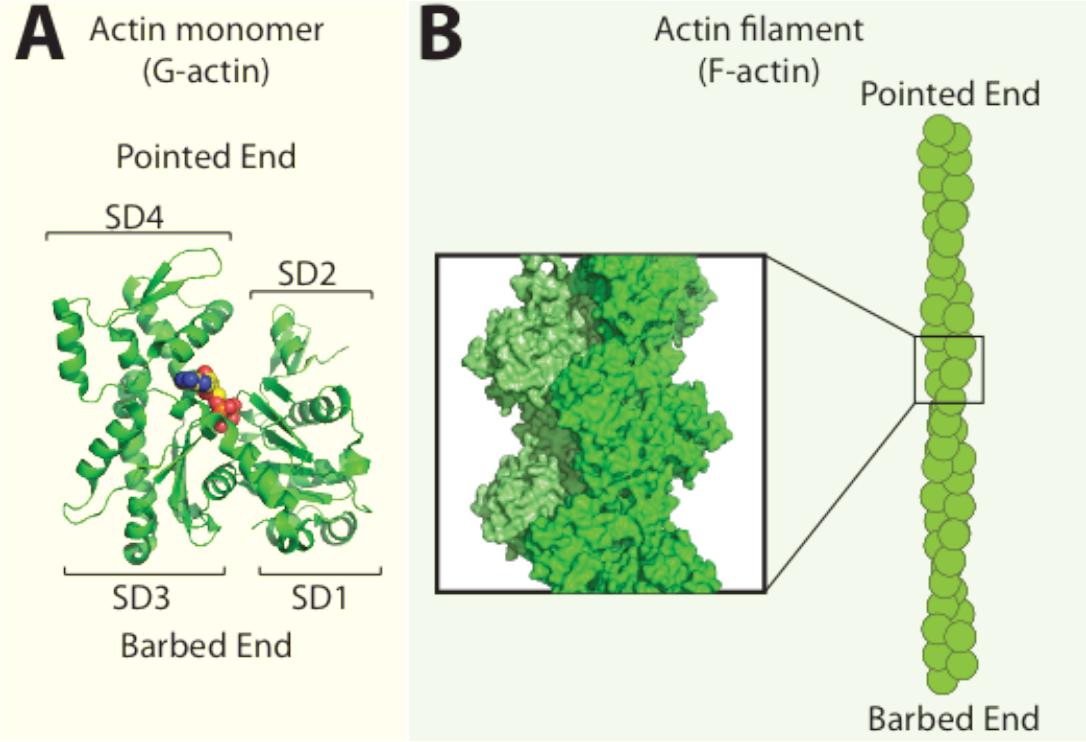

Figure 1-1: Globular actin monomer (G-actin) is assembled into actin filaments (F-actin).
(A) An actin monomer has four subdomains (SD1-4) (PDB: 1NWK, Graceffa and Dominguez, 2003). **(B)** An actin filament (F-actin) is composed of monomeric G-actin (PDB:4A7N, Ecken et al. 2014).

Once actin filaments are assembled from their monomeric subunits, they can be organized into complex networks that promote cellular processes such as cell division, endocytosis, polarity establishment, adhesion, and motility (Figure 1-2). The architecture, dynamics, and mechanical properties of the created actin network must be properly tuned to suit the process involved. Thus, a single base unit, the actin monomer, must be appropriately yet differentially utilized for multiple purposes at the same time within a single common cytoplasm.

Section 1.2 – CONTROLLING ACTIN NETWORK ASSEMBLY IN TIME AND SPACE

Though all actin networks are composed of a similar substrate (actin filaments), their characteristics vary widely in terms of architecture, rigidity, flexibility, and turnover rate, among

others (Figure 1-2). These characteristics are defined by the actin binding proteins (ABPs) that assemble and organize the actin filaments into a defined network. Hundreds of ABPs have been identified in mammalian cells, and they have many different roles including nucleating, elongating, severing, crosslinking, capping, pulling, and disassembling F-actin (Pollard, 2016). In addition, some proteins, such as profilin, interact with G-actin rather than F-actin and control the rate that actin monomers are assembled into filament.

Mammalian cells have 18-20 actin networks, hundreds of actin binding proteins, and multiple actin isoforms, making it difficult to assess the mechanisms behind how multiple actin cytoskeleton networks are assembled at the correct time and place. Therefore, model organisms are used to understand these general mechanisms behind actin cytoskeleton organization and regulation. In particular, the fission yeast *Schizosaccharomyces pombe* is an ideal model to study actin cytoskeleton self-organization (Figure 1-3). Fission yeast contains a simplified actin cytoskeleton, with a single actin isoform. Fission yeast possesses three F-actin networks in vegetative cells, with the F-actin being made by a distinct assembly factor: endocytic actin patches (Arp2/3 complex), polarizing actin cables (formin For3), and the cytokinetic contractile ring (formin Cdc12). Fission yeast additionally contains ~40 known actin-interacting proteins (Stark et al., 2006) that define the properties of these three F-actin networks. As many homologues of mammalian ABPs are present in fission yeast, studies of ABP sorting in fission yeast can have relevance for more complex systems.

Actin monomer binding proteins

Under physiological conditions in vitro, monomeric actin alone is capable of spontaneously assembling into F-actin. In a cell, however, the majority of F-actin is bound by the

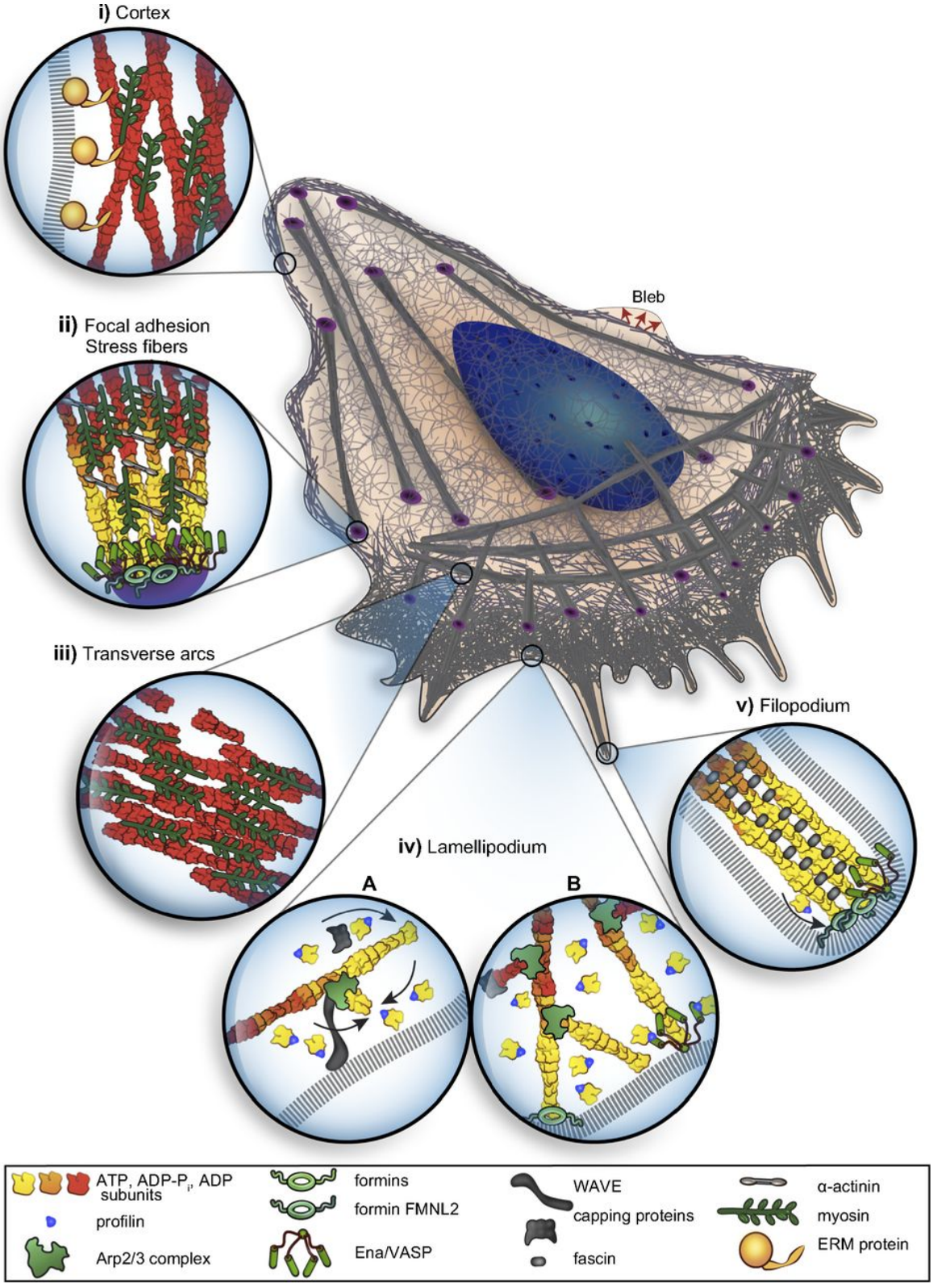

Figure 1-2: Actin binding proteins (ABPs) work together to create F-actin networks for distinct cellular processes in mammalian cells.
Assembly factors formin, Ena/VASP, and Arp2/3 complex assemble the F-actin within actin networks. Combinations of ABPs work together to create actin networks with different properties. Figure adapted from Blanchoin et al. 2014.

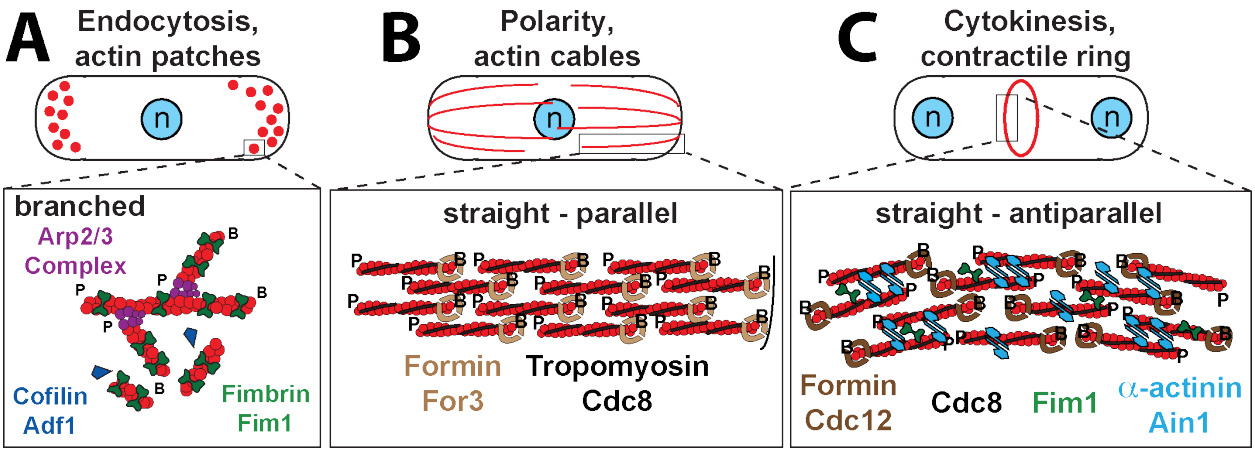

Figure 1-3: Actin binding proteins in the fission yeast *Schizosaccharomyces pombe*.
(A) Endocytic actin patches contain F-actin nucleated by the Arp2/3 complex. Filaments are crosslinked by fimbrin Fim1 and severed by cofilin Adf1. **(B)** Actin cables contain F-actin assembled by the formin For3 and associated with unacetylated tropomyosin Cdc8. (C) The contractile ring is composed of F-actin assembled by the formin Cdc12. Acetylated tropomyosin Cdc8 is associated with the F-actin and α-actinin Ain1 bundles the filaments. Small amounts of fimbrin Fim1 are also associated with the contractile ring.

small actin monomer binding protein profilin (Kaiser et al., 1999). Profilin inhibits the nucleation of new actin filaments, but allows actin monomer addition onto the barbed ends of already assembled actin filaments (Pollard and Cooper, 1984; Pring et al., 1992). Profilin (and other sequestering proteins such as thymosin-β4 in higher eukaryotes (Goldschmidt-Clermont et al., 1992) prevent spontaneous assembly of F-actin. Actin assembly factors then must overcome this inhibition of assembly in order to specifically assemble F-actin at the correct time and place in the cell. There are three primary families of actin nucleators—Arp2/3 complex, formin, and WH2 domain nucleators (Figure 1-4). WH2 domain nucleators are found endogenously in eukaryotic cells and are also utilized by bacterial pathogens in order to excessively and unproductively stimulate F-actin assembly in the host cell, adversely affecting native F-actin processes. However, as this is a recently described family of actin nucleators and their

involvement in actin network assembly and organization is less well understood, Arp2/3 complex and formin will be focused on.

Actin assembly factors: Arp2/3 complex

The Arp2/3 complex is a protein complex composed of seven subunits. Two of the subunits of the complex, Actin Related Proteins 2 and 3 (Arp2 and Arp3) mimic an actin dimer, creating a template upon which a new actin nucleus can be formed (Mullins et al., 1998). The Arp2/3 complex can be activated by several families of proteins, with the most well-known being the Wiskott-Aldrich Syndrome family of Proteins (includes WASP, N-WASP, WASH, and SCAR/WAVE (Kurisu and Takenawa, 2009). Members of the WASP family activate the Arp2/3 complex potentially by adding a third actin monomer to the ARP2/ARP3 dimer mimic, further stabilizing the nucleation event (Marchand et al., 2001; Dayel and Mullins, 2004). Alternatively, WASP could make a conformational change in the Arp2/3 complex that further stimulates its nucleation activity (Goley et al., 2004). The Arp2/3 complex binds with a WASP family activator and actin monomer to the side of a pre-existing 'mother' filament and creates a template for a new actin filament to form. As a result, actin networks assembled by the Arp2/3 complex have a branched appearance and are involved in creating dense networks that provide a pushing force such as at the leading edge of a motile cell (Svitkina and Borisy, 1999) or during vesicle internalization in endocytosis (Winter et al., 1999). Additionally, multiple pathogens express proteins similar to host cell Arp2/3 complex activators in order to hijack the Arp2/3 complex and propel themselves through the cell, promoting their spread from cell to cell (Welch et al., 1998).

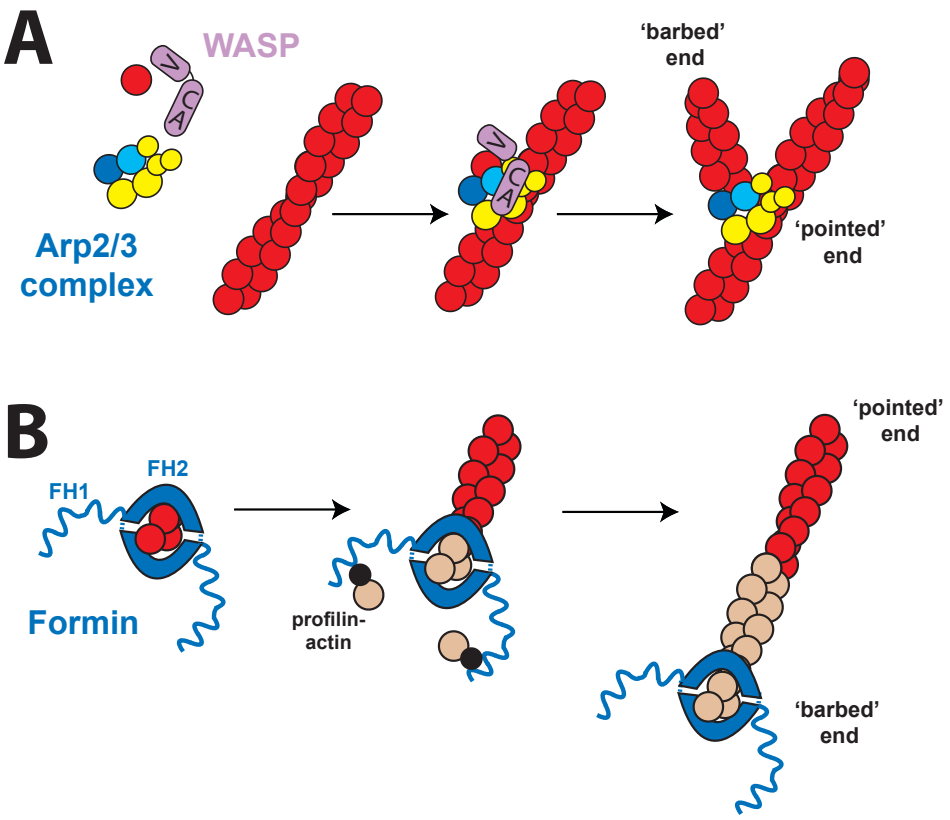

Figure 1-4: Two families of actin assembly factors.
(A) Arp2/3 complex assembles branched actin filaments. Arp2/3 complex activator WASP binds an actin monomer and associates with the Arp2/3 complex, binding to and nucleating a branch off of a pre-existing actin filament. **(B)** Formin nucleates new actin filaments and elongates F-actin by riding processively on the barbed end of an actin filament.

Actin assembly factors: Formins

Formins are assembly factors that can both nucleate new actin filaments and elongate actin filaments by processively associating with the barbed end. All formins have Formin Homology 1 and 2 (FH1 and FH2) domains. A functional formin is a homodimer that utilizes two FH2 domains to create a donut-shaped complex that associates processively with the barbed end of an actin filament. The two FH1 domain 'arms' contain a number of polyproline-rich regions that bind to profilin-actin, enhancing actin association with the barbed end (Paul and Pollard, 2008). Surrounding the FH1 and FH2 domains are regulatory regions that vary greatly

amongst members of the formin family (Chalkia et al., 2008). Many formins contain a Diaphanous inhibitory domain (DID) and/or a Diaphanous autoregulatory domain (DAD). These domains can associate with each other, resulting in autoinhibition of the formin. This autoinhibition can be released by RhoGTPases. Therefore, spatial localization and activation of specific RhoGTPases can activate formins at the correct time and place.

Though much is understood about how these two assembly factor families function on a mechanistic level, many questions remain about how their assembly of F-actin is regulated such that actin networks are assembled at the correct time and place and maintain the proper size. As mentioned above, both families of assembly factors have known upstream activators that regulate their activity. Therefore, the longstanding dogma on actin network regulation is that upstream signaling activates distinct assembly factors at the correct time and place, such that actin network assembly is governed solely by these upstream events (Hall, 1998). These upstream activators are frequently RhoGTPases. The Arp2/3 complex activator WASP is activated by the RhoGTPase Cdc42 (Symons et al., 1996; Leung and Rosen, 2005), while formins are activated by different RhoGTPases depending on the formin (Otomo et al., 2005; Watanabe et al., 1997). Localization and activation of RhoGTPases at the right time and place results in actin assembly at defined locations. For example, RhoA activation is sufficient to induce cleavage furrow formation in HeLa cells (Wagner and Glotzer, 2016), and activation of the actin cable formin For3 is dependent upon release from autoinhibition by Cdc42 (Martin et al. 2007). However, other findings have suggested that activation of an assembly factor alone is not sufficient to generate the proper F-actin network.

Competition between actin assembly factors mediates proper F-actin network formation

There is certainly an important role for upstream signaling in F-actin network establishment. However, findings from multiple studies have suggested that other factors are additionally at play in regulating actin network size (Suarez and Kovar, 2016). A model has been proposed in which a limited pool of actin monomer could result in actin assembly factor competition for actin monomer, restricting actin network size relative to available free actin monomer. Supporting this model, treatment of fission yeast cells with the Arp2/3 complex inhibitor CK-666 resulted in the depletion of one F-actin network, the actin patch, and a corresponding increase in 'ectopic' F-actin assembled by the other two fission yeast assembly factors, the formins For3 and Cdc12 (Burke et al., 2014). However, this ectopic F-actin did not form following CK-666 treatment if actin patches were incapable of disassembling. If actin patches are not disassembled, actin monomer is not released back into the cytoplasm and is not available for use by other assembly factors. Finally, increasing the concentration of actin in the cell resulted in an increase in the number of patches, but not the size of the patch, suggesting that other mechanisms are involved in regulating actin network size. Competition for F-actin has been additionally shown to affect the transition from a static to migratory phenotype in mammalian cells (Lomakin et al., 2015). It was found that inhibition of myosin-II resulted in spontaneous migration of epithelial cells, and it was demonstrated that this is likely due to myosin-II sequestering actin in actomyosin bundles. Upon inhibition of myosin-II, this actin is released and free to polymerize into branched networks at the front end of the cell, stimulating cell motility at the leading edge (Lomakin et al., 2015).

Assembly factor competition for actin monomer is an important mode of regulation that ensures proper monomer distribution to F-actin networks. In a fission yeast cell, Arp2/3 complex

outnumbers formin Cdc12 molecules ~15:1 (Sirotkin et al., 2010; Wu and Pollard, 2005), making it perhaps unsurprising that formin-mediated actin processes are enhanced following the depletion of Arp2/3 complex and its associated actin. However, a small number of formin molecules must still compete with an excess of Arp2/3 complex in order to assemble actin cables and the contractile ring. It has been well-established that profilin enhances formin-mediated F-actin assembly (Kovar et al., 2006; 2003; Romero et al., 2004). In addition, in both fission yeast and mammalian cells, profilin inhibits Arp2/3 complex-mediated actin assembly by competing with its activator, Wsp1 for association with actin monomer (Suarez et al., 2015; Rotty et al., 2015). As Wsp1 assists Arp2/3 complex in the formation of an actin nucleus by bringing in a third actin monomer, preventing Wsp1 from associating with actin monomer slows the rate at which Arp2/3 complex is capable of nucleating new actin filaments (Suarez et al., 2015). Therefore, profilin favors formin-mediated processes both by enhancing formin-mediated assembly and by inhibiting actin assembly by its competitor, the Arp2/3 complex.

Section 1.3—ACTIN BINDING PROTEINS DEFINE THE PROPERTIES OF THE ACTIN NETWORK

Actin assembly factor crosstalk via competition for actin monomer can help to define the initial formation and size of an F-actin network. However, an actin network is composed of more than just actin filaments. Actin binding proteins (ABPs) must additionally assist in modulating the interactions between newly polymerized actin filaments, affecting their flexibility, structure, and organization, molding them for their specific cellular processes. Two types of ABPs: monomer-interacting proteins (profilin), and actin nucleators (Arp2/3 complex, formin, WH2 domain nucleators) have already been discussed. However, ABPs can encompass

a wealth of functions, including bundling, severing, side-binding, pulling, capping, and depolymerizing actin filaments that can function together to assemble the correct F-actin network (Figure 1-2). ABPs can be divided into groups depending on their function (bundling, severing, side-binding, etc.), and into further families depending on their homology. Though there are hundreds of different types of ABPs that perform many different functions, I will focus on three types that are pertinent to this work.

Bundling/crosslinking proteins

Crosslinked F-actin networks are found in a wide variety of F-actin networks, including the lamellipodia (Small et al., 2002), filopodia (Khurana and George, 2014), stress fibers (Hotulainen and Lappalainen, 2006), endocytic actin patches (Young, M.E., Cooper, J.A, Bridgman, P.C., 2004), cables, and the contractile ring. The type and architecture of the network can vary greatly depending on the type of actin crosslinker present in the network. Though some ABPs not typically thought of as crosslinking proteins have cross-linking abilities (two-headed myosin proteins, some formins) a group of ABPs known specifically as bundling/crosslinking proteins mediate much of the direct association between actin filaments. Though most bundling/crosslinking proteins can be considered to be both crosslinkers (create a single link between two actin filaments) and bundlers (multiple links along two parallel actin filaments), certain ABPs, such as filamin, are considered to be crosslinking but not bundling proteins. For the sake of simplicity, the terms bundling and crosslinking will be used interchangeably in this dissertation.

Fission yeast has a variety of ABPs that have been implicated in crosslinking activities (fimbrin Fim1, α-actinin Ain1, formin Fus1, anillin Mid1, IQGAP Rng2 (Li et al., 2016; Scott et

al., 2011; Skau et al., 2011; Takaine et al., 2009). However, the two most well-characterized crosslinkers are fimbrin Fim1 and α-actinin Ain1. Fimbrin Fim1 localizes to actin patches where it assists in creating a dense F-actin network that propels endocytic vesicles into the cell interior (Skau et al., 2011; Young, M.E., Cooper, J.A, Bridgman, P.C., 2004). α-actinin Ain1 localizes to the contractile ring where it dynamically bundles actin filaments during contractile ring formation and constriction (Li et al., 2016).

Severing proteins

Actin filament assembly is important for creating an actin network, but properly disassembling an F-actin network at the right time is crucial for proper network dynamics as well as correct distribution of actin monomer to the different F-actin networks (Burke et al., 2014). Severing proteins are one of the main types of ABPs involved in actin network disassembly. The Actin Depolymerizing Factor (ADF)/cofilin family of ABPs is one of the primary families of severing proteins. ADF/cofilin has been demonstrated to localize to the lamellipodia in mammalian cells, where it functions to disassemble the treadmilling network (Bamburg and Bray, 1987; Theriot, 1997). Fission yeast expresses a single ADF/cofilin, Adf1, that functions predominantly to disassemble endocytic actin patches (Chen and Pollard, 2013; Nakano et al., 2001), though it has an additional role in the assembly of the contractile ring (Chen and Pollard, 2011; Nakano and Mabuchi, 2006b).

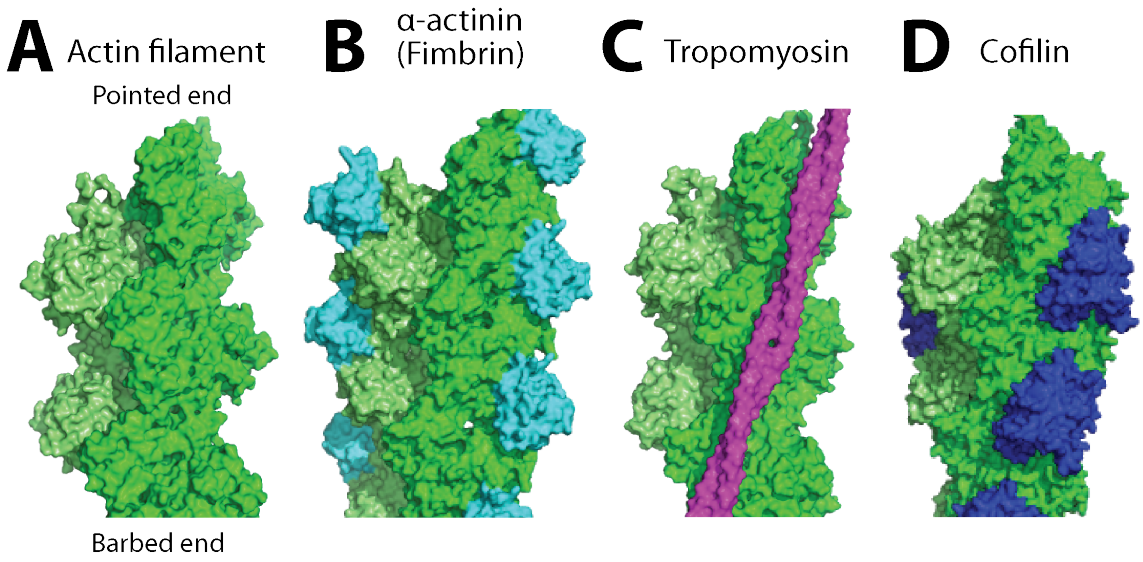

Figure 1-5: Actin binding proteins associate with different regions of the actin filament. **(A)** Cryo-EM structure of an actin filament (PDB: 4A7N, Ecken et al. 2014). **(B)** α-actinin and fimbrin associate with the same region on the actin filament, between subdomain 1 of one actin monomer and subdomain 2 of the next actin monomer nearest to the barbed end. The CH1 domain of human α-actinin is pictured (PDB: 3LUE, Galkin et al. 2010). **(C)** Tropomyosin is a coiled-coil protein that associates with the outside groove of the actin filament (PDB: 3J8A, Ecken et al. 2014). Tropomyosin's binding site does not overlap with the binding site of α-actinin. **(D)** Cofilin associates between subdomain 1 and 2 of adjacent actin monomers (PDB: 3J0S, Galkin et al. 2011). Cofilin's binding site partially overlaps with the binding sites of both α-actinin and tropomyosin.

Side-binding proteins

Tropomyosin is a coiled-coil ABP that binds end-to-end with other tropomyosin molecules to create a cable along the actin filament surface (Hanson and Lowy, 1964) (Figure 1-5C). Tropomyosin is particularly important for skeletal muscle contraction, where it assists in coordinating myosin movement in this cell type (Lehman et al., 1994; Spudich and Watt, 1971). However, tropomyosins are also expressed in other cell types where they are important for proper F-actin network organization. Different tropomyosin isoforms localize to different F-actin networks in the cell, including the focal adhesions, dorsal stress fibers, transverse arcs, and ventral stress fibers (Gunning et al., 2015; Tojkander et al., 2011). Tropomyosins are often characterized as 'gatekeeper proteins', as they are thought to mediate the association of other

ABPs with their specific networks (Gunning et al., 2015). In particular, tropomyosins have been shown to differentially affect myosin and cofilin functions (DesMarais et al., 2002; Ono and Ono, 2002; Strand et al., 2001). Fission yeast has a single tropomyosin gene, *cdc8*, but contains both an acetylated and unacetylated form of the Cdc8 protein. In fission yeast, tropomyosin Cdc8 has been shown to positively regulate formin Cdc12 and myosin-II activities (Clayton et al., 2010; Skau et al., 2009), while negatively regulating myosin-I and cofilin Adf1 activities (Clayton et al., 2010; Skau and Kovar, 2010).

One defining feature of the three ABP families mentioned above is that they are all cooperative—the binding of one protein enhances the likelihood that a second will bind. However, the mechanisms behind their cooperativity are different. Bundling proteins like α-actinin and fimbrin are cooperative by creating a bundle of specific spacing that is favorable for other bundlers of similar spacing to associate with (Winkelman et al., 2016). Cofilin creates a twist in the actin filament upon binding that favors binding of additional cofilins (McGough et al., 1997). Tropomyosin's end-to-end associations favor binding of new tropomyosin molecules with pre-existing tropomyosin cables. Despite our understanding of the functions of individual ABPs and how they work together to create and maintain a specific type of actin network, we still lack a discrete understanding of how a set of ABPs properly localize to the correct F-actin network.

Section 1.4—HOW DO ACTIN BINDING PROTEINS LOCALIZE TO THE CORRECT F-ACTIN NETWORK?

The proper combination of assembly factor activation and ABP coordination results in the formation of the correct F-actin network. However, many different F-actin networks are assembled at the same time within a crowded cytoplasm. Therefore, the mechanisms behind how

actin binding proteins are capable of sorting to the correct F-actin network are unclear. A number of non-mutually-exclusive mechanisms have been proposed describing how ABPs could be recruited to the correct actin network at the right time and place. These mechanisms can be generally broken into two groups: extrinsic (other cellular factors acting on the ABP) or intrinsic (inherent to the ABP itself).

Extrinsic regulation

Much as upstream signaling regulates activation of actin assembly factors at the right time and place, a model of extrinsic regulation postulates that upstream signals could modulate an ABP or actin network such that the ABP is recruited to the correct location. This type of regulation could affect an ABP differently in different regions of the cell or during different cell states such as in specific polarity states or stages of the cell cycle. Extrinsic regulation can then regulate ABPs by ions such as calcium (Namba et al., 1992) or post-translational modifications of the ABP of interest (Shao et al., 2010; Feng et al., 2013). The salient feature in extrinsic regulation is that factors other than the ABPs themselves affect how an ABP segregates to the correct F-actin network. Therefore, reconstituted systems using only purified ABPs of interest will not include factors of extrinsic regulation. As a result, extrinsic regulation is most readily studied in cells or with the use of cellular extracts.

Extrinsic regulation of ABPs via post-translational modifications has been found in a number of systems. In budding yeast, fimbrin Sac6 activity is regulated by phosphorylation at different stages of the cell cycle (Miao et al., 2016). Phosphorylation enhances the ability of Sac6 to associate with F-actin. However, it's still unclear as to how this phosphorylation promotes or affects proper sorting of Sac6 to actin cables. Therefore, though extrinsic regulation may affect

fimbrin's ability to associate with F-actin, intrinsic mechanisms may restrict that association to specific F-actin networks.

Intrinsic regulation

Intrinsic regulation, on the other hand, suggests that the ability of ABPs to sort to the correct network is the result of characteristics inherent to ABPs themselves. These characteristics include features specific to the ABP of interest that affect how or where that ABP interacts with actin filaments (Figure 1-5) or higher-order actin networks, and could include a specific type of actin binding domain or the organization or spacing between actin binding domains. These characteristics can affect the interaction of an ABP with an actin filament by defining the ABP's dynamics (k_{on}/k_{off}) on F-actin or its affinity for a specific actin state (ATP state, flexibility, etc.), or by causing the ABP to impart a specific conformational change on the actin filament (twist, stretch) or higher-order network (spacing between bundles, density of network, etc). Studies of intrinsic regulation are specifically assisted by biochemical techniques, as the ability to in vitro reconstitute a particular actin network from only the ABPs immediately involved suggests that characteristics inherent to those ABPs are sufficient to generate a proper F-actin network, with no extrinsic signaling required.

It has been demonstrated that intrinsic properties of ABPs can cause them to segregate to different regions of an F-actin network. In vivo experiments in *Dictyostelium discoideum* demonstrated that constructs containing only the actin binding domains of α-actinin or filamin localized to the same F-actin networks as the full-length proteins (Washington and Knecht, 2008), suggesting that the actin binding domain defines the localization of the ABP. However, other properties inherent to ABPs may also be involved in their sorting. In vitro, two actin

bundling proteins, fascin and α-actinin, self-sort to distinct regions of a two-filament actin bundle (Winkelman et al., 2016). Fascin is a bundling protein that creates compact bundles of ~8 nm spacing, while α-actinin creates wider bundles of ~40 nm spacing. In addition, other compact bundling proteins fimbrin and espin sort to the same domains as fascin, suggesting that bundle width may be a defining characteristic that can determine what sets of ABPs localize to a specific actin architecture. The above extrinsic and intrinsic factors of regulation are not mutually exclusive, and many types of regulation are almost certainly important for proper ABP sorting.

The actin assembly factor is important for defining F-actin network organization and ABP composition

A combination of 1) proper actin assembly factor activation and regulation and 2) ABP recruitment results in the formation of the correct F-actin network. Therefore, it would make sense that these two processes would be linked. Correspondingly, one of the main models of actin network regulation is that proper network formation is initiated by an assembly factor being activated at a specific time and place. This assembly factor then denotes a specific twist or conformational change upon the assembled actin filaments that promotes recruitment of specific ABPs to those filaments (Michelot and Drubin, 2011). Certain 'upstream' ABPs have intrinsic characteristics that cause them to favor association with actin filaments polymerized by a specific assembly factor. These 'upstream' ABPs then recruit or compete 'downstream' ABPs to or from those same actin filaments, promoting the formation of an actin network with specific associated ABPs.

The idea that an assembly factor could define the set of ABPs that are recruited to an actin network was initially introduced by the discovery of the actin-based propulsion of the

intracellular pathogen *Listeria monocytogenes*. *Listeria* is a bacteria that expresses ActA, an Arp2/3 complex activator, on its surface, creating an explosion of actin assembly at that site, propelling the bacteria through the cytoplasm (Tilney and Portnoy, 1989). Furthermore, coating the surface of a polystyrene bead with ActA and incubating it in cellular extract was sufficient to generate motility (Cameron et al., 1999) and later experiments demonstrated that the presence of seven proteins was sufficient to generate bead-propelling actin tails similar to those observed for *Listeria* in vivo (Loisel et al., 1999). These studies demonstrated that the presence of an actin assembly factor is sufficient to create and organize an F-actin network with a specific architecture and function. Furthermore, these studies demonstrated the power of reconstitution in the identification of components sufficient for F-actin network formation and organization.

The importance of the assembly factor in actin network formation was furthered by work demonstrating that beads coated with budding yeast Arp2/3 complex activator Las17 and incubated in cellular extracts were capable of generating comet tails that recruited the set of ABPs found in actin patches (Michelot et al., 2010). Similarly, incubating formin Bni1-coated beads in cell extracts generated cable-like actin networks containing ABPs found in actin cables, but only when incubated in mitotic cell extracts (Miao et al., 2013). These findings demonstrated that the actin assembly factor is sufficient to assemble an actin network that recruits the correct set of ABPs to it.

In vivo work in fission yeast has additionally suggested the importance of the assembly factor in ABP recruitment. Though fission yeast has a single tropomyosin isoform, Cdc8, it can be either acetylated or unacetylated (Skoumpla et al., 2007), with acetylated Cdc8 localizing to the contractile ring assembled by the formin Cdc12 and unacetylated Cdc8 localizing to actin cables assembled by the formin For3 (Coulton et al., 2010). By swapping the localizations of

Cdc12 and For3, the localization of unacetylated and acetylated Cdc8 also switched, suggesting that the localization of the differently modified Cdc8 to a specific actin network was dependent upon the formin that assembled the actin in that network.

Competition between ABPs mediate their sorting to different F-actin networks

The aforementioned work suggests that the assembly factor likely plays an important role in defining the ABPs that associate with an F-actin network. However, how thousands of ABPs in a cytoplasm all associate with the correct F-actin network is unclear. Our model is that competition between ABPs for association with F-actin is a driving force behind their sorting to the proper F-actin network. A series of competitive interactions in fission yeast has been shown to affect sorting of ABPs to different actin networks. In vitro bulk biochemistry and live cell imaging demonstrated that fimbrin Fim1, a bundling ABP that associates predominantly with actin patches, inhibits association of tropomyosin Cdc8 with actin patches. Furthermore, tropomyosin Cdc8 inhibits severing by cofilin Adf1. Therefore, one of Fim1's primary roles at actin patches is to prevent Cdc8 association so that Adf1-mediated severing can occur (Skau and Kovar, 2010). Furthermore, tropomyosin Cdc8 was found to enhance the activity of Myo51 and Myo52, myosin-V motors found at the contractile ring and actin cables, respectively, but negative affected association of Arp2/3 complex activator myosin-I with actin filaments (Clayton et al., 2010). Fimbrin Fim1 was able to restore the association of myosin-I with actin filaments by inhibiting tropomyosin Cdc8. Together, these results demonstrate that multiple competitive interactions exist between ABPs, and that these interactions can affect their ability to sort to the correct F-actin network on a whole cell scale. Furthermore, they demonstrate the complexity of the ABP sorting problem. Each pair of ABPs has a distinct pair-wise interaction, but each

additional ABP adds a separate layer of complexity to how a set of ABPs interacts with an actin network. Finally, despite understanding which ABPs compete with each other, the molecular mechanisms behind this competition are unclear. Therefore, the work in this dissertation seeks to determine the molecular mechanisms behind how known sets of competitive ABPs compete on actin filaments and how these individual interactions coalesce to promote proper ABP sorting on a whole cell scale.

Summary

It is clear that at each step in actin network formation, cooperative interactions between ABPs (profilin and formin) are important for actin assembly and network maintenance. It is further clear that competitive interactions between assembly factors (Wsp1 vs. profilin, formin vs.. Arp2/3 complex) are equally important for proper actin monomer distribution. Finally, competition between ABPs is also involved in defining which ABPs are associated with a specific F-actin network. Using a combination of in vitro reconstitution of cell networks and in vivo live cell biology, the following work will address both competitive and cooperative interactions amongst ABPs and how those interactions affect the formation, organization, and ABP composition of F-actin networks.

CHAPTER 2: *CHLAMYDOMONAS REINHARDTII* POSSESSES A FORMIN AND PROFILIN THAT ARE OPTIMIZED FOR ACUTE RAPID ACTIN FILAMENT ASSEMBLY

The work in the following chapter was started by previous Kovar lab graduate student Mike Glista. Mike Glista along with Yujie Li, Colleen Skau, and Jennifer Sees performed the work in Figures 2-1, 2-2, 2-3, and 2-4. Yujie Li performed the TIRF in Figure 2-5 and I performed the analysis and created the figure. I performed the experiments and analysis in Figures 2-6 and 2-7. Laurens J. Mets initially identified the formin CrFor1 within the *Chlamydomonas* genome, and collaborators Prachee Avasthi and David Mueller are performing work in *Chlamydomonas* that is forthcoming.

Section 2.1—INTRODUCTION

The actin cytoskeleton is a dynamic system important for diverse cellular processes. *Chlamydomonas reinhardtii* expresses a single conventional actin, IDA5, with 90% identity to mammalian actin, as well as an unconventional actin, NAP (Kato-Minoura, 1998; Lee et al., 1997) with low identity to mammalian actin (64%). Despite two actin genes, few F-actin networks have been identified in *Chlamydomonas*. The minimalistic actin cytoskeleton of *Chlamydomonas* provides a prime opportunity to dissect the mechanisms behind how a specific actin network can be assembled at the correct time and place. An anti-actin antibody and Lifeact marker identified actin surrounding the nucleus during interphase (Onishi et al., 2015; Avasthi et al., 2014; Harper et al., 1992). This actin relocalizes throughout the cell cycle, moving from the anterior of the cell during preprophase and metaphase to the cleavage furrow during cytokinesis (Harper et al., 1992). However, these putative actin networks are not stained by phallicidin (an F-actin-binding toxin), and cytochalasin or latrunculin B treatments have no effect on cell division (Harper et al., 1992; Avasthi et al., 2014) suggesting that this network may be composed of actin monomer or short actin filaments. F-actin has additionally been shown to localize at the base of the flagella, where it has been shown to be important for intraflagellar transport (Avasthi et al., 2014). However, the nature of this actin network has not been well-defined.

The single clearly defined actin network in *Chlamydomonas* is the fertilization tubule. The fertilization tubule is an actin-rich structure found in mating type + gametes (Detmers et al., 1983; Detmers et al., 1985) that protrudes from the 'doublet zone', a region between the two flagella, during mating (Detmers et al., 1983). Phallicidin staining of filamentous actin strongly labeled fertilization tubules (Detmers et al., 1985), and isolation of fertilization tubules found actin to be a main component (Wilson et al., 1997). This simplified actin cytoskeleton of

Chlamydomonas provides the unique opportunity to understand how the cell is capable of regulating its actin cytoskeleton so precisely that actin polymerization occurs only at a very specific place and time. *Chlamydomonas* expresses both a profilin (CrPRF) and a formin (CrFor1). Unlike many profilins, CrPRF has been shown to inhibit ADP exchange of bound actin monomers, suggesting that CrPRF may be a sequestering protein, preventing F-actin assembly in *Chlamydomonas*. The formin CrFor1 has not been characterized and its cellular role in *Chlamydomonas* has not been determined. Therefore, we sought to characterize the formin CrFor1 and determine any potential interactions with CrPRF. Additionally, we wished to determine the role of CrFor1 in *Chlamydomonas* cells. We found that CrPRF is a sequestering protein that inhibits both nucleation and elongation of actin filaments. CrFor1 is capable of overcoming this inhibition and rapidly assembling CrPRF-bound actin.

Section 2.2—MATERIALS AND METHODS

Plasmid construction

Constructs consisting of different components of the formin actin assembly domains (FH1 and FH2) were prepared for bacterial expression. The preparation of Cdc12(FH1FH2) and Cdc12(FH1) constructs has been described (Neidt *et al.*, 2008). The CrFor1 domain constructs were designed based on sequence analysis of the *Chlamydomonas* genome by Laurens Mets ((10P) and (FH2)) and EST analysis by the Susan Dutcher lab (FH1), and were optimized for bacterial expression and custom synthesized by DNA 2.0. All constructs were prepared by standard cloning procedures, consisting of PCR amplification (iProof, Bio-Rad Laboratories) from the commercially prepared DNA. Restriction enzyme cleavage sites and 6x His sequence were included in the reverse primers. PCR products were cloned using restriction enzymes into pET21a (EMD Biosciences) for expression.

Protein purification

All constructs of CrFor1 and CrPRF were expressed in BL21-Codon Plus (DE3)-RP (Agilent Technologies, Santa Clara, CA). Cdc12(FH1FH2) (Kovar et al., 2003), SpPRF (Lu and Pollard, 2001), SpFus1 (Scott et al., 2011), and CrPRF (Kovar et al., 2001) were purified as described previously. CrFor1 constructs were His-tag affinity purified. CrFor1 constructs were expressed with 0.5 mM isopropyl ß-D-thiogalactopyranoside (IPTG; Sigma-Aldrich) for 16 hours at 16°C. Cells were resuspended in extraction buffer (50 mM NaH_2PO_4, pH 8.0, 500 mM NaCl, 10% glycerol, 10 mM imidazole, 10 mM betamercaptoethanol [ßME]) supplemented with 0.5 mM phenylmethylsulfonyl fluoride (PMSF) and protease inhibitors, sonicated, and homogenized in an Emulsiflex-C3 (Avestin, Ottawa, ON, Canada). The homogenate was spun and clarified at 30,000*g* for 15 minutes, then 50,000*g* for 30 minutes and incubated with Talon Metal Affinity Resin (Clontech, Mountain View, CA) for 1 hour at 4°C. The resin was loaded onto a disposable column and washed with 50 mL wash with extraction buffer. CrFor1 was then eluted with Talon elution buffer (50 mM NaH_2PO_4, pH 8.0, 500 mM NaCl, 10% glycerol, 250 mM imidazole, 10 mM ßME) and dialyzed into formin buffer (20 mM HEPES, pH 7.4, 1 mM EDTA, 200 mM KCl, 0.01% NaN3, and 1 mM DTT).

A_{280} of purified proteins was taken using a Nanodrop 2000c Spectrophotometer (Thermo-Scientific, Waltham, MA). Proteins were flash-frozen in liquid nitrogen and kept at -80°C. SNAP-CrFor1(3P,FH2) protein was labeled with SNAP-549 dye (New England Biolabs, Ipswich, MA) as per manufacturer's instructions prior to each TIRF experiment.

Actin was purified from rabbit or chicken skeletal muscle actin as previously described (Spudich and Watt, 1971). For pyrene assembly assays, actin was labeled with N-(1-Pyrene)Iodoacetamide (Life Technologies, Carlsbad, CA) on Cys-374. As the combination of

CrFor1 in the presence of CrPRF selected against actin labeled on Cys-374, actin labeled with Alexa Fluor 488 on lysines (ThermoFisher Scientific, Waltham, MA) was used for TIRF microscopy experiments.

Pyrene assembly and disassembly assays

All pyrene assembly and disassembly assays were carried out in a 96-well plate. Actin assembly was measured by measuring the fluorescence of pyrene-actin (excitation at 364 nm and emission at 407 nm) with a Spectramax Gemini XPS (Molecular Devices) or Safire2 (Tecan) fluorescent plate reader following reaction initiation. For spontaneous assembly assays, a 15 μM mixture of 20% pyrene-labeled Mg-ATP-actin monomer with 100X anti-foam 204 (0.005%; Sigma) was placed in the upper well of a 96 well non-binding black plate. Formin and/or profilin, 10X KMEI (500 mM KCl, 10 mM $MgCl_2$, 10 mM ethylene glycol tetraacetic acid [EGTA], and 100 mM imidazole, pH 7.0), and Mg-Buffer G (2 mM Tris, pH 8.0, 0.2 mM ATP, 0.1 mM MgCl2 and 0.5 mM DTT) were placed in the lower row of the plate. Reactions were initiated by mixing contents of the lower wells the actin monomers in the upper wells with a twelve-channel pipetman (Eppendorf).

For seeded assembly assays, 5.0 μM unlabeled Mg-ATP-actin was preassembled in the upper row of the plate, followed by addition of anti-foam, formin and/or profilin, and Mg-Buffer G. A 2.0 μM mixture of 20% pyrene-labeled actin with Mg-Buffer G was placed in the lower plate row. Mixing actin monomers in lower wells with pre-assembled actin filaments in upper wells initiated reactions.

For depolymerization assays, a 5.0 μM mixture of unlabeled and 20% pyrene-labeled Mg-ATP-actin monomers was preassembled in the upper row of the plate for two hours, followed by

addition of anti-foam. Formin, 10X KMEI and Mg-Buffer G were placed in the lower plate row. Reactions were initiated by mixing lower wells with upper wells, diluting the pre-assembled filaments to 0.1 μM.

Profilin FH1 affinity assays

The affinity of profilin for formin(FH1) was determined by measuring the change in profilin's intrinsic tryptophan fluorescence by excitation at 295 nm and emission at 323 nm (). Profilin (1.0 μM) was incubated with a range of formin(FH1) concentrations for 30 min, then profilin fluorescence was read in a Safire2 fluorescence plate reader and plotted versus formin(FH1) concentration. The fluorescence of formin(FH1) alone was subtracted from the fluorescence in the presence of profilin. Dissociation constants (K_d) were determined by fitting a quadratic function to the dependence of the concentration of bound profilin on the concentration of formin(FH1).

Polymerization and depolymerization rate determination

Actin assembly rates were determined from spontaneous assembly reactions by measuring the slopes of actin assembly following the lag phase to 50% of total actin assembly. Assembly rates from preassembled actin seeds were determined by a linear fit to the first 100 seconds of assembly. Depolymerization rates were determined by a linear fit to the first 100-300 seconds of the reaction.

The affinity of formin CrFor1 for barbed ends was determined as previously described (Kovar et al., 2006). We fit the plot of the dependence of the assembly or disassembly rate on formin concentration using the equation $V_i = V_{if} + (V_{ib} - V_{if})$ ((K_d + [ends] + [formin] –

$\sqrt{((K_d + [ends] + [formin])2 - 4[ends][formin])/2[ends]))}$, where V_i is the observed elongation or depolymerization rate, V_{if} is the elongation or depolymerization rate of free barbed ends, V_{ib} is the elongation or depolymerization rate of bound barbed ends, [ends] is the concentration of barbed ends, and [formin] is formin concentration. The nucleation efficiency was calculated by dividing the slope of the spontaneous assembly rate by *k*+ in the absence and presence of profilin and dividing by the formin concentration (Kovar et al., 2006). Depolymerization rates are normalized to the rate of actin assembly alone and expressed as a percent of the standard actin assembly rate.

Rhodamine phalloidin staining of F-actin

Unlabeled Mg-ATP-actin was assembled as per standard spontaneous assembly reactions. Actin filaments were then incubated with 1 μM TRITC-Phalloidin (Fluka Biochemika, Switzerland) for 5 minutes. Reactions were terminated by diluting assembled filaments in fluorescence buffer (50 mM KCl, 1 mM $MgCl_2$, 100 mM DTT, 20 μg/ml catalase, 100 μg/ml glucose oxidase, 3 mg/ml glucose, 0.5% methylcellulose, and 10 mM imidazole, pH 7.0) and were absorbed to coverslips coated with 0.05 μg/μl poly-L-lysine. Fluorescence microscopy images were collected on an Olympus IX-81 microscope and cooled CCD camera (Orca-ER, Hamamatsu).

Low-speed sedimentation assays

Sedimentation assays were performed as previously described (Skau et al., 2010). 15 μM Mg-ATP actin monomers were spontaneously assembled for 1 hour in 10 mM imidazole, pH 7.0,

50 mM KCl, 5 mM $MgCl_2$, 1 mM EGTA, 0.5 mM DTT, 0.2 mM ATP and 90 μM $CaCl_2$ to generate F-actin. Filamentous actin was then incubated with CrFor1 or SpFus1 for 20 minutes at 25ºC and spun at 10,000g at 25ºC. Supernatant and pellets were separated by 15% SDS-PAGE gel electrophoresis and stained with Coomassie Blue for 30 minutes, destained for 16 hours and analyzed by densitometry with ImageJ.

TIRF microscopy

Time-lapse TIRF microscopy movies were obtained using a iXon EMCCD camera (Andor Technology, Belfast, UK) fitted to an Olympus IX-71 microscope with through-the-objective TIRF illumination. Mg-ATP-actin (20% Alexa 488-labeled) was mixed with a polymerization mix (10 mM imidazole (pH 7.0), 50 mM KCl, 1 mM MgCl2, 1 mM EGTA, 50 mM DTT, 0.2 mM ATP, 50 μM CaCl2, 15 mM glucose, 20 μg/mL catalase, 100 μg/mL glucose oxidase, and 0.5% (400 centipoise) methylcellulose) to induce F-actin assembly (Winkelman et al., 2014). Where stated, formin or profilin was added to the polymerization mix prior to mixing with actin and initiating F-actin polymerization. The mixture was then added to a flow chamber and imaged at 10 s intervals at room temperature. For bead assays, Wsp1 and formin beads were prepared as previously described (Loisel et al., 1999). Carboxylated Polybeads (Polysciences, Warrington, PA) were coated with Wsp1 or CrFor1 and flowed into the TIRF chamber prior to initiating the reaction.

Section 2.3—RESULTS

CrPRF inhibits nucleation and elongation of actin filaments

In a cell, the majority of unassembled G-actin is bound to profilin (Carlsson et al., 1977; Kaiser et al., 1999; Lu and Pollard, 2001). Profilin inhibits the nucleation of new actin filaments,

but once an actin filament has been formed, allows the addition of profilin-bound actin monomers to the barbed end of a growing actin filament (Pollard and Cooper, 1984). Additionally, mammalian profilins promote ADP-to-ATP exchange within their bound actin, though plant profilins do not (Mockrin and Korn, 1980; Goldschmidt-Clermont et al., 1992; Perelroizen et al., 1996).

Chlamydomonas profilin CrPRF is found in both the cytoplasm and flagellar compartments of the cell, localizing at the base of the flagella in vegetative cells and below the fertilization tubule in mating type + gametes (Kovar et al., 2001). Previous work showed that unlike typical profilins, CrPRF inhibits the nucleotide exchange of bound G-actin, suggesting its role as potent sequesterer of G-actin (Kovar et al., 2001). Consistent with its role as a sequestering protein, we found that actin assembly was inhibited in the presence of CrPRF in a concentration-dependent manner (Figure 2-1A). By observing growth of actin filaments using TIRF microscopy, we found that CrPRF inhibited not only nucleation, but also elongation of actin filaments (Figure 2-1B), suggesting that CrPRF potently sequesters G-actin.

As *Chlamydomonas* has minimal F-actin networks, a sequestering profilin such as CrPRF could be ideal for proper F-actin organization by preventing spontaneous actin assembly. However, F-actin polymerization within the fertilization tubule still needs to occur at the correct time and place during mating. Therefore, we speculated that an actin assembly factor such as a formin may be responsible for rapid actin assembly at fertilization tubule sites.

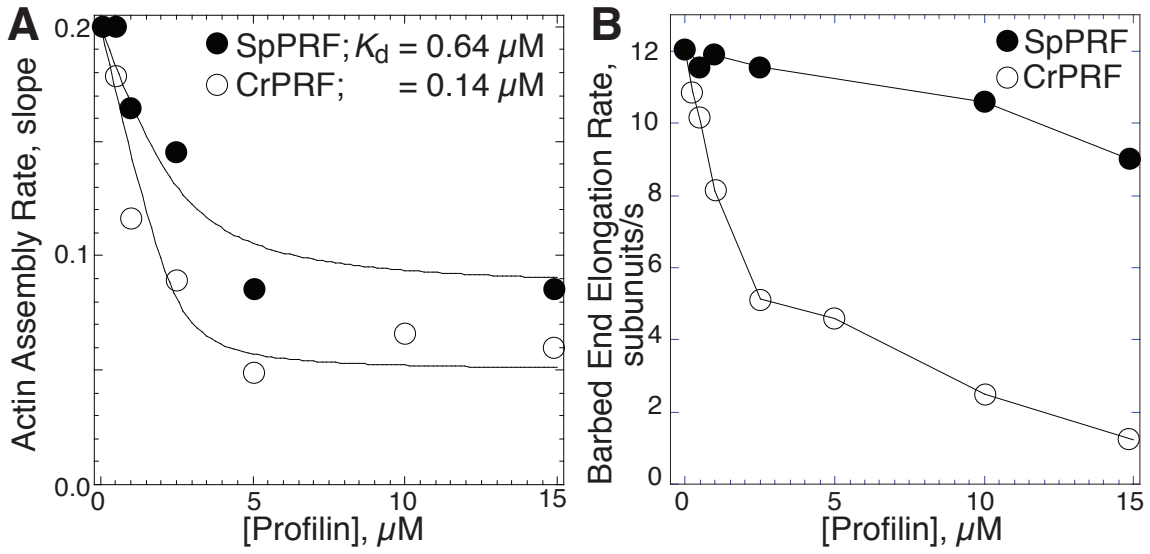

Figure 2-1: CrPRF inhibits nucleation and elongation of actin filaments.
(A) Slopes of spontaneous pyrene actin assembly assays (1.5 μM Mg-ATP actin, 20% pyrene labeled) with increasing concentrations of fission yeast profilin SpPRF or *Chlamydomonas reinhardtii* profilin CrPRF. Curve fits reveal affinities of SpPRF and CrPRF for actin monomer. **(B)** Barbed end elongation rates of 1.5 μM Mg-ATP actin (10% Alexa-488 labeled) in the presence of increasing concentrations of SpPRF or CrPRF, measured by TIRF microscopy.

CrFor1 efficiently nucleates but weakly elongates actin filaments

Formins are a conserved family of actin assembly factors that both nucleate and elongate actin filaments. Formins contain a formin homology 1 (FH1) and formin homology 2 (FH2) domain along with flanking regulatory regions. Functional formins are dimers, with two FH2 domains interacting head-to-tail to create a donut-shaped dimer capable of creating a stable actin 'nucleus'**.** In addition, the FH2 dimer maintains processive association with the barbed end of an actin filament as it elongates (Goode and Eck, 2007) The unstructured FH1 domains are rich in proline-rich motifs (PRMs) that bind to profilin and promote rapid association of profilin-actin with the barbed end of an elongating filament. In order to investigate the actin assembly properties of the formin CrFor1, we created a set of constructs containing the CrFor1 FH1 and FH2 domains, alone or in combination (Figure 2-2A).

CrFor1's capacity to stimulate actin assembly was investigated by measuring the effect of CrFor1 on actin polymerization over time using spontaneous pyrene actin assembly assays. In pyrene assembly assays, 20% of actin monomer is labeled N-(1-Pyrene)Iodoacetamide, a fluorophore that fluoresces when near other pyrene molecules. Therefore, the pyrene fluorescence signal increases over time upon F-actin polymerization (Figure 2-2B). CrFor1 containing the FH2 alone (CrFor1(FH2)) or both the FH1 and FH2 domains (CrFor1(3P,FH2)), and (10P,FH2) all stimulated actin assembly in a concentration-dependent manner (Figure 2-2B,C). Additionally, each CrFor1 construct tested was more efficient in stimulating polymerization than the fission yeast formin Cdc12(FH1,FH2) (Figure 2-2B,C). Though these results indicate an increase in actin assembly in the presence of CrFor1, spontaneous pyrene assembly assays are unable to differentiate between an increase in the nucleation and/or elongation of actin filaments, leaving us unable to determine if this increase in assembly is due to an increase in actin nucleation or the elongation of pre-existing actin filaments.

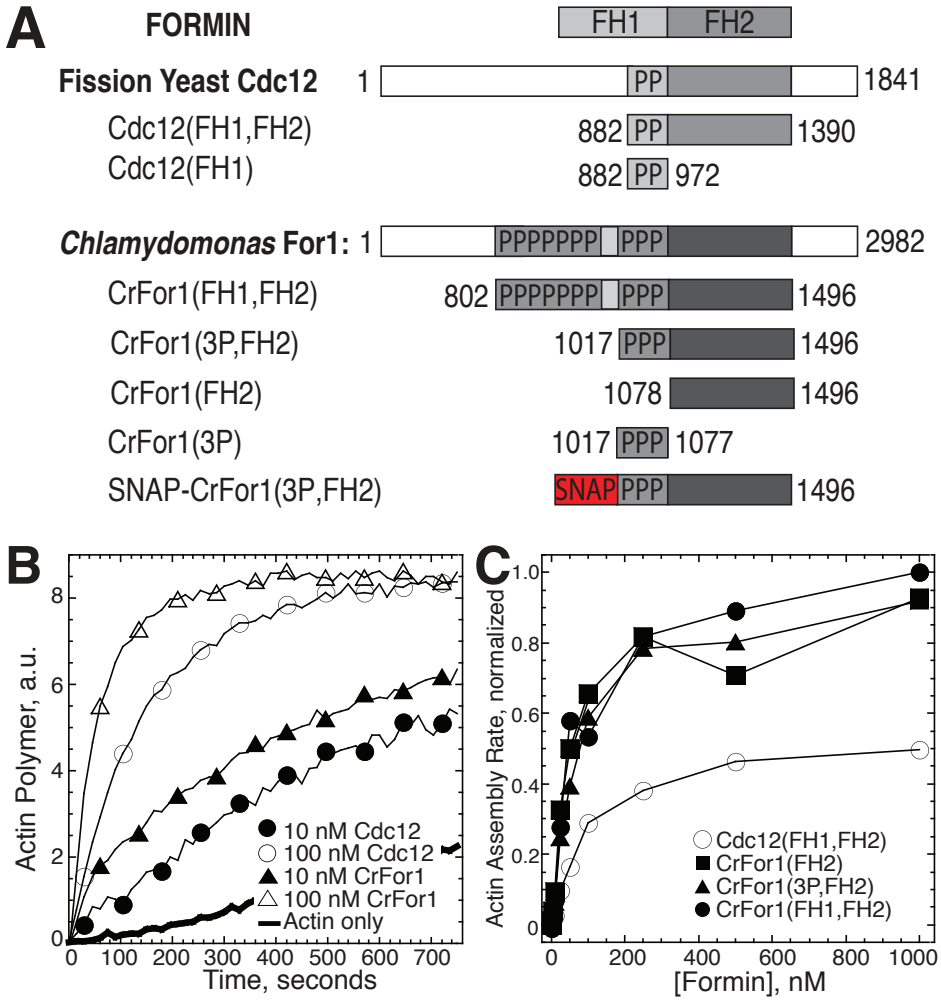

Figure 2-2: CrFor1 efficiently nucleates actin filaments.
(A) Domain organizations of fission yeast formin Cdc12 and *Chlamydomonas reinhardtii* formin CrFor1 and created constructs. Numbers denote amino acid residue. Each "P" denotes a putative profilin binding site of at least 6 prolines within 8 residues. **(B,C)** Spontaneous pyrene actin assembly assays of 2.5 μM Mg-ATP actin, 20% pyrene labeled. (B) Plot of pyrene fluorescence over time for actin alone (thick curve) or 10 nM (●) or 100 nM (○) of Cdc12(FH1,FH2) or 10 nM (▲) and 100 nM (△) of CrFor1(3P,FH2). **(C)** Plot of the dependence of the normalized actin assembly rate (slope) on the concentration of Cdc12(FH1,FH2) (○), CrFor1(FH2) (■), CrFor1(3P,FH2) (▲), and CrFor1(10P,FH2) (●).

In order to determine the effect of CrFor1 on actin filament elongation, we performed seeded assembly assays. In the presence of actin filament seeds, the effect of actin polymerization due to nucleation of new filaments is minimized, and the elongation of existing seed barbed ends is the primary factor involved in the observed actin assembly rates. Adding

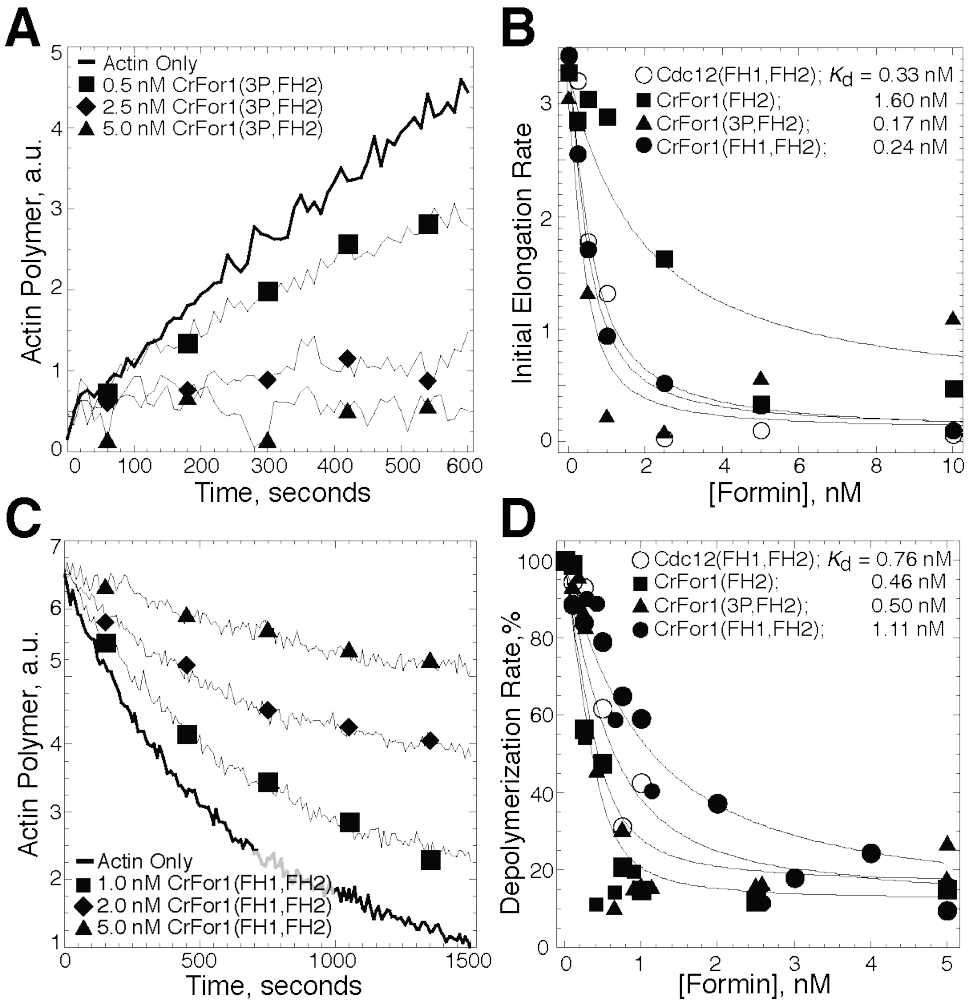

Figure 2-3: CrFor1 weakly elongates actin filaments.
(A,B) Seeded assembly assays of 2.0 µM Mg-ATP actin, 20% pyrene labeled. **(A)** Plot of pyrene fluorescence over time for actin alone (thick line) or in the presence of 0.5 nM (■), 1.0 nM (⬥), or 2.5 nM (▲) CrFor1(3P,FH2). **(B)** Plot of the dependence of the initial barbed end assembly rate on the concentration of Cdc12(FH1,FH2) (○), CrFor1(FH2) (■), CrFor1(3P,FH2) (▲), and CrFor1(10P,FH2) (●). **(C,D)** F-actin disassembly assays; depolymerization of 5 µM actin filaments (50% pyrene labeled) after dilution to 0.1 µM in the absence (thick curve) or presence of 0.1 nM (■), 0.25 nM (⬥), or 0.5 nM (▲) CrFor1(3P,FH2). **(D)** Dependence of the rate of depolymerization on the concentration of the indicated formin. Curve fits reveal equilibrium dissociation constants for CrFor1(FH2) (■), CrFor1(3P,FH2) (▲), CrFor1(10P,FH2) (⬥), and Cdc12(FH1,FH2) (●).

CrFor1(3P,FH2) to seeded assembly reactions reduced the rate of actin assembly in a concentration dependent matter (Figure 2-3A), suggesting that CrFor1 inhibits actin filament elongation, and that the majority of actin assembly observed in spontaneous pyrene assays is due

to nucleation. By fitting the initial rate of polymerization over a range of formin concentrations, we obtained formin dissociation rate constants (K_d) in the low nanomolar range for each construct. The affinities of the formin constructs for filament barbed ends were similar for CrFor1(FH2) (K_d=1.6 nM), CrFor1(3P,FH2) (K_d=0.17 nM), CrFor1(FH1,FH2) (K_d=0.24 nM), and Cdc12(FH1,FH2) (K_d=0.33 nM) (Figure 2-3B).

The barbed end affinity of each formin construct was verified by disassembly assays. In the presence of sub-nanomolar concentrations of CrFor1 constructs, the rate of F-actin depolymerization was significantly reduced (Figure 2-3C). Curve fits revealed affinities for the filament barbed ends similar to those determined by seeded assembly for CrFor1(FH2) (K_d=0.40 nM), CrFor1(3P,FH2) (K_d=0.40 nM), CrFor1(10P,FH2) (K_d=0.68 nM), and Cdc12(FH1,FH2) (K_d=0.76 nM) (Figure 2-3D). Together, these results indicate that CrFor1 potently stimulates actin nucleation, while inhibiting actin filament elongation. In addition, like other formins, CrFor1 binds actin filament barbed ends with an affinity in the low nanomolar range.

Universal profilin SpPRF is utilized by CrFor1

We have demonstrated that *Chlamydomonas* formin CrFor1 has potent nucleation activity but poorly elongates actin filaments. Similarly, in the absence of profilin, the fission yeast formin Cdc12 has high nucleation activity, but poorly elongates actin filaments. However, in the presence of fission yeast profilin SpPRF, Cdc12 rapidly elongates actin filaments (Kovar et al., 2003; 2006). We speculated that CrFor1 may similarly utilize profilin to rapidly elongate F-actin. We first tested the ability of profilin CrPRF to bind to the FH1 domains of formins Cdc12 and CrFor1. CrPRF had similar affinities for the FH1 domains of formins CrFor1 and Cdc12 as SpPRF (Figure 2-4B,C), all within the low micromolar range. We additionally tested the ability

of both profilins to bind PLP, and found that CrPRF had a lower affinity for PLP than the fission yeast profilin SpPRF (397 ± 63 μM and 40 ± 2.6 μM, respectively) (Figure 2-4A,C).

Although profilin was found to bind to CrFor1's FH1 domain, the capacity of a formin to add profilin-actin to filament barbed ends depends on the complementarily of the profilin with both the FH1 and FH2 domains of the formin (Neidt et al., 2009; Bestul et al., 2015). We initially tested the ability of CrFor1 to elongate SpPRF-bound actin, as SpPRF is one of the profilins most widely compatible with different formin isoforms (Neidt et al., 2009; Bestul et al., 2015). We found that CrFor1 containing both the FH1 and FH2 domains (CrFor1(3P,FH2)) rapidly accelerated actin assembly in the presence of fission yeast profilin SpPRF (Figure 2-4D,E). On the other hand, the presence of SpPRF inhibited actin assembly by CrFor1 containing the FH2 domain alone (Figure 2-4D,E). The actin assembly rates measured in the presence of SpPrf with CrFor1(3P,FH2) were greater than those of SpPRF with Cdc12(FH1,FH2) over a range of SpPRF concentrations, as well as in the absence of profilin (Figure 2-4E), indicating that CrFor1(3P,FH2) has efficient actin assembly activity in the presence of the universal profilin, SpPRF.

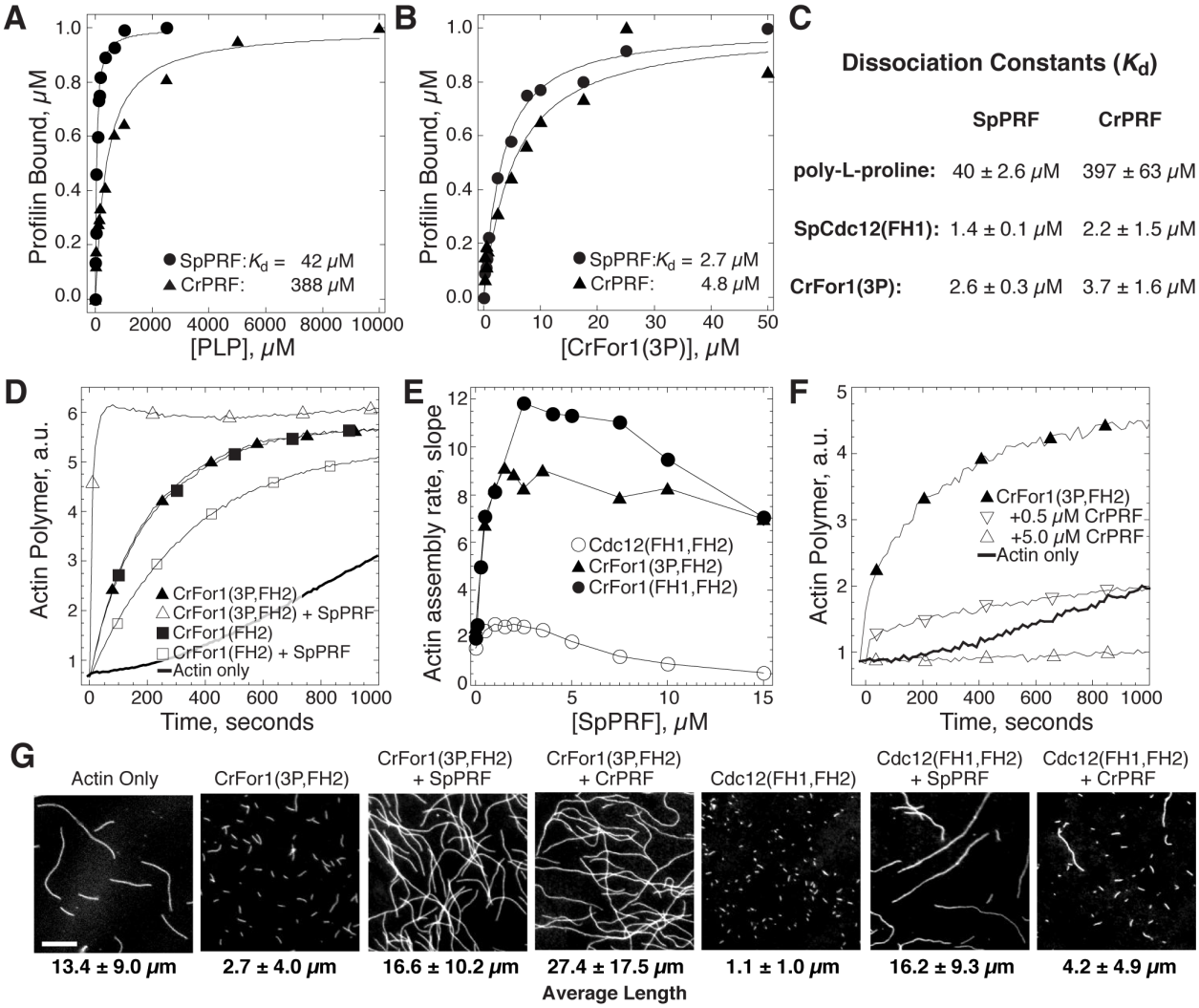

Figure 2-4: CrFor1 stimulates the assembly of profilin-actin.

(A-C) Affinity of profilin for poly-L-proline and FH1 domains. Dependence of SpPRF (●) and CrPRF (▲) intrinsic tryptophan fluorescence on the concentration of poly-L-proline (A) and CrFor1(3P) **(B)**. **(C)** Average affinity of SpPRF and CrPRF for poly-L-proline, Cdc12(FH1) and CrFor1(3P); n≥3 experiments. **(D-F)** Spontaneous assembly of 2.5 µM Mg-ATP actin (20% pyrene-labeled). **(D)** Plot of pyrene fluorescence over time for actin alone (thick curve), or with 10 nM CrFor1(FH2) in the absence (■) or presence (□) of 2.5 µM fission yeast profilin SpPRF, or with 10 nM CrFor1(3P,FH2) in the absence (▲) or presence (▵) of 2.5 µM SpPRF. **(E)** Dependence of the actin assembly rate (slope) on the concentration of SpPRF for reactions containing 10 nM CrFor1(3P,FH2) (▲) or 10 nM Cdc12(FH1,FH2) (●). **(F)** Plot of pyrene fluorescence over time for actin alone (thick curve), or in the presence of 10 nM CrFor1(3P,FH2) alone (▲), or with 0.5 µM (▿), or 5.0 µM (▵) CrPRF. **(G)** Fluorescence micrographs of actin filaments taken 10 minutes after the initiation of the indicated reactions with 10 nM formin and 2.5 µM profilin. Samples were labeled with rhodamine-phalloidin and adsorbed to glass coverslips coated with poly-L-lysine. Scale bar, 5 µm.

CrPRF-bound actin is utilized specifically by CrFor1

We next examined the ability of CrFor1 to assemble CrPRF-bound actin. In spontaneous assembly assays, the pyrene fluorescence measured in reactions containing CrFor1 and CrPRF was sharply reduced relative to actin alone or actin in the presence of CrFor1, even at low CrPRF concentrations (Figure 2-4F). While this could indicate that CrPRF was severely inhibiting actin polymerization, our spontaneous assembly assay relies on measuring changes in pyrene fluorescence over time and we suspected that CrPRF was potentially distorting this readout. It is possible that CrPRF could bind with a much higher affinity to unlabeled actin monomer than to pyrene-conjugated actin monomer, leading to polymerization of only unlabeled actin in the presence of formin and CrPRF. Alternatively, CrPRF could directly quench the fluorescence of pyrene-actin that had been incorporated into filament.

To test this observation, we directly visualized actin filaments formed by spontaneous assembly in the presence of different profilin-formin combinations. Reactions were prepared as in the bulk assembly experiments described above and allowed to proceed for 600 seconds. Polymerization was then stopped by dilution and F-actin stained with TRITC-Phalloidin to allow visualization of filaments by fluorescence microscopy. Micrographs revealed many small actin filaments (average length, 2.7 ± 4.0 μm), indicative of efficient nucleation by CrFor1. In the presence of either SpPRF or CrPRF, CrFor1 facilitated the formation of long actin filaments (average length, 16.6 ± 10.2 μm and 27.4 ± 17.5 μm, respectively). Interestingly, although CrFor1 could utilize either SpPRF or CrPRF to elongate filaments, Cdc12 was unable to form long filaments in the presence of CrPRF (average length, 4.2 ± 4.9 μm) (Figure 2-4G), suggesting that CrPRF is tailored for elongation by CrFor1. Together, these results indicate that CrFor1 is capable of efficient actin filament nucleation, and in the presence of its complimentary

profilin CrPRF, rapidly elongates these filaments. In addition, the inability of Cdc12 to elongate CrPRF-associated actin suggests that CrFor1 and CrPRF are tailored to precisely and rapidly polymerize F-actin.

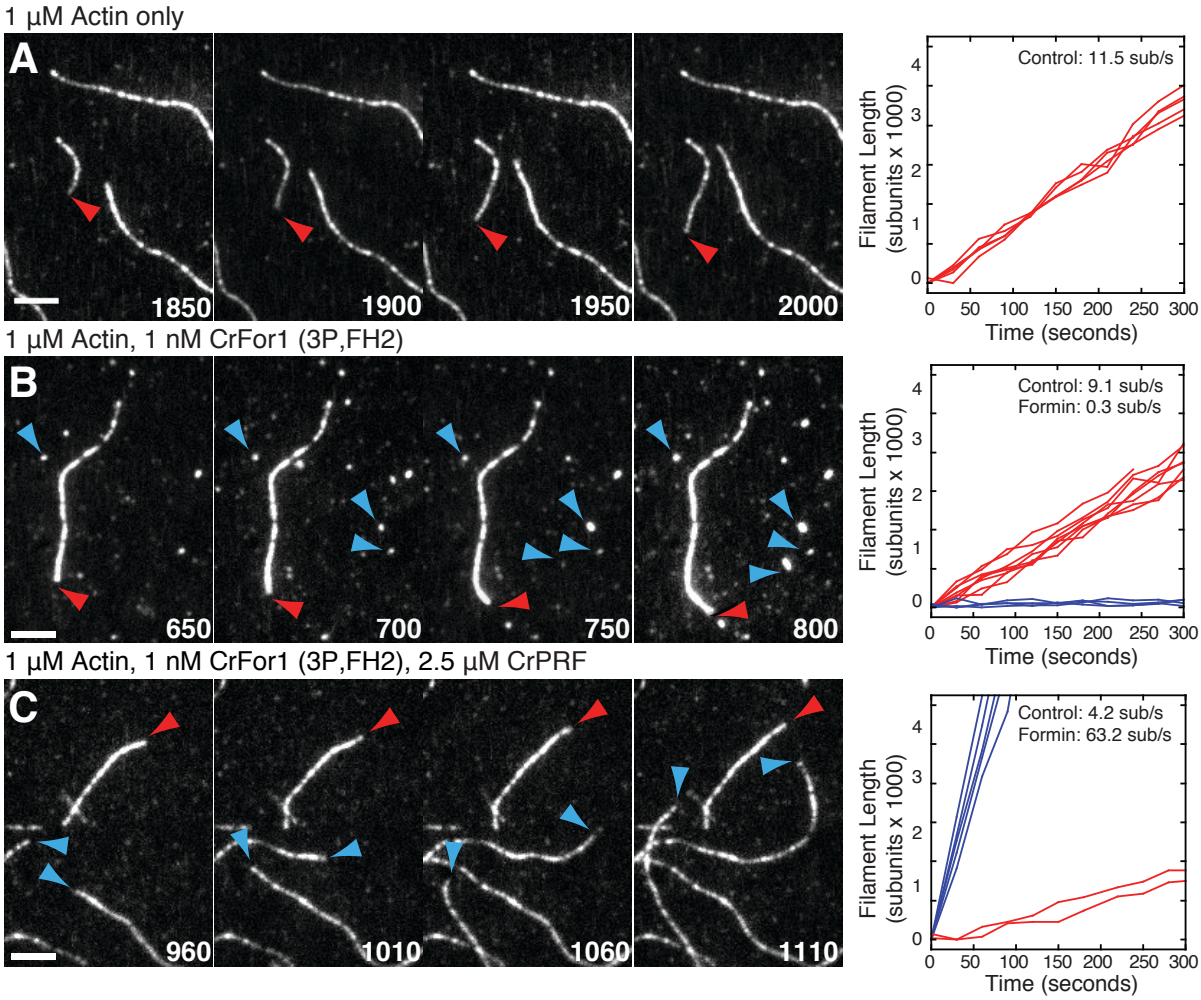

Figure 2-5: CrFor1 rapidly elongates actin filaments in the presence of CrPRF. **(A,C,E)** TIRF microscopy of 1 µM Mg-ATP actin (10% Alexa 488-labeled) in the presence of CrFor1(3P,FH2) and/or CrPRF. Red arrowheads denote control (non-formin bound) filaments. Blue arrowheads denote CrFor1-associated filaments. Scale bars, 5 µm. Time in sec. **(B,D,F)** Rates of filament growth for control filaments (red lines) and CrFor1-associated filaments (blue lines).

CrFor1 rapidly and processively elongates actin filaments in the presence of CrPRF

In order to directly examine the effect of CrPRF on CrFor1-mediated actin assembly, we visualized the elongation of individual actin filaments over time using Total Internal Reflection Fluorescence (TIRF) microscopy. Actin filaments alone (control) elongated at a rate of 11.5 subunits per second (Figure 2-5A). In the presence of CrFor1 (3P,FH2), two populations of filaments were observed: actin filaments elongating at the control rate (9.1 sub/s, red arrowheads), and actin filaments elongating at a significantly reduced rate (0.3 sub/s, blue arrowheads) (Figure 2-5B). Our interpretation is that the slow-growing filaments are bound by CrFor1, which is inhibiting their elongation, while control rate filaments are not bound by CrFor1. In the presence of CrFor1 and CrPRF, two distinct populations of filaments were again observed: actin filaments elongating at a rate slower than the control rate (4.2 sub/s) and rapidly elongating actin filaments (63.2 sub/s) (Figure 2-5C). As CrPRF slows actin filament elongation, the control rate is slower in these reactions, while CrFor1 can efficiently utilize CrPRF-bound actin to rapidly elongate actin filaments.

Our results suggest that CrFor1 and CrPRF work together to rapidly elongate F-actin. In order to directly visualize and confirm this finding, we created a SNAP-tagged construct of CrFor1(3P,FH2) capable of being labeled in TIRF microscopy experiments. In the absence of CrPRF, red CrFor1 is associated with small, slow growing actin filaments (Figure 2-6A, blue arrowheads), consistent with our finding that CrFor1 can nucleate actin filaments but inhibits actin filament elongation. In the presence of CrPRF, CrFor1-associated actin filaments elongate rapidly (Figure 2-6B,D) compared to control filaments (Figure 2-6C).

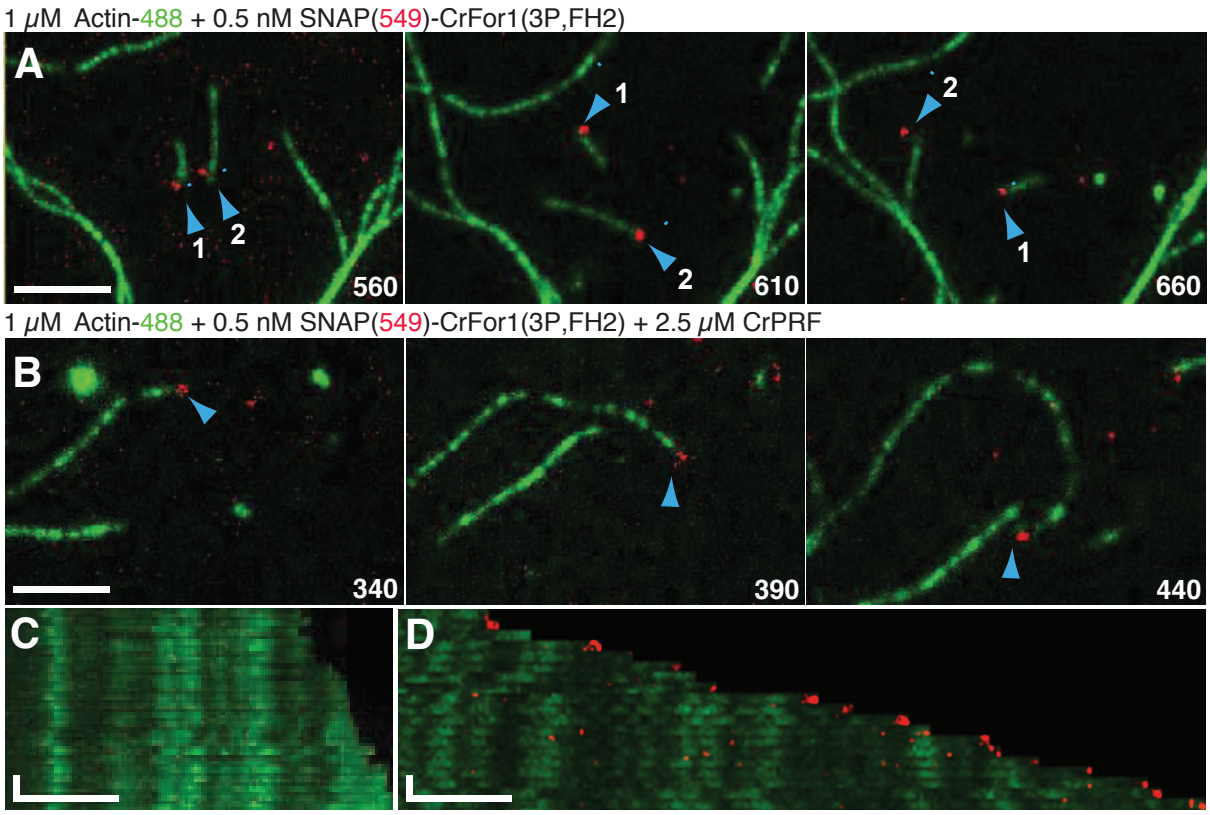

Figure 2-6: CrFor1 is processive in the absence or presence of CrPRF.
(A-D) Two-color TIRF microscopy of 1 µM Mg-ATP actin (10% Alexa 488-labeled) with 0.5 µM SNAP-CrFor1(3P,FH2) (549-labeled) in the presence or absence of 2.5 µM CrPRF. Blue arrowheads denote formin-bound filaments. Numbers next to arrowheads denote distinct formin-bound filaments. **(A)** 0.5 µM SNAP-CrFor1(3P,FH2) alone. **(B)** 0.5 µM SNAP-CrFor1(3P,FH2) in the presence of 2.5 µM CrPRF. **(C)** Kymograph of control filament from **(B)**. **(D)** Kymograph of formin-bound filament from **(B)**. Scale bars, x-axis, 5 µm. Time bars, y-axis, 30 sec.

CrPRF favors formin- over Arp2/3 complex-mediated assembly.

We have demonstrated that CrPRF promotes rapid actin assembly by CrFor1 and that this enhanced actin assembly is specific for CrFor1. In addition to enhancing formin-mediated elongation, profilin has also been shown to tune F-actin network formation by inhibiting Arp2/3 complex-mediated actin assembly (Suarez et al., 2015; Rotty et al., 2015). As CrPRF is a potent sequestering protein, we speculated that it may also be an inhibitor of the Arp2/3 complex by competing for actin monomer with Arp2/3 complex activator Wsp1 (Suarez et al., 2015). In

order to test this, we performed bead assays in which fission yeast Arp2/3 complex activator Wsp1 or formin CrFor1 is attached to a polystyrene bead within a standard TIRF microscopy chamber. Actin alone and CrPRF-bound actin are flowed sequentially into the microscopy chamber in order to assess actin filament assembly under each condition. When initially incubated with actin alone, CrFor1-bound beads poorly assemble F-actin (Figure 2-7D (1),E), similar to what we observed in standard TIRF assays (Figure 2-5C, 2-6A). However, when CrPRF-bound actin is flowed into the TIRF chamber, rapid actin filament assembly occurs (Figure 2-7D(2),E). Photobleaching the F-actin following the flow of CrPRF-bound actin shows the reoccurrence of high fluorescence at the site of the bead (Figure 2-7D(3),F), indicative of rapid actin filament assembly by CrFor1 at the bead surface. Conversely, beads coated with Wsp1 showed normal actin assembly following incubation with actin and Arp2/3 complex (Figure 2-7A(1),E). However, filament growth was halted following incubation with CrPRF-bound actin (Figure 2-7B(2),E). Photobleaching of F-actin shows very little F-actin assembly at filament barbed ends, consistent with CrPRF inhibition of actin filament elongation. In addition, very little F-actin assembly occurs at the bead, demonstrating inhibition of Arp2/3 complex-mediated assembly at the bead surface (Figure 2-7B(3),F).

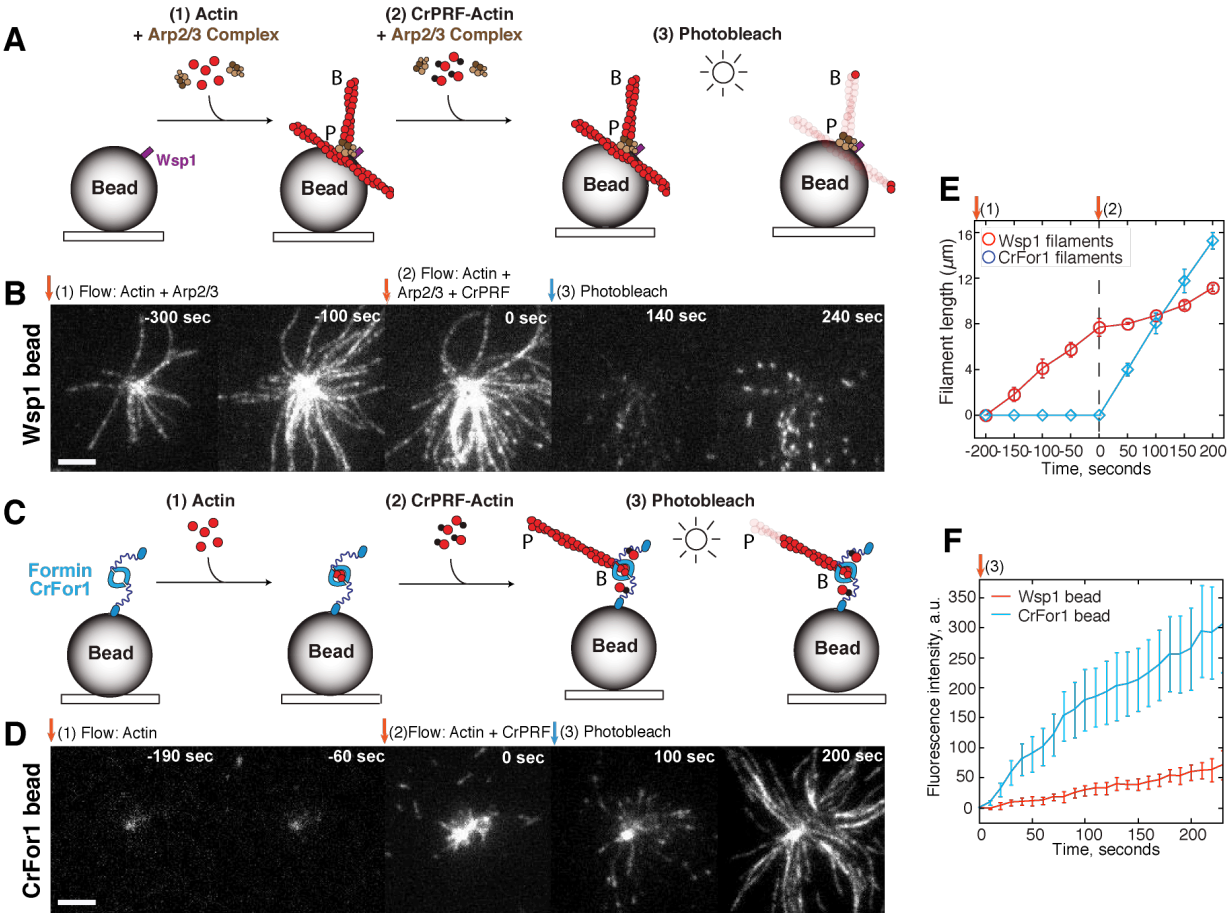

Figure 2-7: CrPRF favors formin- over Arp2/3 complex-mediated assembly.
(A-F) TIRF microscopy bead assays. Fission yeast Arp2/3 complex activator Wsp1 or formin CrFor1 is adsorbed to a polystyrene bead and the effect of CrPRF-actin on network formation is observed. 'B' indicates actin filament barbed ends, and 'P' indicates pointed ends. **(A-B)** TIRF microscopy experiments containing beads coated with Wsp1. TIRF chamber is flowed with 1.5 μM Mg-ATP actin (10% Alexa 488-labeled) and 30 nM Arp2/3 complex (1), then actin, Arp2/3 complex, and 2.5 μM CrPRF (2). Filaments are photobleached (3) following second flow to observe where new filament assembly occurs. **(C-D)** TIRF microscopy experiments containing beads coated with CrFor1. TIRF chamber is flowed with actin (1), then actin and CrPRF (2), then photobleached (3). **(E)** Quantification of actin filament length over time for filaments associated with Wsp1 (red) or CrFor1 (blue) beads. (1) indicates flow of actin and (2) indicates flow of CrPRF + actin. Error bars=s.e., n=5 filaments. Scale bar, 5 μm. **(F)** Quantification of fluorescence intensity (indicative of actin assembly) at the surface of a Wsp1-coated (red line) or CrFor1-coated (blue line) bead following flow-in of CrPRF-actin and photobleaching.

Section 2.4—DISCUSSION

CrFor1 in fertilization tubule formation

We speculate CrPRF works to sequester G-actin in the *Chlamydomonas* cell. Specifically during mating, CrFor1 is activated and rapidly assembles CrPRF-bound actin to create the fertilization tubule. Fertilization tubule formation in *Chlamydomonas* occurs near the membrane at a site between the two flagella. Prior to fertilization tubule formation, this site is characterized by two parallel electron-dense regions called the membrane zone (immediately adjacent to the membrane) and doublet zone (slightly interior) (Goodenough and Weiss, 1975; Detmers et al., 1983). In a mature fertilization tubule, the pointed ends of actin filaments are attached at the doublet zone (Detmers et al., 1983) while the membrane zone is present at the far end of the extended fertilization tubule, near the F-actin barbed ends. As formins are typically membrane-anchored, CrFor1 is potentially localized to the membrane zone, which extends from the doublet zone following F-actin formation. Fertilization tubules are capable of partially forming in the presence of cytochalasin D (Detmers et al., 1983), suggesting that actin polymerization is specifically important for extended formation and maturation of the fertilization tubule. Future work will involve determining the factors that regulate CrFor1 activity and other ABPs that are involved in proper organization of F-actin at that site.

CrPRF as a regulator of F-actin assembly

We have demonstrated that regulation of the simplified actin cytoskeleton in *Chlamydomonas* is due to the actin-sequestering abilities of the profilin CrPRF and its utilization by the formin CrFor1. We have demonstrated that CrPRF is an unusual profilin that sequesters actin monomers, inhibiting both the nucleation and elongation of F-actin. CrFor1 is able to utilize CrPRF-bound actin in order to rapidly assemble actin filaments. On the other hand, CrPRF is poorly utilized by fission yeast formin Cdc12 and inhibits Arp2/3 complex-mediated actin assembly, providing a mechanism by which F-actin can be assembled at the precise time and place by CrPRF and CrFor1. We have previously shown that the profilin defines the rate of formin-mediated actin assembly (Neidt et al., 2009). The presence of tailored formin-profilin pairs (Bestul et al., 2015) suggests that this interaction is crucial for controlling utilization of an actin monomer pool. The *Chlamydomonas* profilin CrPRF appears to be an extreme example of this, as CrPRF-bound actin is inhibited from polymerizing in the absence of CrFor1. Therefore, the *Chlamydomonas* actin cytoskeleton may present a model by which a single actin network can be assembled at the correct time and place. Actin monomers can be tightly sequestered throughout the cell, inhibiting spontaneous actin polymerization as well as utilization by the majority of actin assembly factors. However, at a single site, a precisely tailored actin assembly factor can be activated that is capable of utilizing the previous unattainable actin monomer pool. Though this tightly sequestered monomer pool is useful for an organism that needs few F-actin networks, the majority of cell types have multiple F-actin networks that must be maintained simultaneously within the same cytoplasm. Therefore, in more complex organisms, the presence of multiple profilin isoforms expressed at different levels could regulate network size by controlling actin utilization by formin (Mouneimne et al., 2012).

Additionally, we showed that CrPRF inhibits actin assembly mediated by the fission yeast Arp2/3 complex, further biasing CrFor1-mediated assembly by inhibiting its competitor for actin monomer (Suarez and Kovar, 2016; Suarez et al., 2015). *Chlamydomonas* has an Arp2/3 complex, but any activators are currently unidentified (Kollmar et al., 2012). The Arp2/3 complex may be involved in assembly and maintenance of the F-actin involved in intraflagellar transport, as treatment with Arp2/3 complex inhibitor CK-666 resulted in flagellar shortening (Avasthi et al., 2014). The presence of other potential F-actin networks provides the additional possibility that other F-actin assembly factors are also present in *Chlamydomonas*. The inability of latrunculin and cytochalasin treatments to affect cytokinesis may be a result of their inability to bind *Chlamydomonas* actin(s). Future work will involve determining the nature of the F-actin networks involved in cytokinesis and intraflagellar transport and CrPRF's role in ensuring proper F-actin distribution to each network.

CHAPTER 3: COMPETITION BETWEEN TROPOMYOSIN, FIMBRIN, AND COFILIN DRIVES THEIR SORTING TO DISTINCT ACTIN FILAMENT NETWORKS

PREFACE

The work in the following chapter was performed with assistance from Glen Hocky, Alisha Morganthaler, and Katie Homa. Alisha Morganthaler and Katie Homa performed the experiments and analysis in Figure 3-1. Glen Hocky performed the modeling in Figures 3-4F, 3-5, and 3-6B,C. I completed and analyzed the rest of the experimental data and created all of the figures. Our collaborator Sarah Hitchcock-DeGregori assisted in identifying initial tropomyosin Cdc8 residues to mutate for fluorescent labeling in TIRF and provided valuable feedback in writing the manuscript.

Section 3.1—INTRODUCTION

The self-organization of complex structures from interactions between basic components is a general phenomenon of chemistry and material sciences, as well as more complicated biological systems (Karsenti, 2008). Examples include the generation of self-segregating PAR domains in the developing *C. elegans* embryo (Hoege and Hyman, 2013; Goldstein and Macara, 2007) and the organization of a mitotic spindle around DNA-coated microspheres (Heald et al., 1996). How individual interactions within the cell coalesce to generate complex patterns or structures remains a fundamental biological question. The actin cytoskeleton is an ideal system to study complex cellular self-organization. Multiple functionally diverse F-actin networks, each with a distinct architecture and dynamics, assemble at the correct time and place within a single crowded cytoplasm. Distinct sets of actin binding proteins (ABPs) help to define the characteristics of each F-actin network by performing tasks such as actin filament (F-actin) nucleation, bundling, severing, and capping (Pollard, 2016). Therefore, proper localization of ABPs to the correct network is crucial to generate F-actin networks defined for specific processes. The biochemical activity and cellular functions of many individual ABPs have been well-studied. However, we are only beginning to understand how ABPs function in concert, how they compete with each other for association with individual actin filaments, and how these interactions contribute to the proper sorting of ABPs to diverse F-actin networks on a whole-cell scale (Michelot and Drubin, 2011; Skau and Kovar, 2010; Jegou and Romet-Lemonne, 2016).

Fission yeast has proven an ideal, simplified system in which to study fundamental questions concerning actin network self-organization. Fission yeast has three primary actin cytoskeleton networks, in which all of the actin filaments are assembled by a distinct actin assembly factor: endocytic actin patches (assembled by the Arp2/3 complex), polarity-

establishing actin cables (formin For3), and the cytokinetic contractile ring (formin Cdc12). Moreover, each of these actin networks has a distinct set of ABPs associated with them. We hypothesize that competition between ABPs for association with actin filaments is a driving force behind the sorting of ABPs to the correct F-actin network. Previous work has shown that competition between ABPs tropomyosin, fimbrin, and cofilin result in the exclusion of tropomyosin from actin patches (Skau and Kovar, 2010). In this study, we use a combination of multi-color TIRF microscopy (TIRFM) and mathematical modeling to examine the mechanistic detail behind this series of competitive ABP interactions in fission yeast. By understanding ABP activity at a detailed, mechanistic level, we can gain insight into how the physical properties of an ABP might dictate its interactions with other ABPs and furthermore, its association with a specific actin network. In particular, we focus on tropomyosin Cdc8, a central player in this competitive scheme (Balasubramanian et al., 1992),Skau et al., 2009),Skoumpla et al., 2007)). We show that tropomyosin Cdc8 is a highly cooperative ABP that rapidly coats actin filaments. We suggest that this cooperativity occurs from end-to-end interactions with other tropomyosin molecules and potentially by indirect interactions across the actin filament. We show that tropomyosin Cdc8's cooperativity also results in its efficient displacement specifically from F-actin bundles by fimbrin Fim1. Finally, we show that cofilin Adf1 severing enhances fimbrin-mediated bundling, resulting in the generation of a dense F-actin network that is capable of efficiently displacing tropomyosin Cdc8.

Section 3.2—MATERIALS AND METHODS

Tropomyosin Cdc8 mutagenesis

All plasmid design and construction was performed using SnapGene software (from GSL Biotech; available at snapgene.com). Three amino acids in *S. pombe* tropomyosin Cdc8--Leucine 38, Isoleucine 76, and Aspartate 142--were chosen as potential labeling sites for mutation to cysteine. These three sites for mutagenesis were chosen based on four criteria: (1) localization on the outside of the coiled coil (at *b, c,* or f locations), (2) low sequence conservation amongst fungal tropomyosins (Cranz-Mileva et al., 2013) (3) present outside the first half of each period and therefore unlikely to affect tropomyosin association with actin (Barua et al., 2013), and (4) present away from C-terminal end so as to not affect end-to-end associations between tropomyosin molecules. To create Cdc8 mutants L38C, I76C, and D142C for protein expression, QuikChange Site-Directed Mutagenesis (Agilent Technologies, Inc., Santa Clara, CA) was used to engineer distinct base pair substitutions within acetylation-mimic Cdc8 expression vector pET3a-AS-Cdc8 (Monteiro et al., 1994) and modifications were confirmed by sequencing. In vitro high-speed sedimentation assays and preliminary TIRFM assays at high Cdc8 concentrations determined that the I76C and D142C tropomyosin Cdc8 mutants behaved closest to wild-type Cdc8 in ability to bind to actin filaments (Figure 3-1B,C,D). In addition, replacing the endogenous *cdc8* gene in fission yeast with each of these mutants demonstrated that the I76C and D142C mutants more closely complemented the wild-type than the L38C mutant (Figure 3-1E,F,G). As a result of this in vitro and in vivo analysis, a labeled I76C mutant was used in TIRFM assays for the rest of the study.

All three mutations were introduced within exon 2 of the *cdc8* gene. For insertion of Cdc8 mutants into the *S. pombe* genome, the portion of the Cdc8 mutant corresponding to exon 2

of Cdc8 was amplified from pET3a-AS-Cdc8*mut* protein expression vectors (using primers AAGGCGCGCCAGATCTAAAATTAATGCCGCTCGTGCTGAG and CAAGCTAAACAGATCTCTACAAATCCTCAAGAGCTTGGTGAAC), and the product was cloned into gene targeting vector pFA6-kanMX6 at BglII using In-Fusion HD Cloning (Clontech Laboratories, Mountain View, CA). cdc8*mut*-kan was then amplified (using primers AGGTATGAGATGATAGCTTTTCATTGGAAAATCAAGTTGCTAATATTTGCTTTTTATT TAGAAAATTAATGCCGCTCGTGC and AGAAGATATAAAAAAGGTGGTATGTTTCTTCTATGTTCGTCAAGCTTTTCGCTATGA ATTCGAGCTCGTTTAAAC) and transformed into a *cdc8-27* strain. Colonies were screened for absence of temperature sensitivity and resistance to kanamycin. Candidate colonies were then screened for proper insertion by PCR and sequenced to confirm insertion at the *cdc8* locus**.**

Cofilin Adf1 mutagenesis

Three mutations were made in *S. pombe* cofilin Adf1 for labeling in TIRFM experiments. Endogenous cysteines were converted to alanines (C12S and C62A) and aspartate 34 was converted to cysteine (D34C) as previously described for cofilin from *S. cerevisiae* (Suarez et al., 2011). These mutations were made by QuikChange Site-Directed Mutagenesis in expression vector pMW-SpCofilin (Skau and Kovar, 2010). Modifications were confirmed by sequencing.

Protein purification and labeling

Fimbrin Fim1, cofilin Adf1 (WT and mutant D34C, C12S, C62A)**,** tropomyosin AlaSer-Cdc8 (WT and L38C, I76C and D142C mutants) were expressed in BL21-Codon Plus (DE3)-RP (Agilent Technologies, Santa Clara, CA) and purified as described previously (Skau and Kovar,

2010). Actin was purified from chicken skeletal muscle or rabbit skeletal muscle (Pel-Freez, Rogers, AR) as described previously (Spudich and Watt, 1971). A_{280} of purified proteins was taken using a Nanodrop 2000c Spectrophotometer (Thermo-Scientific, Waltham, MA). Protein concentration was calculated using extinction coefficients Fim1: 55,140 M^{-1} cm^{-1}, Cdc8 (WT and mutants): 2,980 M^{-1} cm^{-1}, Adf1 (and mutant): 13,075 M^{-1} cm^{-1}. Proteins were labeled with CF^{TM} 405M (Sigma-Aldrich, St. Louis, MO), TMR-6-maleimide (Life Technologies, Grand Island, NY) or Cy5-monomaleimide (GE Healthcare, Little Chalfont, UK) dyes as per manufacturer's protocols immediately following purification, and were flash-frozen in liquid nitrogen and kept at -80oC. Tropomyosin Cdc8 was reduced with DTT prior to labeling. For proteins labeled on one cysteine residue (Cdc8 and Adf1 mutants), labeling efficiency was determined by taking the absorbance at the emission max of the dye and calculating the coupling efficiency (Kim, Y. et al 2008). All reported tropomyosin Cdc8 concentrations are concentrations for the two-chain (dimer) molecule.

Glass preparation for TIRFM

Coverslips and microscope slides (#1.5; Fisher Scientific) for TIRFM were prepared by washes in acetone, isopropanol, and water followed by sonication for 30 minutes in isopropanol. Washed glass was then cleaned by plasma cleaning for 3 minutes using a Harrick PDC-32G plasma cleaner (Harrick Plasma, Ithaca, NY). Cleaned coverslips and microscope slides were immediately passivated by incubation in 1 mg/mL PEG-Si (5,000 MW) in 95% ethanol for 18 hours (Winkelman et al., 2014). Coverslips and slides were then rinsed in ethanol and water and flow chambers were created as described previously (Zimmermann et al., 2015).

TIRF microscopy (TIRFM)

Time-lapse TIRFM movies were obtained using a cellTIRF 4Line system (Olympus) fitted to an Olympus IX-71 microscope with through-the-objective TIRF illumination and a iXon EMCCD camera (Andor Technology). Mg-ATP-actin (15% Alexa 488-labeled) was mixed with labeled or unlabeled actin binding proteins and a polymerization mix (10 mM imidazole (pH 7.0), 50 mM KCl, 1 mM MgCl2, 1 mM EGTA, 50 mM DTT, 0.2 mM ATP, 50 μM CaCl2, 15 mM glucose, 20 μg/mL catalase, 100 μg/mL glucose oxidase, and 0.5% (400 centipoise) methylcellulose) to induce F-actin assembly (Winkelman et al., 2014). The mixture was then added to a flow chamber and imaged at 2.5 or 5 s intervals at room temperature.

Fluorescence intensity line scans

Line scans were performed by drawing a line of 3 pixel width along the actin filament and recording the fluorescence intensity along the line using "Plot Profile" in FIJI (Schindelin, J. et al. 2012; Abramoff et al. 2004). The same region of interest was then applied to the actin binding protein channel of interest. If necessary, the region of interest was adjusted to account for filament movement during channel switching.

Tropomyosin Cdc8 coating of actin filaments

The occupancy of Cdc8 on actin filaments was determined from one frame from each TIRFM movie. For each movie, the frame of interest was chosen based on actin filament density (between 7 and 11 μm of filament per square μm). Segmented line ROIs were used to measure total actin filament length (488 channel) and total Cdc8 cable length (647 channel) at that frame. History of the TIRFM movie as well as Cdc8 fluorescence intensity was used to

determine sites at which two Cdc8 cables were present on a single actin filament stretch, and in these cases each Cdc8 stretch was counted as a separate measurement. As there are two Cdc8 cables on a single actin filament, Total Cdc8 Occupancy=Total Cdc8 Length/(Actin Filament Length*2). Single vs. double Cdc8 occupancy was determined by measuring the length of single- vs. double-Cdc8-coated stretches and calculating the total length of single- or double-coated stretches divided by total actin filament length.

Free Cdc8 was calculated by ([Cdc8 added]-250*(Total Cdc8 Occupancy)/4)*0.001 (adapted from Hsiao et al. 2015). 250 (nM) refers to the filamentous actin concentration at the average timepoint that total Cdc8 occupancy was measured. The F-actin concentration determined by spontaneous pyrene assembly assay. 4 refers to the ratio of bound Cdc8 to filamentous actin (1:4) (Kurahashi et al. 2002). The data was fit to a Hill equation $\theta=[L]^n/(K_d+[L]^n$ where θ is the fraction of actin sites that are bound by tropomyosin Cdc8, [*L*] is the free tropomyosin Cdc8 concentration, K_d is the apparent dissociation constant, and n is the Hill coefficient.

Actin binding protein fluorescence intensity on actin filaments

The fluorescence intensity of fimbrin Fim1, tropomyosin Cdc8, or cofilin Adf1 was used to determine amount of ABP associated with actin filaments under different conditions. Analysis was performed on movie frames with a similar filament density for each compared condition. Segmented line ROIs (line width 5 pixels) were used to define each actin filament in the actin channel (488 channel). ROIs were then transferred to the ABP channel of interest and mean fluorescence intensity was measured for each actin filament. For comparing single actin filaments to F-actin bundles, the history of the actin channel and the actin fluorescence intensity

was used to determine single filament versus bundled regions and separate ROI sets were generated and used to measure fluorescence intensity.

Residence time measurements

To calculate residence times for individual cofilin Adf1 or tropomyosin Cdc8 molecules, a high total concentration of Adf1 or Cdc8 was included in the TIRFM assay to ensure total coating of the actin filaments (5 μM Adf1 or 2.5 μM Cdc8). ~20% of Adf1 or Cdc8 was labeled with Cy5 dye in order to visualize the extent of coating of the protein on F-actin. The actin and Cy5-labeled Adf1 or Cdc8 was visualized every 10 seconds. A low (0.5-1%) percentage of Adf1 or Cdc8 was labeled with TMR in order to visualize single molecules, and fast imaging (5 frames/sec) was performed in this channel. To measure residence time of Adf1 in the presence of Cdc8, 2.5 μM of unlabeled Cdc8 was included in the reaction. Single molecules were tracked using MTrackJ (Meijering et al., 2012). Only single molecules that moved were tracked, as static molecules were assumed to be adsorbed to the coverglass. Both censored and uncensored events were obtained and Kaplan-Meier analysis (Kaplan and Meier, 1958) with fit to a single exponential f(x) = x0 * exp^(−x/T1) was used to determine residence time and k_{off}.

Site of initial tropomyosin Cdc8 binding event

Site of first tropomyosin Cdc8 binding event on an actin filament was determined by observing TIRFM movies performed at tropomyosin Cdc8 concentrations at the inflection point of the Hill plot (1.25 μM tropomyosin Cdc8). As our resolution limit is 100 nm, and individual tropomyosin Cdc8 molecules may only briefly associate with the actin filament before

dissociating or forming a 'seed', we cannot determine explicitly the number of tropomyosin Cdc8 molecules in each of these initial association events.

At the point of first observation of tropomyosin Cdc8 binding, the length of the actin filament was measured as well as the distance from the pointed end to the site of tropomyosin Cdc8 binding. The barbed and pointed ends of the actin filament were identified by observing photobleaching of the older, pointed end of the actin filament that occurred over time.

In order to compute the first binding times of a molecule to a substrate, we modeled the reaction as a master equation with two states, bound and unbound, with unbound transforming to bound at rate k_{12} and the reverse process occurring with rate $k_{21} = 0$. Once a binding event has been observed for a filament, that filament cannot go back to having been never bound. Let P (t) be a vector representing the populations of the two states.

$$\frac{d\vec{P}}{dt} = \mathbb{W}\vec{P} \qquad \text{(Eq. 1)}$$

where W is a rate matrix whose columns must sum to zero. Hence:

$$\mathbb{W} = \begin{bmatrix} k_{22} & k_{12} \\ k_{21} & k_{11} \end{bmatrix} = \begin{bmatrix} 0 & k_{12} \\ 0 & -k_{12} \end{bmatrix} \qquad \text{(Eq. 2)}$$

In the case of binding to an extending actin substrate, if we assume an average constant growth rate v_{grow}, the length of the substrate $l(t) = v_{grow}t$. With the assumption of uniform binding affinity, the rate of going from unbound to singly bound k_{12} depends on time, and in particular can be written $k_{on}l(t) = k_{on}v_{grow}t$ and we emphasize that k_{on} is the rate per unit length of observing Cdc8 stably residing on a filament, which arises from the complex cooperative binding process discussed above and below.

Equation 1 is solved formally by the equation

$$\vec{P}(t) = e^{\int_0^t \mathbb{W}(t')dt'}\vec{P}(0) \qquad \text{(Eq. 3)}$$

in which case:

$$\vec{P}(t) = \exp\left(\begin{bmatrix} 0 & \frac{k_{on}v_{grow}t^2}{2} \\ 0 & \frac{-k_{on}v_{grow}t^2}{2} \end{bmatrix}\right)\vec{P}(0) = \begin{bmatrix} 1 & 1 - e^{-\frac{k_{on}v_{grow}t^2}{2}} \\ 0 & e^{-\frac{k_{on}v_{grow}t^2}{2}} \end{bmatrix}\vec{P}(0) \qquad \text{(Eq. 4)}$$

Hence, since $\vec{P}(0) = \begin{pmatrix} P_2(0) \\ P_1(0) \end{pmatrix} = \begin{pmatrix} 0 \\ 1 \end{pmatrix}$, $P_1(t) = e^{-\frac{k_{on}v_{grow}t^2}{2}}$, the probability of a first binding event happening at time t = τ is the probability of still being unbound at time τ, $P_1(\tau)$, times the rate of binding at time τ, $k_{12}(\tau)$, hence:

$$P(\tau) = k_{12}(\tau)P_1(\tau) = k_{on}v_{grow}\tau\, e^{-\frac{k_{on}v_{grow}\tau^2}{2}} \qquad \text{(Eq. 5)}$$

Given this equation for the binding time, we can also determine the probability of binding to a particular site on the actin filament which has been in the filament for an amount of time τ_{age}, $P(\tau_{age})$.

Under our assumptions, at time t, the actin filament has length $l(t) = v_{grow}t$ and the probability of tropomyosin Cdc8 binding anywhere along the filament is uniform. The probability of binding at a distance x_0 from the end of the actin filament of length l is

$$P_{bind}(x_0|l) = \begin{cases} 1/l & l \geq x_0 \\ 0 & l < x_0 \end{cases} \qquad \text{(Eq. 6)}$$

Consequently, given our assumption of a constant average growth rate v_{grow}, the probability of

binding to a spot of a given age τ_{age} is

$$P_{bind}(\tau_{age}|l = v_{grow}t) = \begin{cases} \frac{1}{v_{grow}t} & \tau_{age} \leq t \\ 0 & \tau_{age} > t \end{cases} \quad \text{(Eq. 7)}$$

In order to determine the probability that a molecule binds to a part of the substrate of age τ_{age}, we must integrate Eq. 7 against the probability that the binding event happened at time t, as given by Eq. 5. Therefore,

$$P_{bind}(\tau_{age}) = \int_0^\infty dt\, P_{bind}(\tau_{age}|l = v_{grow}t)P(t) \quad \text{(Eq. 8)}$$

$$= \int_{\tau_{age}}^\infty dt\, k_{on} e^{-\frac{k_{on}v_{grow}t^2}{2}} \quad \text{(Eq. 9)}$$

$$= \sqrt{\frac{k_{on}v_{grow}}{2}} \int_{\tau_{age}\sqrt{\frac{k_{on}v_{grow}}{2}}}^\infty dx\, e^{-x^2} \quad \text{(Eq. 10)}$$

$$= \sqrt{\frac{\pi k_{on}v_{grow}}{2}}\, \text{erfc}\left(\tau_{age}\sqrt{\frac{k_{on}v_{grow}}{2}}\right) \quad \text{(Eq. 11)}$$

where erfc(x) is the so-called complementary error function and can be evaluated numerically. Using these equations, we can choose k_{on} to fit the data in Figure 3-4A and we find that a value of 4×10^{-6} sec^{-1} nm^{-1} gives good agreement with the data.

Numerical simulation

The validity of the aforementioned expressions can be tested by comparison with a simple simulation. The simulation methodology moreover provides a way to mimic the noise level that would arise due to sample size limitations. A Monte Carlo scheme can be performed

by taking discrete time steps of size dt and at each time assuming the probability of binding in that time dt is

$$P_{bind}(dt) = 1 - e^{-k_{on} v_{grow} t \, dt} \quad \text{(Eq. 12)}$$

Tropomyosin Cdc8 Spreading Rates

Elongation rates of individual tropomyosin Cdc8 cables were determined by creating a region of interest (ROI) of an individual actin filament in the actin 488 channel over many time points. The actin ROIs were then applied to the tropomyosin Cdc8 (647) channel and adjusted slightly if necessary to account for movement of the actin filament during channel switching. A kymograph of the Cdc8 647 channel was created from the ROIs using an adapted version of Kymograph - Time Space Plot ImageJ plugin (http://www.embl.de/eamnet/html/kymograph.html). Spreading rates were determined from kymographs by identifying examples of constant growth over at least 15 seconds (3 frames). The distance of growth over time was calculated to determine a rate of spreading.

Site of second tropomyosin Cdc8 binding event

In order to determine whether the two tropomyosin Cdc8 cables on each side of the actin filament are influenced by each other, we first quantified whether a second Cdc8 binding event on an actin filament was more or less likely to bind at a site that is already bound by tropomyosin Cdc8 on one side. First tropomyosin Cdc8 binding events were determined as stated above, and those actin filaments were observed until a second tropomyosin Cdc8 binding event occurred, and whether or not the binding occurred at a site already occupied by Cdc8 or not was determined. At that frame, the length of the actin filament as well as the total Cdc8 cable length was calculated to determine current percent occupancy of Cdc8 on the actin filament. These

'current occupancies' were then binned into 0-12.5%, 12.5-25% or 25-50% occupancy. Initial occupancy cannot exceed 50% as one Cdc8 binding event could at most cover one side of the actin filament, or half of the available binding sites.

Second binding probability analysis

In order to determine whether the proportion of observed second binding events that bind opposite a tropomyosin-bound segment (Figure 3-4C) would be expected in the absence of indirect cooperativity, or whether they are more likely given inclusion of some positive or negative indirect cooperativity factor, we performed a bootstrapping-type analysis on the n=37 observed events. For this analysis, we asked: given the experimental data, what is the probability that the second binding events are binding randomly vs. binding in a biased fashion towards or against a tropomyosin-coated segment?

For an actin filament of length L_a and a first tropomyosin cable of length L_1 starting at position x_1 (in the range 0 to L_a-L_1) along the actin filament, we need to determine the probability of a second tropomyosin cable of length L_2 binding across from the first tropomyosin cable. We can then compare the probability generated from different models with our experimental results. To account for experimental resolution, we divide the actin filament into a grid of 100 nm segments. In order to compute the probability of the second binding event overlapping with the first tropomyosin cable, we count the number of places the second cable can bind that overlaps with the first cable of length L1, and divide by the total number of potential places a second cable of length L2 could bind. As a helical actin filament has two grooves, there are twice as many potential binding sites on F-actin unoccupied by tropomyosin as on those with a single tropomyosin cable. However, if there is any overlap of second

tropomyosin cable binding with the first tropomyosin cable, we presume there was only one potential binding face. For random binding, binding to each actin site is given an equivalent likelihood. To account for potential indirect cooperativity, we perform a weighted sum, where the second tropomyosin cable binding is proportionally more or less likely by a factor of *c* at all sites overlapping with the first cable of tropomyosin. The probability of an overlapping binding is hence given by the following 3 expressions:

$$N_1 = 2\sum_{x=0}^{L_a-L_2}\big((x+L_2)<x_1\big)\big|\big(x>(x_1+L_2)\big)$$

$$N_2 = \sum_{x=0}^{L_a-L_2}\begin{cases}(x_1-x)+c\big(L_2-(x_1-x)\big) & x<x_1\ \&\ (x+L_2)>x_1\\ \big(L_2-\big((x_1+L_1)-x\big)\big)+c((x_1+L_1)-x) & x\geq x_1\&(x<x_1+L_2)\end{cases}$$

(with the terms in outer parentheses being restricted to minimum value 0 and maximum L_2)

$$p_2 = \frac{N_2}{N_1+N_2}$$

We can then compare the expected outcomes for random (c=1X) vs. positive or negative indirect cooperativity values (c=2X or c=0.5 respectively) (Figure 3-4C). Finally, we performed a bootstrapping analysis. For each experimentally observed set of events, where a given (L_a, L_1, and x_1) was measured, we compute the probability that a cable of length L_2 binding would overlap with the first tropomyosin Cdc8 cable (p_2). We then re-perform the 37 experiments 5000 times with a chosen indirect cooperativity factor *c*, choosing randomly with probability p_2 whether or not overlapping binding occurred. Binning these events similar to the experimental data, we can compute the values shown in Figure 3-4C.

Lattice model of Tropomyosin Cdc8 loading and spreading

In order to probe the microscopic origins of the high cooperativity observed for tropomyosin Cdc8 (Figure 3-2B), we wished to distinguish between two potential cooperative mechanisms: (1) end-to-end cooperativity and (2) indirect cooperativity (Figure 3-2C). We distinguished between these two models by modeling the binding kinetics of tropomyosin Cdc8 to a growing actin filament using a lattice model (Figure 3-6Bi, 3-6Ci). As two distinct tropomyosin Cdc8 cables can bind to an actin filament (one on the surface of each groove of the helical actin filament), we represent the actin filament as a lattice with two rows representing the two actin surfaces potentially bound by tropomyosin Cdc8. Each tropomyosin Cdc8 molecule interacts across four actin monomers, meaning that a bound tropomyosin Cdc8 extends over the length of 8 actin monomers total. Therefore, as each tropomyosin Cdc8 cable is represented separately, we ascribe to each lattice site a length l of approximately 21.6 nm (assuming an approximate actin spacing of 2.7 nm). The dynamics of tropomyosin Cdc8 molecules associating with this lattice were then simulated using a kinetic Monte Carlo procedure (Newman and Barkema, 1999). First, consider the case for a non-elongating actin filament, represented by a fixed lattice of length N. Each potential tropomyosin Cdc8 binding site can either be occupied (1) or unoccupied (0) by tropomyosin. We describe binding site site i in row j as x_{ij}. For every unoccupied site, there is a base on-rate k_{on} (0->1) and for every occupied site there is a base off-rate k_{off} (1->0). To include the effect of end-to-end cooperativity, the on-rate for unoccupied site ij is multiplied by a factor of w and the off-rate for occupied site ij is divided by a factor of w for each occupied immediate neighbor in the same row, (See Figure 3-6Bi or table below for diagram). Using these parameters, we ran a model describing tropomyosin Cdc8 binding with end-to-end cooperativity as the sole form of cooperativity (Figure 3-6B). In order to additionally

probe the potential role of indirect cooperativity, we adjusted the same model to include additional parameters for indirect cooperativity. In this model, on-rates are multiplied by a factor *c* and off-rates are divided by a factor *c* for each occupied site in the opposite row (row 1-j) (Figure 3-6Ci). All possible on rates are shown below:

Situation	**Rate 0->1 for X**	**Rate of 1->0 for X**
0X0 ?0?	k_{on}	k_{off}
1X0 ?0?	$w*k_{on}$	$(w)^{-1}*k_{off}$
0X1 ?0?	$w*k_{on}$	$(w)^{-1}*k_{off}$
1X1 ?0?	w^2*k_{on}	$(w^2)^{-1}*k_{off}$
0X0 ?1?	$c*k_{on}$	$(c)^{-1}*k_{off}$
1X0 ?1?	$c*w*k_{on}$	$(cw)^{-1}*k_{off}$
0X1 ?1?	$c*w*k_{on}$	$(cw)^{-1}*k_{off}$
1X1 ?1?	$c*w^2*k_{on}$	$(cw^2)^{-1}\ k_{off}$

Table 1: Rates of tropomyosin Cdc8 association and dissociation under specific lattice model parameters.
Column 1 (Situation) describes the current tropomyosin Cdc8 occupancy. Each row represents one face of the actin filament with three potential Cdc8 binding sites. X represents the association or dissociation site of interest, 0 represents a site with no Cdc8 molecule bound, 1 represents a site with Cdc8 bound, and ? represents a site with unknown Cdc8 occupancy. Column 2 (Rate 0→1 for X) describes the parameters applicable for a Cdc8 association event at site X. Column 2 (Rate 1→0 for X) describes the parameters applicable for a Cdc8 dissociation event at site X. Further description can be found in text.

For a lattice size 2xN sites, there are precisely 2xN possible events with rates selected from the table above. The dynamics up to a chosen time *max_time* or until the lattice is completely filled are then solved using kinetic Monte Carlo (Newman and Barkema, 1999). In order to factor in an elongating actin filament, an additional type of event representing actin filament growth is

included, with a rate equal to the input growth rate of actin, v_{grow}. In this case, whenever that event is selected by the algorithm, time is advanced and N is set equal to

N = floor(new_time*site_extension_rate)

To make kymographs and to compute the occupancy of tropomyosin Cdc8 as accurately as possible, we processed the output raw simulation data in 3 ways:

1) In TIRFM experiments, ~20% of tropomyosin Cdc8 molecules are labeled. Hence, in our kymographs, we replace 80% of the occupied sites with 0s.
2) The experiments are limited by optical resolution. To approximate this, each remaining occupied site is "broadened" by filling in adjacent sites in the same row within a radius of 100 nm (+/- 4 sites), the experimental resolution.
3) The two rows are summed together to give fluorescence values of 0 1 or 2 at each site along the actin filament.

The coverage data in Figure 3-6Biii and 3-6Ciii is computed by averaging this fluorescence level over the filament at the time when the filament has length 6 μm over 24 such simulations. 6 μm was the average length of the actin filaments at the frame used for quantification of tropomyosin Cdc8 coverage in TIRFM experiments. In order to choose the values of w, c and k_{off}, we first fixed c, and tried combinations of k_{off} and w which gave (a) the best match to the data shown in Figure 3-2B as k_{on} is scanned, and (b) gave kymographs whose first time for observed binding is similar to what is observed experimentally.

In Figure 3-7, k_{off} is measured from single molecule tropomyosin Cdc8 events on an actin filament fully coated by tropomyosin Cdc8. In our model, the microscopic k_{off} corresponding to this situation is $k_{off}^{measured} = k_{off}^{model}/w^2/c$. Using k_{off}^{model} values far from those measured in Figure 3-7 did not give good agreements to the data. Constraining k_{off} to precisely the value measured

results in a single value of w which best matched the experimental data (Figure 3-2B, parameters k_{off}=116.8 sec^{-1}, w=40), with the results from these simulations shown in Figure 3-6B. However, these simulations do not match the experimental single/double coverage data (Figure 3-6A, bottom). Relaxing the restraint on k_{off} does not alleviate this problem. For a fixed value of c>1, there is a single w which best matches the experimental data. For c=1.25, while these simulations match the experimental data (Figure 3-2B), they over-stabilize double cable association. Hence, we slightly relax the restriction on k_{off} and the simulations with parameters (k_{off}=300 sec^{-1},w=125,c=1.25) match the experimental data (Figure 3-6A) very closely as well as qualitatively reproducing many of the aspects we have observed for tropomyosin loading.

We note that a limitation of this model is that it does not allow for any "frame shifts" in the tropomyosin Cdc8 binding. Hence there cannot be defects in tropomyosin Cdc8 occupancy on a cable that is smaller than 4 actin monomers in these representations, and we do not allow the tropomyosin to "slide" except by binding and unbinding. The first part of this could be addressed by using a lattice of 4x higher resolution. However, since we do not know how to account for the end-to-end cooperativity in this case, or how to represent the sliding dynamics, we have chosen the simpler representation for the purposes of this study.

The rates of a lattice with these w and c parameters fixed can be written in terms of energies for a two-row Ising model in a field. Since this system is still 1 dimensional in nature, for the infinite-length case any equilibrium properties of the system can be derived using a transfer matrix approach (Tsuchiya and Szabo, 1982) in the same way as for a standard Ising model (except that the transfer matrix is 4x4). However, given that the growth of the actin filament as well as the way that the data is analyzed play significant roles in the coverage fractions

computed, we have found the simulations useful since they are able to replicate the full dynamics as shown in Figure 3-6Bii and 3-6Cii.

Bundling quantification

The percentage of actin filaments bundled was quantified at similar actin filament densities (between 800 and 1100 μm) for each experiment. The total actin filament length in the chamber was measured manually by creating ROIs for every actin filament. ROIs for every segment of actin filament present in a bundle were then created, and the ratio of actin filament present in a bundle vs. total actin filament length was quantified.

Quantification of fold-change in fluorescence intensity

Fold-change in fluorescence intensity over time was taken by taking a total fluorescence measurement of the entire TIRFM field for each frame of the movie.

Severing rate quantification

Severing was quantified by first identifying a region of the movie before extensive bundling and/or filament growth occurred that may have affected quantification. ROIs were created for all single filaments and two-filament bundles at that time point and total filament length was measured. Severing events that occurred within those filaments prior to the selected frame were quantified, and severing events per micron per second was calculated. We were only able to directly observe severing of single filaments and two-filament bundles, and were unable to determine severing rate within the dense bundles generated by a combination of fimbrin Fim1 and cofilin Adf1.

Pyrene assembly assays

Spontaneous assembly assays were carried out in a 96 well plate with 9μM of 10% pyrene-labeled actin monomer in the upper well. WT Cofilin or TMR labeled Cofilins were mixed with 10X KMEI (500 mM KCl, 10 mM $MgCl_2$, 10 mM ethylene glycol tetraacetic acid [EGTA], and 100 mM imidazole, pH 7.0) and placed in the lower row of the plate. Pyrene fluorescence readout over time was detected using a Safire2 (Tecan, Durham, NC) fluorescence plate reader.

DAPI/Calcofluor

Fission yeast cells were grown in YE5S media at 25ºC for 24-36 hours. Cells were fixed in 100% cold methanol and nuclei and septa were visualized using DAPI (nuclei) and calcofluor (septa). For staining, cells were incubated in 300 μL of 50 mM sodium citrate and 4 μL Calcofluor White Stain (Fluka Analytical, Sigma-Aldrich, St. Louis, MO) at 37ºC for 5 minutes. Cells were then washed with 1 mL 50 mM sodium citrate, and resuspended in 15 μL sodium citrate and 4 μL DAPI stock (1 mg/mL in H20, Life Technologies, Carlsbad, CA). Stained cells were kept on ice until imaging. Cells were imaged using differential interference contrast (DIC) and epifluorescence with an Orca-ER camera (Hamamatsu, Bridgewater, NJ) fitted to an IX-81 microscope (Olympus, Tokyo, Japan), with a 60X 1.4 N.A. Plan Apo objective.

High-Speed Sedimentation assays

Sedimentation assays were performed as previously described (Skau and Kovar, 2010). 15 μM Mg-ATP actin monomers were spontaneously assembled in 10 mM imidazole, pH 7.0, 50

mM KCl, 5 mM $MgCl_2$, 1 mM EGTA, 0.5 mM DTT, 0.2 mM ATP and 90 μM $CaCl_2$ for 1 hour to generate filaments. F-actin was then incubated with tropomyosin mutants (2 μM) for 20 minutes at 25ºC and spun at 100,000g at 25ºC. Supernatant and pellets were separated by 15% SDS-PAGE gel electrophoresis and stained with Coomassie Blue for 30 minutes, destained for 16 hours and analyzed by densitometry with ImageJ.

Section 3.3—RESULTS

Tropomyosin Cdc8 is cooperative on single actin filaments

Tropomyosin is an actin binding protein that is a central player in actin binding protein sorting and actin network organization in many organisms (Gunning et al. 2015). Tropomyosin is a two-chained, parallel coiled-coil composed of two polypeptide chains with the characteristic heptad-repeat of hydrophobic residues, identical in the case of Cdc8 (Figure 3-1A). In many organisms, including fission yeast, the tropomyosin coiled coil associates end-to-end, to form continuous tropomyosin cables that extend along both sides of the helical actin filament (Hanson and Lowy, 1964; Spudich et al., 1972). While in vertebrates one tropomyosin molecule spans 6 or 7 actins in the filament, depending on the isoform, yeast tropomyosins are shorter: both tropomyosins in *S. cerevisiae* span 4 or 5 actins while *S. pombe* contains a single tropomyosin, Cdc8, that spans 4 actin monomers (Kurahashi et al., 2002). Although tropomyosin Cdc8 from *S. pombe* has been purified and characterized in steady state bulk assays (Cranz-Mileva et al., 2015; Skau et al., 2009; Skoumpla et al., 2007), our understanding of the mechanism of tropomyosin loading and unloading on the actin filament, as well as how it interacts with other ABPs at the single filament level is unclear. Multi-color TIRFM has been successfully used in the past as a sensitive probe to study the detailed interactions between multiple ABPs and actin (Winkelman et al., 2014; 2016; Jansen et al., 2015; Bombardier et al., 2015). In order to study the interactions

of tropomyosin with actin filaments, we first created an *S. pombe* tropomyosin Cdc8 that could be labeled for visualization in TIRFM (Figure 3-1, Methods).

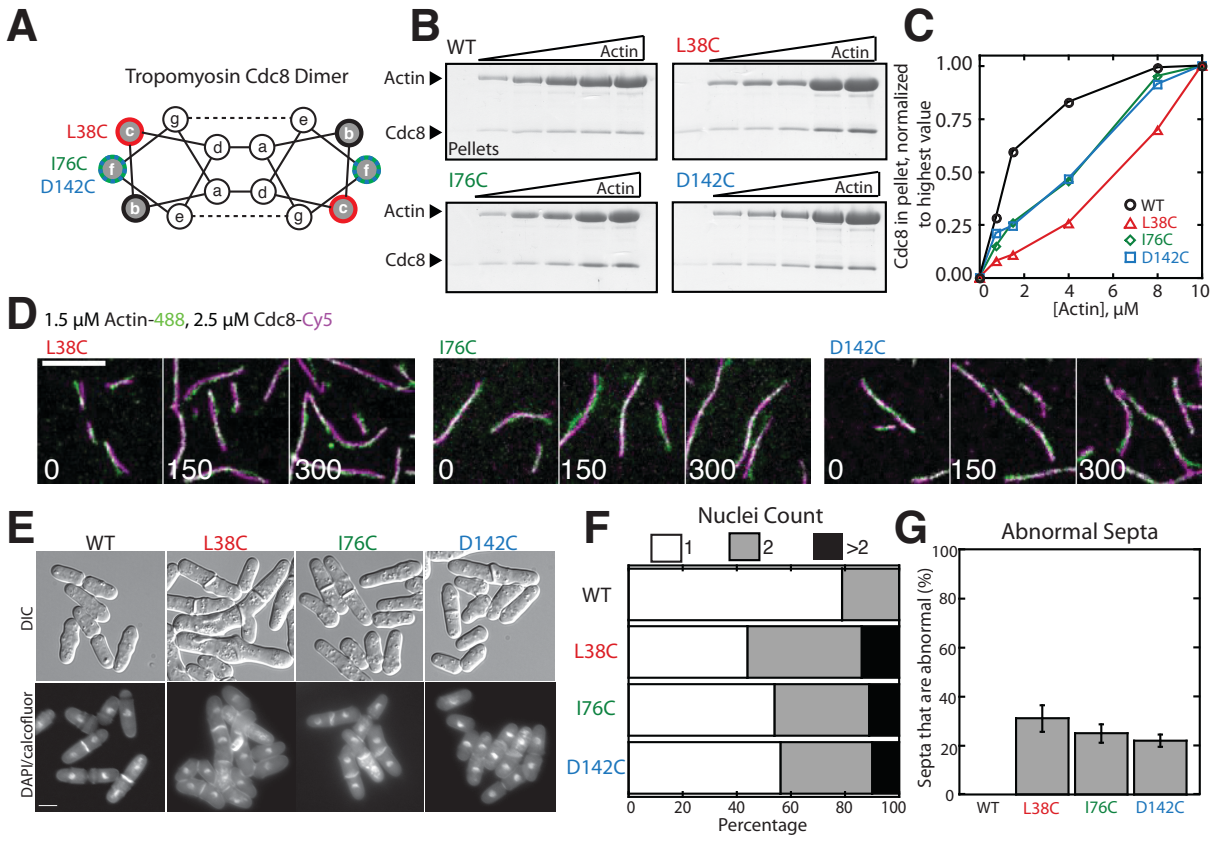

Figure 3-1: Characterization of Tropomyosin Cdc8 mutants L38C, I76C, and D142C. **(A)** Characteristic tropomyosin coiled-coil heptad repeat organization. Residues with low sequence conservation localized at b-, c-, or f-sites on the outside of the coiled-coil were chosen for mutation to cysteine. **(B-C)** High-speed sedimentation assay of 1 μM of wild-type (WT) or mutant (L38C, I76C, or D142C) tropomyosin Cdc8 binding to increasing (0-10 μM) concentrations of actin **(B)** and quantification of tropomyosin Cdc8 in pellet **(C)**. **(D)** Two-color TIRFM of 1.5 μM Mg-ATP actin (15% Alexa 488-labeled) and 2.5 μM tropomyosin Cdc8 mutants L38C (left), I76C (middle), or D142C (right) (Cy5-labeled). **(E)** Morphology of cells with tropomyosin Cdc8 mutants replacing endogenous tropomyosin *cdc8* gene. **(F-G)** Quantification of number of nuclei **(F)** and abnormal septa **(G)** in cells expressing tropomyosin *cdc8* mutants. Scale bar, 5 μm.

We examined in detail the loading characteristics of tropomyosin Cdc8 on actin filaments at a range of concentrations. At concentrations below 1 μM Cdc8, no labeled Cdc8 was observed to bind to actin filaments. However, at 1 μM Cdc8, short stretches of Cdc8 binding were

observed on actin filaments. These stretches were dynamic and varied in size over time, but could be as small as the observable limit of 100 nm and generally remained within ~0.5-2 μm or ~2% of total actin filament coverage for the duration of the movie (Figure 3-2A,B). At 1.25 μM Cdc8, spreading of Cdc8 cables from initial 'seeds' was observed, with ~40% of actin filament sites coated with Cdc8 (Figure 3-2A,B). Finally, at concentrations of 2 μM Cdc8 or higher, ~98% of actin filament sites were coated with Cdc8 (Figure 3-2A,B). This rapid shift in actin filament occupancy over a small Cdc8 concentration range indicates a high degree of cooperativity. Fitting the data to a Hill function gave a Hill coefficient of 14.6 (Figure 3-2B). This Hill coefficient is higher than that of other cooperative ABPs such as cofilins (Hill=~4-10) (la Cruz, 2009), human α-actinin 4 (Hill=2.5), human fascin (Hill=2.3) (Winkelman et al., 2016), and other tropomyosins (Hill=1.6-5.0) (Skórzewski et al., 2009; Hsiao et al., 2015). We hypothesized that this high degree of cooperativity is a result of the previously demonstrated end-to-end binding between tropomyosin molecules ('end-to-end cooperativity') (Figure 3-2C). However, the cooperativity of other tropomyosins on F-actin has been found to not directly correlate with their end-to-end binding ability, suggesting that other interactions may additionally influence tropomyosin's cooperativity on F-actin (Tobacman, 2008). We wondered whether indirect interactions between tropomyosin Cdc8 cables on opposing sides of the actin filament or via long-range interactions along the length of the actin lattice may also contribute to tropomyosin Cdc8's observed cooperativity ('indirect cooperativity') (Figure 3-2C). We focused on investigating a potential role for indirect cooperativity in tropomyosin Cdc8 loading onto an actin filament by observing (Figure 3-3) and quantifying (Figure 3-4) tropomyosin Cdc8 loading events in detail under conditions near the inflection point of the Hill plot (1.25 μM Cdc8).

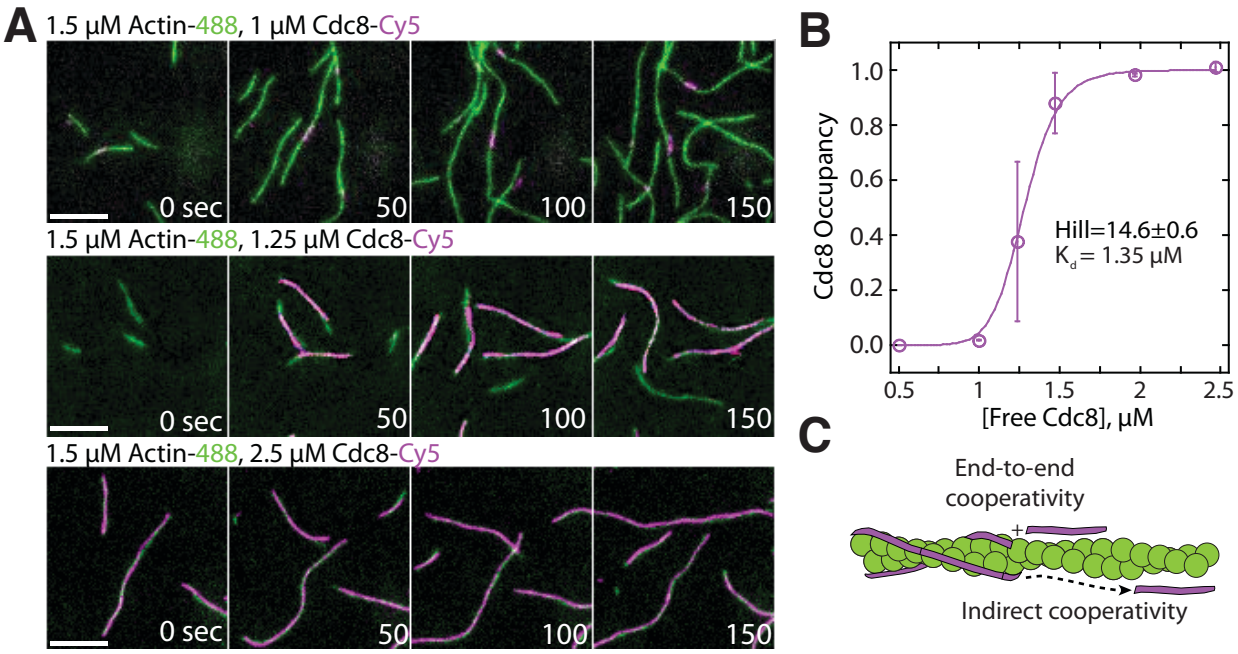

Figure 3-2: Tropomyosin Cdc8 loads cooperatively onto actin filaments.
(A) Two-color TIRFM of 1.5 μM Mg-ATP actin (15% Alexa 488 labeled) with a range of concentrations of tropomyosin Cdc8 (Cy5-labeled). Scale bar, 5 μm. **(B)** Plot of the fraction of actin filament bound by tropomyosin Cdc8 ('Cdc8 occupancy') over free tropomyosin Cdc8 concentration. Data were fit to a Hill function, revealing a Hill coefficient >1 that indicates cooperativity. Error bars represent SE; n=2 reactions. **(C)** Schematic of tropomyosin Cdc8 loading onto an actin filament. Observed cooperativity of tropomyosin Cdc8 could be the result of end-to-end binding of tropomyosin molecules ('End-to-end cooperativity') and/or indirect interactions between tropomyosin molecules via changes in the actin filament ('Indirect cooperativity').

Two Tropomyosin Cdc8 cables load onto a single actin filament

By examining both timelapse (Figure 3-3A) and kymograph (Figure 3-3B) data of an elongating actin filament and the tropomyosin Cdc8 molecules associated with it, we can observe the distinct loading and spreading behavior of tropomyosin Cdc8. Tropomyosin Cdc8 loading is

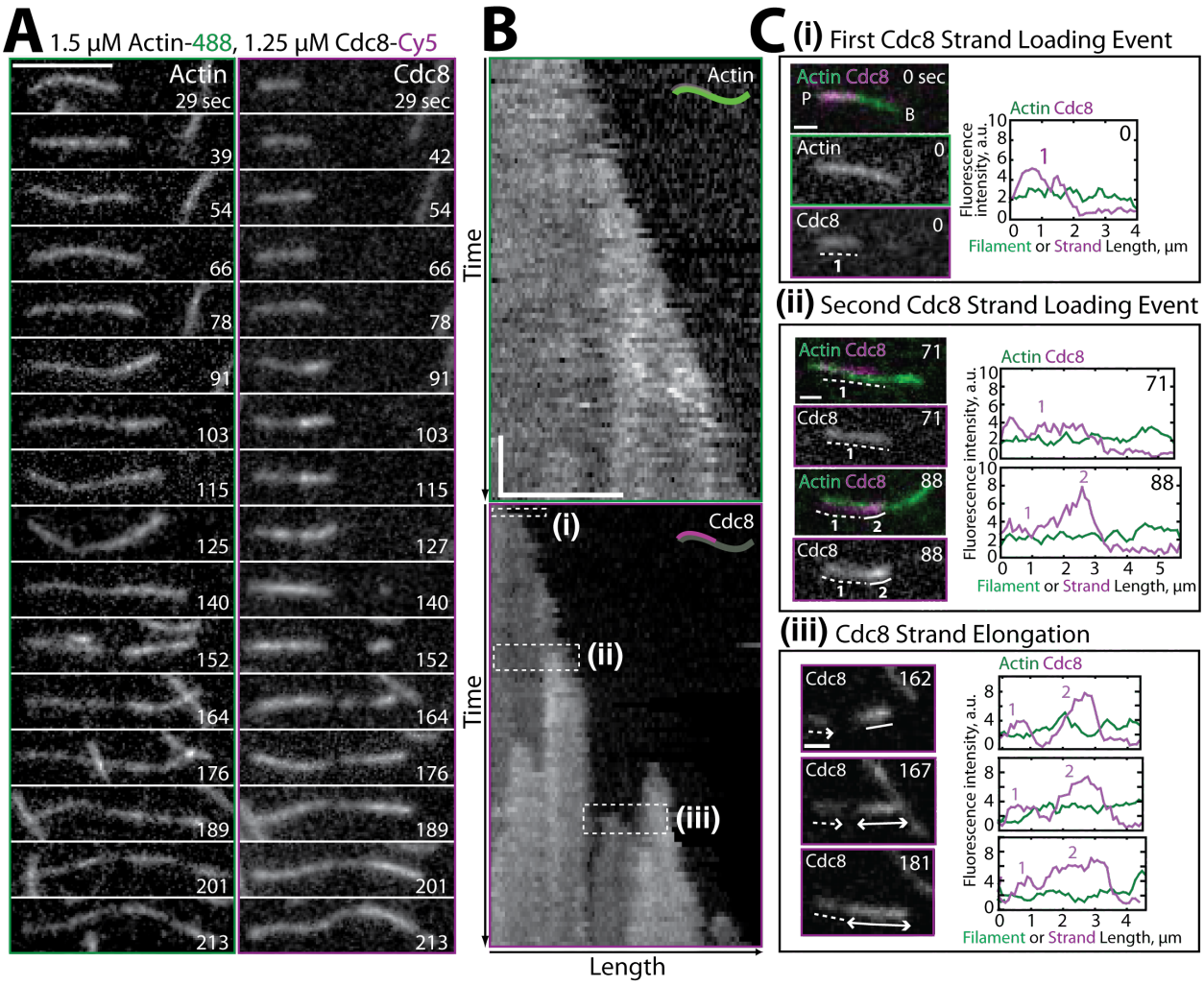

Figure 3-3: Two distinct Tropomyosin Cdc8 cables load cooperatively onto a single actin filament.

(A-B) Two-color TIRFM of 1.5 μM Mg-ATP actin (15% Alexa 488) with 1.25 μM tropomyosin Cdc8 (Cy5-labeled). **(A)** Timelapse of an elongating actin filament **(left)** and tropomyosin Cdc8 loading and spreading events **(right)**. Scale bar, 5 μm. **(B)** Kymograph of the elongating actin filament and associated tropomyosin Cdc8 events**.** The first tropomyosin Cdc8 cable loading event **(i)**, second tropomyosin Cdc8 cable loading event **(ii)**, and tropomyosin Cdc8 cable spreading event **(iii)** are boxed. Scale bar, 5 μm. Time bar, 30 sec. **(C)** Fluorescent images and corresponding fluorescence intensity line scans of actin (green) and tropomyosin Cdc8 (magenta) from the boxed regions in **(B)**. Scale bar, 1 μm. **(Ci)** A single tropomyosin Cdc8 cable on an actin filament segment. The dotted line (1) marks one tropomyosin Cdc8 cable on the actin filament segment. **(Cii)** A second tropomyosin Cdc8 cable loading event on an actin filament. Dotted (1) and solid (2) lines mark the first and second tropomyosin cables on the actin filament segment. **(Ciii)** A spreading tropomyosin Cdc8 cable. Arrows denote spreading direction of first (dotted line, 1) and second (solid line (2) tropomyosin Cdc8 cables. Scale bars, 1 μm.

complex and characterized by several initial 'seed' events, followed by tropomyosin Cdc8 cable spreading towards both the barbed and pointed end of the actin filament, interrupted by frequent stops and starts (Figure 3-3A,B). Sites of initial tropomyosin Cdc8 seed association can be observed by an increase in tropomyosin Cdc8 fluorescence at the site of binding (Figure 3-3Ci). Unlike *Drosophila* tropomyosin Tm1A (Hsiao et al., 2015), first tropomyosin Cdc8 binding events have no initial preference for the barbed or pointed end of the actin filament, with binding patterns consistent with random binding (Figure 3-4A, Figure 3-5). Once an initial tropomyosin Cdc8 site was initiated, tropomyosin Cdc8 cable spreading toward the barbed and pointed end occurred at similar average rates (3.2 and 2.4 Cdc8 molecules sec^{-1}, μM^{-1}, respectively). However, there was considerable variation in spreading rates in both directions, between 1-6 Cdc8 molecules sec^{-1}, μM^{-1} (Figure 3-4B). As the majority of tropomyosin Cdc8 molecules associated directly adjacent to a previously-bound tropomyosin Cdc8, these findings suggest that end-to-end binding is one key feature contributing to the high cooperativity of tropomyosin.

Ultrastructural studies of mammalian and *S. pombe* tropomyosins have shown that a single actin filament can accommodate two tropomyosin cables, one on each side of the helical actin filament (Hanson and Lowy, 1964; Skoumpla et al., 2007). In our TIRFM assays, we are able to observe the loading of these two distinct Cdc8 cables on the same actin filament (Figure 3-3Cii). Secondary loading events are identified by a doubling in fluorescence at the site of a previous tropomyosin Cdc8 loading event (Figure 3-3C, right panels). Our ability to observe two distinct tropomyosin cables on a single stretch of F-actin allows us to assess the involvement of actin-mediated interactions in tropomyosin Cdc8 cooperativity. The single pixel resolution in our TIRFM experiments is 100 nm, or a continuous stretch of ~5 tropomyosin Cdc8 molecules

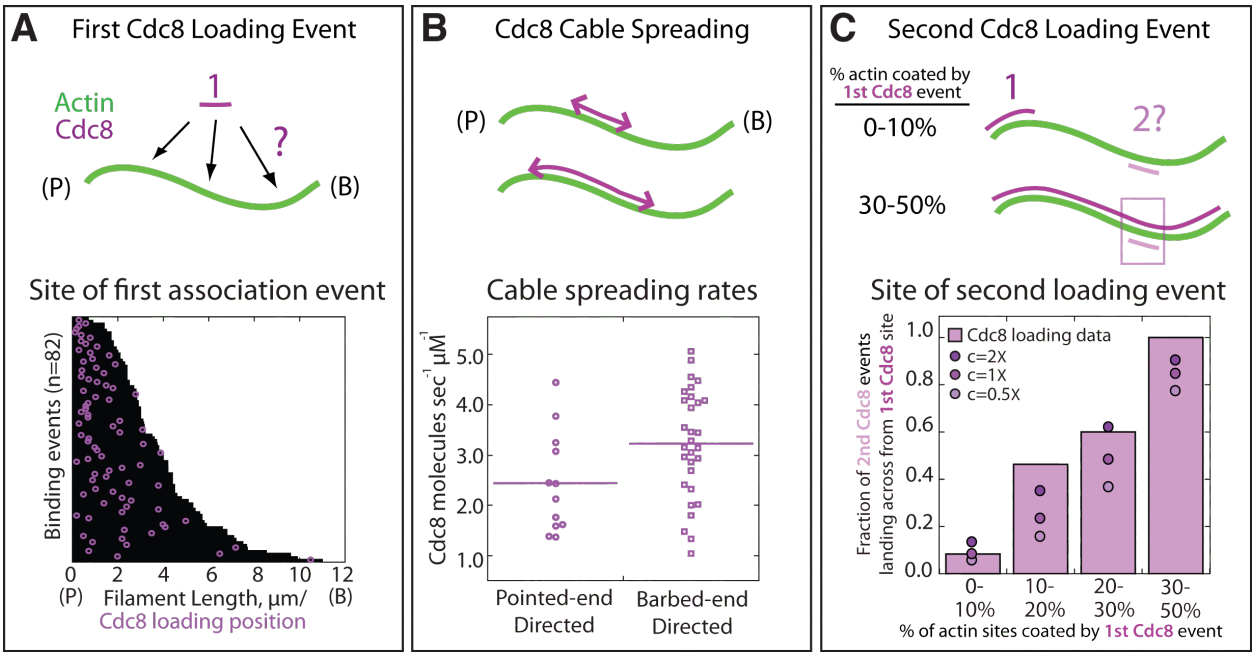

Figure 3-4: Quantification of loading and spreading of first and second Tropomyosin Cdc8 cables.

Two-color TIRFM of 1.5 µM Mg-ATP actin (15% Alexa 488) with 1.25 µM tropomyosin Cdc8 (Cy5-labeled). **(A) (Top)** Depiction of potential sites for the first tropomyosin Cdc8 loading event. The actin filament and tropomyosin Cdc8 molecule are depicted by green and purple lines, respectively. **(Bottom)** Plot of the first tropomyosin Cdc8 association event (purple circles) on actin filaments (black lines), with F-actin pointed ends (P) aligned at the left. n=82 events. **(B) (Top)** Depiction of tropomyosin Cdc8 cable spreading toward the barbed (B) and pointed (P) ends of actin filaments. **(Bottom)** Spreading rates of tropomyosin Cdc8 cables toward the barbed or pointed end. n>12 events. **(C) (Top)** Depiction of site of second tropomyosin Cdc8 loading event, which can occur at a naked actin site (top cartoon) or across from the first-bound tropomyosin Cdc8 cable (bottom cartoon). The larger percentage of the F-actin surface coated by the initial tropomyosin Cdc8 cable (1) increases the probability that the second tropomyosin Cdc8 cable (2) will associate across from a site already bound by Cdc8. **(Bottom)** Plot of the fraction of second tropomyosin Cdc8 events that associate with a F-actin site already coated by tropomyosin Cdc8, binned by percentage of F-actin already coated by tropomyosin Cdc8 (light purple bars). n=38 events. Modeling of predicted degree of association given no indirect cooperativity (c=1X, purple circles), positive indirect cooperativity (c=2X, dark purple circles), and negative indirect cooperativity (c=0.5X, light purple circles).

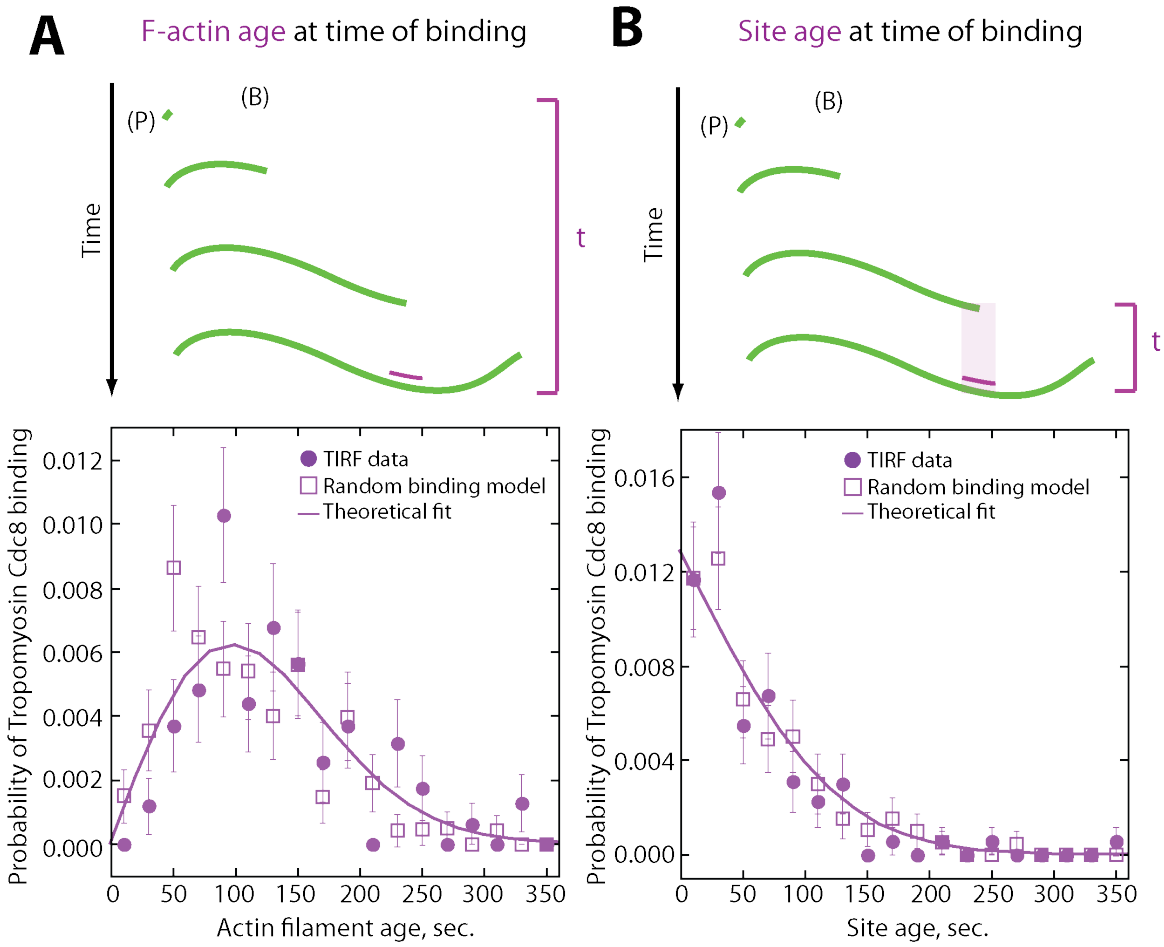

Figure 3-5: Tropomyosin Cdc8 first-binding events are consistent with random binding. **(A-B)** Modeling of random binding compared to experimental data of first tropomyosin Cdc8 binding events. Experimental TIRFM data (purple filled circles), theoretical fit of random binding (purple line) and random binding model with generated noise (purple open square). **(A) (Top)** Depiction of actin filament age at time of initial tropomyosin Cdc8 binding. **(Bottom)** Analysis and modeling of age of the actin filament at time of initial tropomyosin Cdc8 binding. **(B) (Top)** Depiction of age of site first bound by tropomyosin Cdc8 at time of tropomyosin Cdc8 binding. **(Bottom)** Analysis and modeling of age of tropomyosin Cdc8-bound site at time of binding.

bound end-to-end. Given our resolution, though we assume that the observed tropomyosin spreading events are the result of end-to-end binding between tropomyosin Cdc8 molecules, we cannot differentiate between tropomyosin end-to-end binding and distinct, unconnected tropomyosin molecules associating with actin. However, we can use the two distinct tropomyosin cables to examine indirect tropomyosin interactions via the actin filament as (1) the

two tropomyosin cables on opposing sides of the actin filament been shown to not directly interact and (2) we can differentiate between the two cables by an increase in fluorescence intensity (Figure 3-3C). Therefore, we sought to determine whether these two distinct tropomyosin Cdc8 cables loaded independently, or if there was a potential interaction between the two (presumably mediated by an indirect interaction across the actin filament).

To determine whether there was an interaction between the two tropomyosin cables, we examined second Cdc8 loading events. In a first tropomyosin Cdc8 loading event, a tropomyosin Cdc8 'seed' forms and elongates along one face of the actin filament. Second tropomyosin Cdc8 loading events can then occur either on the actin face opposite the first tropomyosin Cdc8 cable (Figure 3-4C, purple box), or on either face at an unbound stretch of the actin filament. As expected, if the first tropomyosin Cdc8 stretch covered a higher fraction of the actin face before the second event occurred, the second Cdc8 event was more likely to occur at the site of an initial Cdc8 seed (Figure 3-4C, purple bars). However, comparing our data to a model of random binding suggested that our observed likelihood of binding opposite a first tropomyosin Cdc8 stretch was higher than what would be predicted for random binding (Figure 3-4C, c=1X circles). Adding in an indirect cooperativity factor of 2 (doubling the likelihood of binding opposite a first tropomyosin Cdc8 cable) more closely replicated the data (Figure 3-4C, c=2X circles). These findings suggest that although initial Cdc8 molecules bind stochastically on the actin filament, there is a bias for subsequent Cdc8 molecules to bind opposite previously-established Cdc8 stretches, indicating a potential role for indirect cooperativity (Figure 1C).

Modeling of tropomyosin Cdc8 loading onto growing actin filaments

The preference of second Cdc8 loading events for already Cdc8-occupied regions described above is based on a statistical calculation from a limited number of second Cdc8 binding events (n=37). To further address whether indirect cooperativity plays a role in tropomyosin Cdc8 loading, we created two variations of a lattice simulation describing tropomyosin Cdc8 loading onto a growing actin filament. The first model described tropomyosin Cdc8 loading given only end-to-end cooperativity (w), while the second model described tropomyosin Cdc8 loading given both end-to-end (w) and indirect cooperativity (c) across the actin filament (Figure 3-6B,C). We wished to determine whether either model was sufficient to reproduce the complex behavior observed in experiments (Figure 3-6A). To select values of w, c and k_{off}, we first fixed c, and varied k_{off} and w until generating (1) the best match to the experimental data in Figure 3-2B as k_{on} is scanned, (2) similar k_{off} to single molecule experimental measurements (Figure 3-7) (3) kymographs whose first time for observed binding is similar to what is observed experimentally (Figure 3-5). For the first model, cooperativity occurs only via end-to-end binding (w) (Figure 3-6Bi). By generating a simulated kymograph using those parameters, we can replicate many of the observed tropomyosin loading characteristics, specifically the frequent starts and stops and differences in spreading rate (Figure 3-6Bii). However, if we quantify the fraction of actin filament that is coated by a single Cdc8 cable or by two Cdc8 cables in the model and the experimental data, we see a much higher fraction of actin filament that is doubly coated in the experimental data (Figure 3-6Aiii) when compared to the end-to-end binding model (Figure 3-6Biii), suggesting that end-to-end binding alone may not be able to fully account for tropomyosin behavior as observed experimentally.

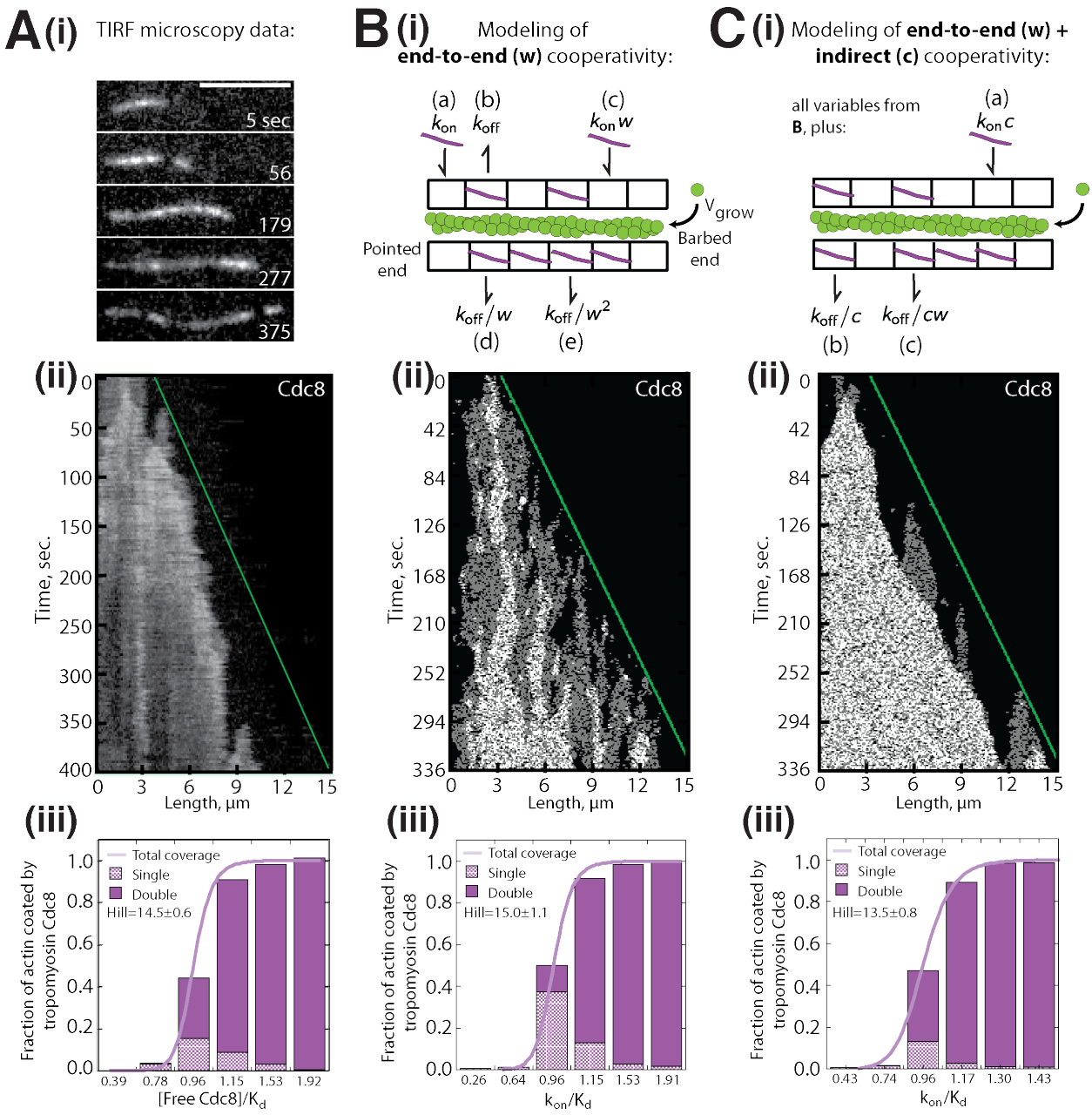

Figure 3-6: Modeling of Tropomyosin Cdc8 dynamics on growing actin filaments.
(Ai-iii) Two-color TIRFM of 1.5 µM Mg-ATP actin (15% Alexa 488) with 1.25 µM tropomyosin Cdc8 (Cy5-labeled). **(Ai-ii)** Timelapse and corresponding kymograph of tropomyosin Cdc8 loading and spreading. The green line indicates the actin filament barbed end. Scale bar, 5 µm. **(Aiii)** Quantification of fraction of F-actin coated by one (Single, checkered purple) or two (Double, solid purple) tropomyosin Cdc8 cables. Total coverage (purple line) is from initial quantification in Figure 1B. n=2 reactions. **(Bi-iii)** Modeling of tropomyosin Cdc8 association with an actin filament with exclusively end-to-end interactions. **(Bi)** Lattice model schematic with parameters for actin elongation (v_{grow}), rates of association ($k_{on,}$ (a)) or dissociation (k_{off}, (b)) of single tropomyosin Cdc8 molecules with the actin filament, and rates of association (k_{on}*w (c), k_{on}/w^2) and dissociation (k_{off}/w (d), k_{off}/w^2 (e)) at sites within a tropomyosin Cdc8 cable. **(Bii)** Kymograph of simulated loading and spreading

Figure 3-6 (cont.) of modeled tropomyosin Cdc8 under parameters in **(Bi).** The green line indicates the actin filament barbed end. **(Biii)** Quantification of simulated data from end-to-end cooperativity model. **(Ci-iii)** Modeling of tropomyosin Cdc8 association with an actin filament that includes both end-to-end interactions and indirect cooperativity. **(Ci)** Schematic of lattice model, which includes all parameters from **(B)** as well as additional parameters added for **(C)**: rates of association (k_{on}*c, (a)) and dissociation (k_{off}*c, (b)) of tropomyosin Cdc8 molecules across from a site already bound by a tropomyosin Cdc8 molecule, and rates of association (k_{off}*cw) and dissociation (k_{off}/cw (c)) of tropomyosin Cdc8 molecules within a cable and across from an already-bound Cdc8. **(Cii)** Kymograph of simulated loading and spreading of modeled tropomyosin Cdc8 under parameters in **(Ci). (Ciii)** Quantification of simulated data from end-to-end with indirect cooperativity model.

To determine the potential role of indirect cooperativity, we then added positive indirect cooperativity via parameter c (Figure 3-6Ci). An indirect cooperativity (c) value of 1.25 most closely replicated our experimental data (Figure 3-6Ciii). This model also replicated the observed dynamics of tropomyosin loading (Figure 3-6Cii), and replicated the observed bias towards double-coating of actin filaments by tropomyosin (Figure 3-6Ciii, compare to Figure 3-6Aiii). These findings, along with the second Cdc8 binding event data (Figure 3-4C), are consistent with a role for indirect cooperativity in the high overall cooperativity of tropomyosin.

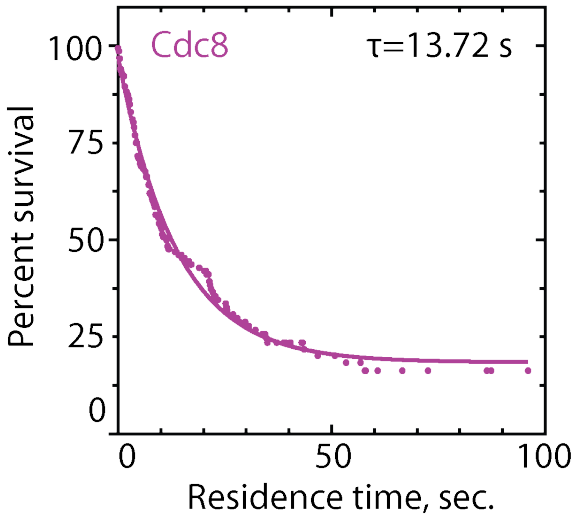

Figure 3-7: Residence time of tropomyosin Cdc8 on actin filaments.
Three-color TIRFM of 1.5 µM Mg-ATP actin (15% Alexa 488-labeled) and 2.5 µM tropomyosin Cdc8 (0.5% TMR-labeled and 30% Cy5-labeled). Residence time of single tropomyosin Cdc8-TMR molecules on F-actin was quantified in the presence of tropomyosin Cdc8-Cy5 in order to determine that full Cdc8 coverage of F-actin occurred. n=102 events.

Fimbrin Fim1 actively displaces Tropomyosin Cdc8 from F-actin bundles

We have demonstrated that tropomyosin Cdc8's high degree of cooperativity allows it to rapidly coat actin filaments. This ability to rapidly assemble onto actin filaments is likely important in a cellular context as it allows tropomyosin to quickly define the functional composition of an F-actin network by associating with F-actin and inhibiting certain ABPs from associating with it (Gunning et al., 2015). In fission yeast, tropomyosin Cdc8 has been shown to inhibit actin patch ABPs cofilin Adf1, Arp2/3 complex, and myosin-I Myo1 (Skau and Kovar, 2010). Though tropomyosin's presence at the contractile ring and actin cables is useful to prevent the association of those ABPs at those locations, mechanisms must be in place to prevent tropomyosin from associating with actin patches and disrupting the association of actin patch ABPs. Tropomyosin Cdc8's association with actin patches is regulated by competition with another ABP, fimbrin Fim1 (Skau and Kovar, 2010). Fimbrin Fim1 is an F-actin crosslinking protein that localizes predominantly to actin patches in fission yeast (Nakano et al., 2001; Wu et al., 2001). Though tropomyosin Cdc8 does not localize to actin patches in a wild-type cell, in a *fim1*Δ cell, tropomyosin Cdc8 localizes to actin patches, suggesting that fimbrin Fim1 prevents tropomyosin association with patches in a wild-type context. In addition, fimbrin Fim1 can compete tropomyosin Cdc8 off of actin filaments in in vitro bulk sedimentation assays (Skau and Kovar, 2010). Though this previous work suggests that a competitive interaction exists between fimbrin Fim1 and tropomyosin Cdc8, the mechanism by which fimbrin prevents tropomyosin association with actin filaments is unclear. We suspected that fimbrin Fim1 could potentially inhibit the initial (and already poor) ability of tropomyosin Cdc8 to associate with F-actin. On the other hand, fimbrin Fim1 could result in the removal tropomyosin Cdc8 already associated with actin filaments. In order to differentiate between these and other potential mechanisms, we

used three-color TIRFM with labeled actin, fimbrin Fim1, and tropomyosin Cdc8 to observe the interplay of fimbrin Fim1 and tropomyosin Cdc8 on the same actin filaments. We find that the majority of single actin filaments in the reaction chamber are initially coated by tropomyosin Cdc8 (Figure 3-8, first panel), with loading and spreading patterns similar to those observed in the absence of fimbrin. However, as actin filaments become bundled by fimbrin Fim1 (Figure 3-8A,C), the amount of fimbrin Fim1 on these bundles increases and tropomyosin Cdc8 is actively displaced from actin filament bundles (Figure 3-8B,C). Kymographs of elongating and bundling actin filaments show that tropomyosin displacement occurs in a cooperative manner at the bundled site, where tropomyosin cables appears to be 'stripped' away from initial sites of removal (Figure 3-8D). Quantification of fluorescence intensity of fimbrin Fim1 and tropomyosin Cdc8 at single actin filaments, two-filament actin bundles, and actin bundles containing more than two filaments indicates that fimbrin Fim1 intensity increases at actin bundles (Figure 3-8E), while tropomyosin Cdc8 intensity decreases at actin bundles (Figure 3-8F), indicating that tropomyosin Cdc8 displacement by fimbrin Fim1 occurs preferentially at sites of actin filament bundling (Figure 3-8F). These findings suggest that the cooperativity of tropomyosin Cdc8 assists not only its assembly onto filaments but also its thorough displacement specifically from F-actin that is crosslinked into bundles or other higher-order networks.

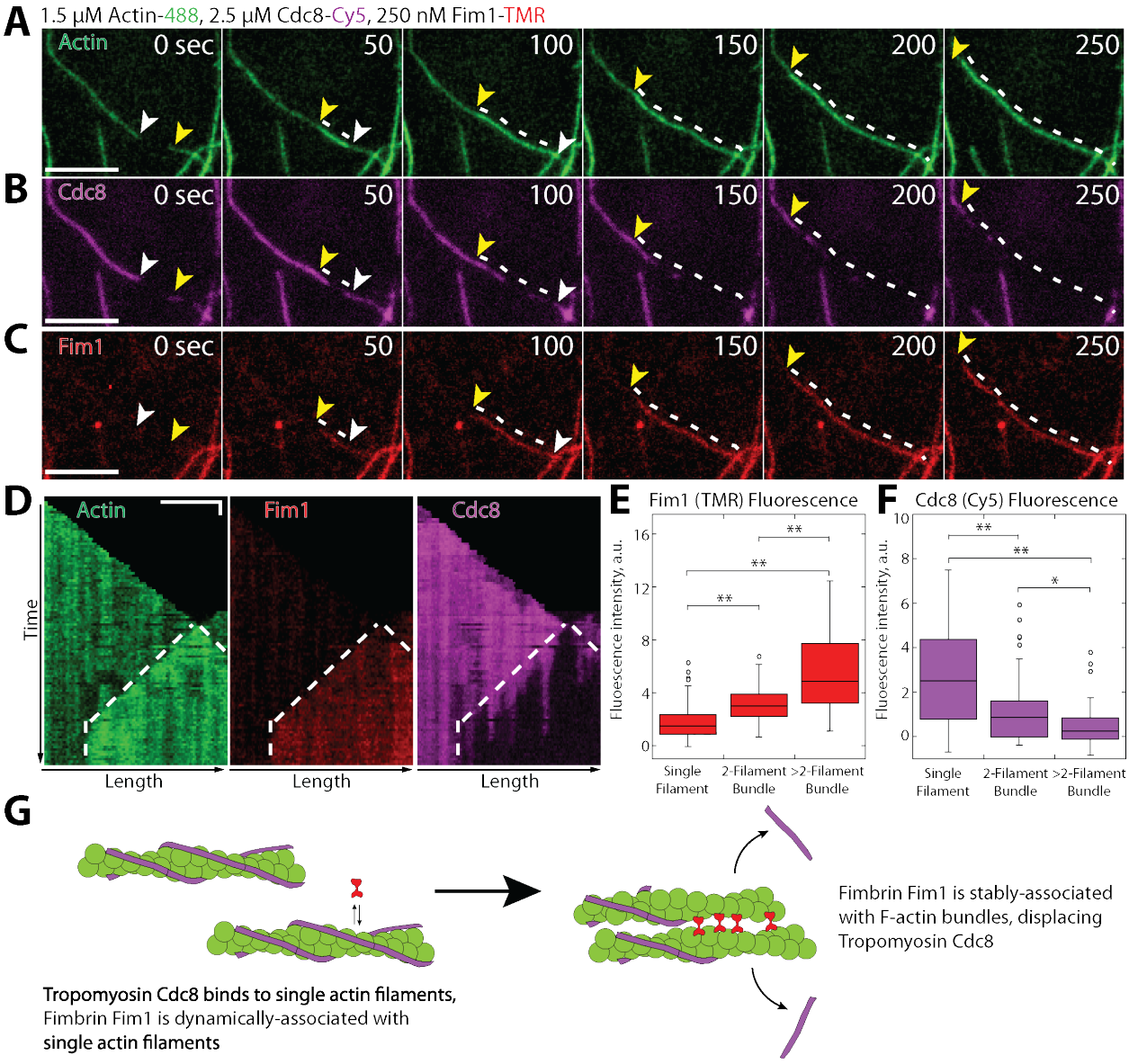

Figure 3-8: Fimbrin Fim1-mediated bundling induces cooperative removal of Tropomyosin Cdc8.

(A-D) Three-color TIRFM of 1.5 µM Mg-ATP actin (15% Alexa 488-labeled) with 2.5 µM tropomyosin Cdc8 (Cy5-labeled) and 250 nM fimbrin Fim1 (TMR-labeled). Arrowheads and dotted lines mark actin filament barbed ends and bundled region, respectively. **(D)** Kymographs of actin, fimbrin Fim1, and tropomyosin Cdc8 during bundle formation. Dotted lines indicate the bundled region. Scale bars, 5 µm. Time bar, 30 sec. **(E-F)** Box plots of the amount of fimbrin Fim1-TMR **(E)** or tropomyosin Cdc8-Cy5 **(F)** fluorescence on single actin filaments, two-filament bundles, or bundles containing more than two filaments. Open circles indicate outliers. n≥42 measurements. Asterisks indicate statistically significant differences, t test: *p<0.05, **p<0.00005. **(G)** Cartoon model of how fimbrin Fim1 and tropomyosin Cdc8 affect each other's association with single and bundled actin filaments.

Tropomyosin Cdc8 inhibits initial Cofilin Adf1 binding to actin filaments

Cofilin Adf1 is a severing protein that localizes predominantly to actin patches and is required for proper patch dynamics (Nakano and Mabuchi, 2006a; Nakano et al., 2001). Cofilin Adf1 is typically thought of as an important factor in F-actin network disassembly by severing actin filaments and allowing recycling of the actin monomers (Chen and Pollard, 2013). Competition between tropomyosins and cofilins in many systems has been well-established (Bernstein and Bamburg, 1982; Ono and Ono, 2002; DesMarais et al., 2002; Kuhn and Bamburg, 2008). In fission yeast, in vitro TIRFM has shown that cofilin Adf1-mediated severing is decreased in the presence of tropomyosin Cdc8 (Skau and Kovar, 2010). We used multi-color TIRFM to investigate whether Cdc8 inhibits Adf1-mediated severing by decreasing the initial association of Adf1 with F-actin, or by another mechanism. Wild-type Adf1 labeled with a cysteine-reactive dye was not observed to associate with F-actin (data not shown). We therefore engineered an Adf1 labeling mutant (C12S, C62A, D34C) for use in TIRFM, based on a similar strategy used for budding yeast ADF/cofilin Cof1 (Figure 3-9, Methods) (Suarez et al., 2011). The TMR-labeled cofilin mutant bound to actin less well than wild-type cofilin Adf1, but was observed to bind to actin in a cooperative manner and sever actin filaments at boundaries of cofilin bound/unbound regions (Figure 3-9), characteristics previously observed for cofilins from *S. pombe* and other organisms (Andrianantoandro and Pollard, 2006; la Cruz, 2009; La Cruz, 2005; Hayakawa et al., 2014; Michelot et al., 2007).

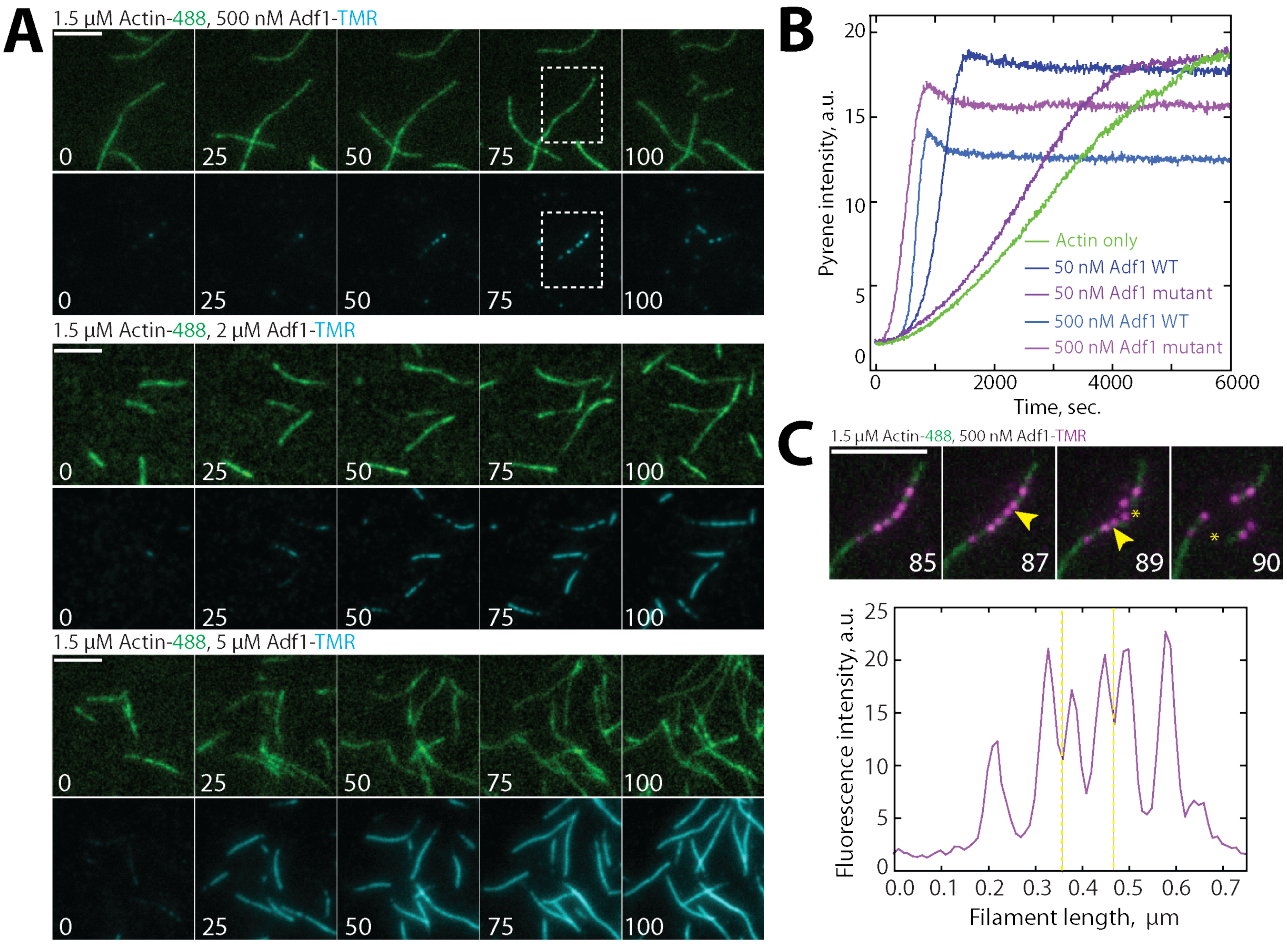

Figure 3-9: Characterization of Cofilin Adf1 labeling mutant.
(A) Two-color TIRFM of 1.5 µM Mg-ATP actin (15% Alexa 488) with a range of concentrations of cofilin Adf1 mutant (C12S, C62A, D34C) (TMR-labeled). Scale bar, 5 µm. **(B)** Spontaneous assembly assay of 1.5 µM actin (10% pyrene-labeled) and 50 or 500 nM of WT cofilin Adf1 (green lines) or cofilin Adf1 labeling mutant (blue lines). **(C)** Actin filament severing occurs at cofilin Adf1 boundaries. **(Top)** Two-color TIRF microscopy of 1.5 µM Mg-ATP actin (15% Alexa 488) 500 nM cofilin Adf1 mutant (C12S, C62A, D34C) (TMR-labeled). Yellow arrowhead and asterisks indicate future sites of severing and severing events, respectively. Scale bar, 5 µm. **(Bottom)** Linescan of cofilin Adf1 fluorescence (purple) along actin filament before severing. Yellow dotted line indicates sites of severing.

Using this new reagent, we found that at high (5 µM) cofilin Adf1 concentrations, the majority of F-actin was rapidly coated with cofilin Adf1 (Figure 3-9, 3-10A). However, in the presence of tropomyosin Cdc8, little cofilin Adf1 was observed to initially associate with F-actin (Figure 3-10A,B,C). Over time, however, cofilin Adf1 began to associate with actin filaments at small 'clusters' near the pointed end that then spread cooperatively along the actin filament

(Figure 3-10B). Importantly, though tropomyosin Cdc8 affected this initial association (k_{on}) of cofilin with actin filaments, the k_{off} of cofilin Adf1 for F-actin was unaffected by the presence of tropomyosin Cdc8 (Figure 3-10E), suggesting that tropomyosin Cdc8 inhibits only the initial association of cofilin Adf1 with an actin filament. These findings are supported by three-color TIRFM utilizing labeled actin, cofilin Adf1, and tropomyosin Cdc8. Labeled tropomyosin Cdc8 and cofilin Adf1 show mutually exclusive localization (Figure 3-10E) on actin filaments. Initially, the majority of actin filaments are coated with tropomyosin Cdc8. Over time, cofilin Adf1 puncta arise, displacing tropomyosin from those regions. Cofilin Adf1 domains then spread in a cooperative manner, displacing tropomyosin Cdc8 from the regions it binds (Figure 3-10D). As actin filaments grow, tropomyosin continues to associate at the growing barbed end, where cofilin Adf1 is not yet associated, but is frequently displaced by cofilin Adf1 over time. As cofilin has been shown to preferentially associate with ADP-actin (Andrianantoandro and Pollard, 2006), we suspect that the transition from ADP-Pi- to ADP-actin increases the k_{on} of cofilin Adf1 for ADP-bound actin, allowing a few cofilin Adf1 molecules to associate with the actin filament. Cofilin Adf1 then cooperatively spreads from these regions of association, and displaces tropomyosin Cdc8. Together, this data suggests that while tropomyosin Cdc8 inhibits the initial binding of cofilin Adf1 to actin filaments, cofilin Adf1 is capable of associating and displacing segments of tropomyosin Cdc8 at later timepoints.

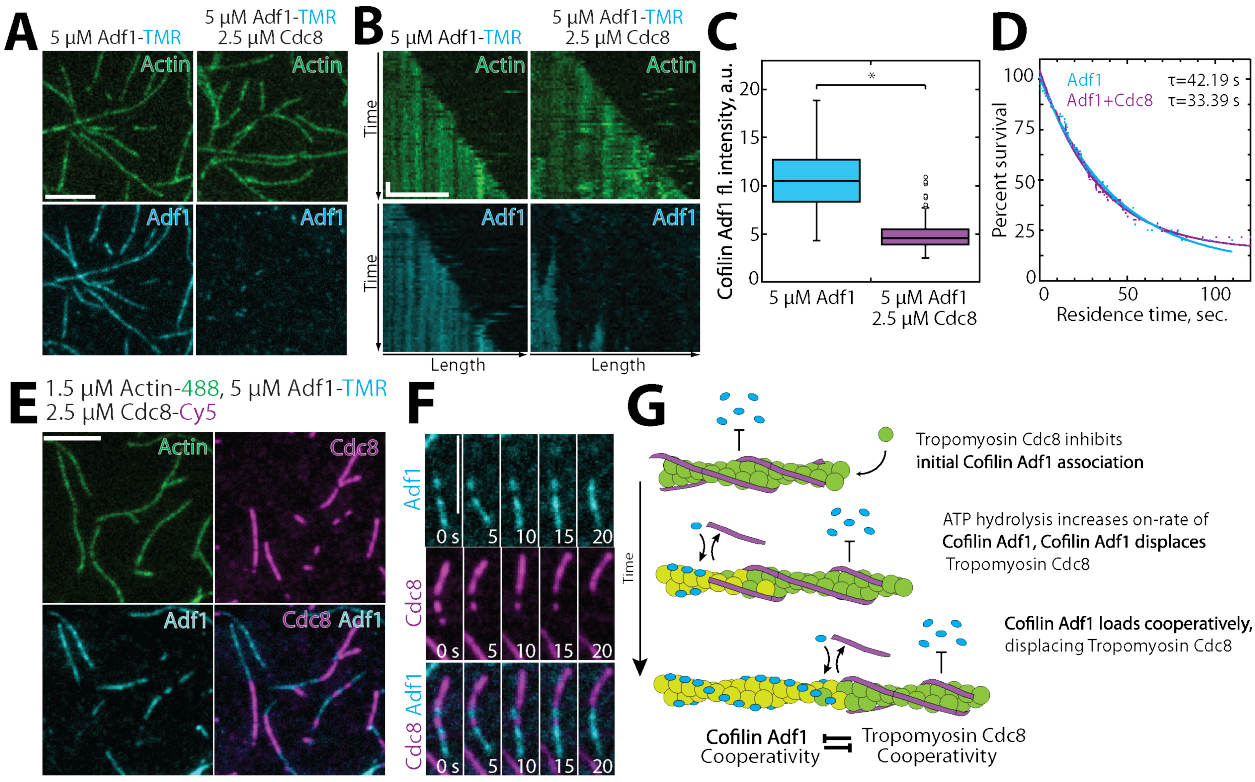

Figure 3-10: Tropomyosin Cdc8 inhibits initial binding of Cofilin Adf1 to actin filaments.

(A-C) Two-color TIRFM of 1.5 μM Mg-ATP actin (15% Alexa 488 labeled) with 5 μM cofilin Adf1 (TMR-labeled) in the presence or absence of 2.5 μM tropomyosin Cdc8 (unlabeled). **(A)** Micrograph of cofilin Adf1 association with actin filaments in the absence or presence of tropomyosin Cdc8. **(B)** Kymograph of an elongating actin filament (top) and associated cofilin Adf1 (bottom) in the absence or presence of unlabeled tropomyosin Cdc8. Scale bar, 5 μm. Time bar, 30 sec. **(C)** Average cofilin Adf1 fluorescence intensity on actin filaments in the absence or presence of unlabeled tropomyosin Cdc8. n≥145 measurements. Open circles indicate outliers. Asterisks indicate statistically significant differences, t test: *p<0.00005**. (D)** Residence time of single cofilin Adf1 (TMR-labeled) molecules in the absence or presence of unlabeled tropomyosin Cdc8. n≥81 events. **(E-F)** Three-color TIRFM of 1.5 μM Mg-ATP actin (15% Alexa 488 labeled) with 5 μM cofilin Adf1 (TMR-labeled) and 2.5 μM tropomyosin Cdc8 (Cy5-labeled). **(E)** Micrograph of actin filaments associated with cofilin Adf1 and tropomyosin Cdc8. Scale bar, 5 μm. **(F)** Timelapse of cofilin Adf1 association with an actin filament, and subsequent dissociation of tropomyosin Cdc8. Scale bar, 5 μm. **(G)** Cartoon model of how tropomyosin Cdc8 and cofilin Adf1 affect each other's association with F-actin.

Fimbrin Fim1 and Cofilin Adf1 synergize to quickly generate a dense F-actin network

Within an actin patch, a dense array of branched filaments provides the structure to propel a newly-generated endocytic vesicle into the cell (Young et al., 2004, Collins et al., 2011). It has been postulated that Fimbrin Fim1 may be required for proper patch motility indirectly, by inhibiting tropomyosin Cdc8 binding, allowing cofilin severing to occur (Skau and Kovar, 2010) However, a fimbrin Fim1 mutant incapable of bundling but capable of displacing tropomyosin Cdc8 from actin filaments still shows abnormal patch dynamics (Skau et al., 2011), suggesting that fimbrin Fim1 has an additional role aside from inhibition of tropomyosin Cdc8. Therefore, we first wanted to examine the relationship between fimbrin Fim1 and cofilin Adf1 utilizing labeled proteins in vitro. We find that cofilin Adf1 and fimbrin Fim1 are capable of localizing to the same actin filaments, with both localizing to single actin filaments and multi-filament bundles (Figure 3-11B). Mutually-exclusive boundaries are not as obvious as in the case of tropomyosin Cdc8 and cofilin Adf1 (Figure 3-10E), and often fimbrin Fim1 and cofilin Adf1 are observed to localize to the same F-actin bundles (Figure 3-11B). However, domains can still be observed, with cofilin Adf1 frequently excluding fimbrin Fim1 from association with single filaments, while fimbrin Fim1 excludes cofilin Adf1 from bundled regions (Figure 3-11C). Severing is often observed at these single filament/bundle interfaces (Figure 3-11C), likely because of sharp changes in cofilin Adf1 amount or actin filament flexibility between those two regions (McCullough et al., 2008; Suarez et al., 2011; Elam et al., 2013). Consistent with this finding, the cofilin Adf1 severing rate is increased in the presence of fimbrin Fim1 (Figure 3-11F). The severing rate was measured only at single filaments and small bundles where it could be easily observed, and is therefore potentially lower than the actual severing rate (Figure 3-11F, indicated by an asterisk). In fact, severing appears to occur extensively within bundles,

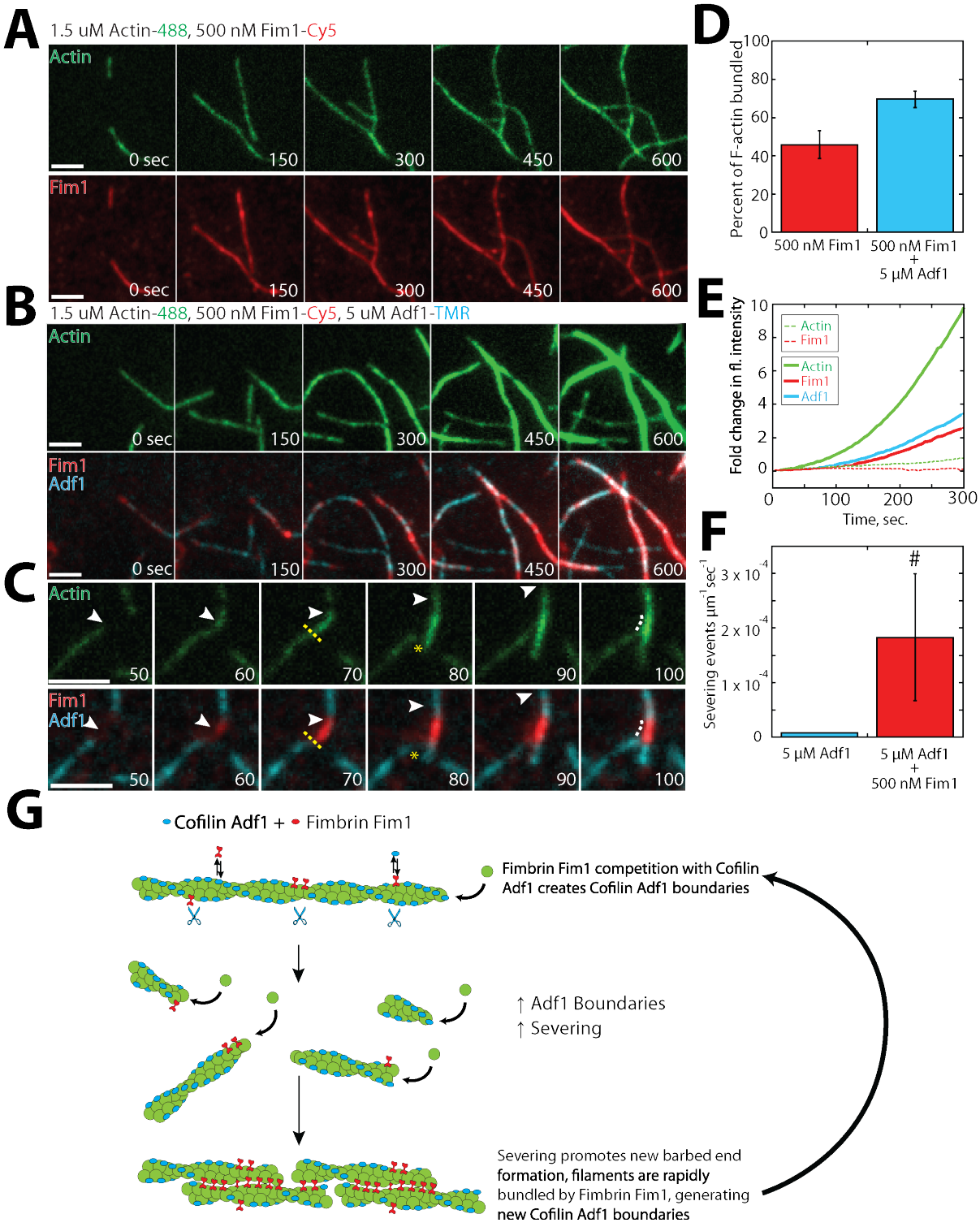

Figure 3-11: Fimbrin Fim1 and Cofilin Adf1 competition generates a dense F-actin network.

(A) Timelapse of two-color TIRFM of 1.5 µM Mg-ATP actin (15% Alexa 488-labeled) with 500 nM fimbrin Fim1 (Cy5-labeled). **(B)** Timelapse of three-color TIRFM of 1.5 µM Mg-ATP actin (15% Alexa 488-labeled) with 500 nM fimbrin Fim1 (Cy5-labeled) and 5 µM

Figure 3-11 (cont). cofilin Adf1. **(C)** Timelapse showing severing at the boundary between a fimbrin Fim1-mediated bundle and a single actin filament. White arrow indicates the elongating actin filament barbed end. A yellow dotted line and asterisk indicate the severing site and severing event, respectively. **(D)** Quantification of percent of total actin filaments bundled with fimbrin Fim1 alone or fimbrin Fim1 and cofilin Adf1. Error bars represent SE; n=2 reactions. **(E)** Fold-change over time in total fluorescence intensity for either actin (dotted green line) and fimbrin Fim1 (dotted red line) in the absence of cofilin Adf1, or for actin (solid green line), fimbrin Fim1 (solid red line), and cofilin Adf1 (solid blue line) in the presence of cofilin Adf1. **(F)** Severing rate of high concentrations of cofilin Adf1 alone or in the presence of fimbrin Fim1. # indicates under-reporting, as severing events could not be measured on dense bundles. Error bars represent SE; n=2 reactions. **(G)** Cartoon model of how cofilin Adf1 and fimbrin Fim1 influence each other's interactions with actin and affect F-actin network formation.

as fimbrin Fim1-mediated bundles become extremely large and dense in the presence of cofilin Adf1 (Figure 3-11B), as each severing event results in the formation of a new, elongating barbed end. This rapid generation of barbed ends can be quantified via fold-change in actin fluorescence over time (Figure 3-11E, solid lines), compared to experiments lacking cofilin Adf1 (Figure 3-11E, dashed lines). Together, these findings support a potential role for cofilin Adf1 as both a disassembly factor (via severing) and an assembly factor (via generation of new barbed ends). We speculate that the presence of fimbrin Fim1 on actin patches may be important not only for exclusion of tropomyosin Cdc8 from the network but also for enhancement of cofilin Adf1 severing via generation of single filament/bundle interfaces.

Fimbrin Fim1 and Cofilin Adf1 work together to displace Tropomyosin Cdc8 from actin filaments

Our findings and previous work suggest that the synergistic activities of fimbrin Fim1 and cofilin Adf1 may serve to inhibit the association of tropomyosin with actin filaments (Skau and Kovar, 2010). In order to determine if this is the case, we used four-color TIRFM to examine how this combination of proteins affects each other's interactions with actin filaments. As in the previous experiments with fimbrin Fim1 and cofilin Adf1 (Figure 3-11), a dense, bundled actin network was formed, containing filaments coated with both cofilin Adf1 and fimbrin Fim1. Tropomyosin Cdc8, on the other hand, rapidly dissociated from nearly every actin filament in the chamber (Figure 3-12A,B,C). Upon close examination, we can observe individual growing actin filaments that are initially coated with tropomyosin Cdc8 (Figure 3-12B, right panel). These filaments are often severed at bundle/single filament boundaries (Figure 3-12Bi). The severing events create new actin filament barbed ends that are encompassed into actin bundles, where tropomyosin Cdc8 is displaced by fimbrin Fim1 (Figure 3-12Bii). We do not observe cofilin Adf1 directly displacing tropomyosin Cdc8, and therefore we suspect that cofilin Adf1's primary role in displacing tropomyosin Cdc8 is by rapidly generating short actin filaments that can be encompassed into actin bundles mediated by fimbrin Fim1.

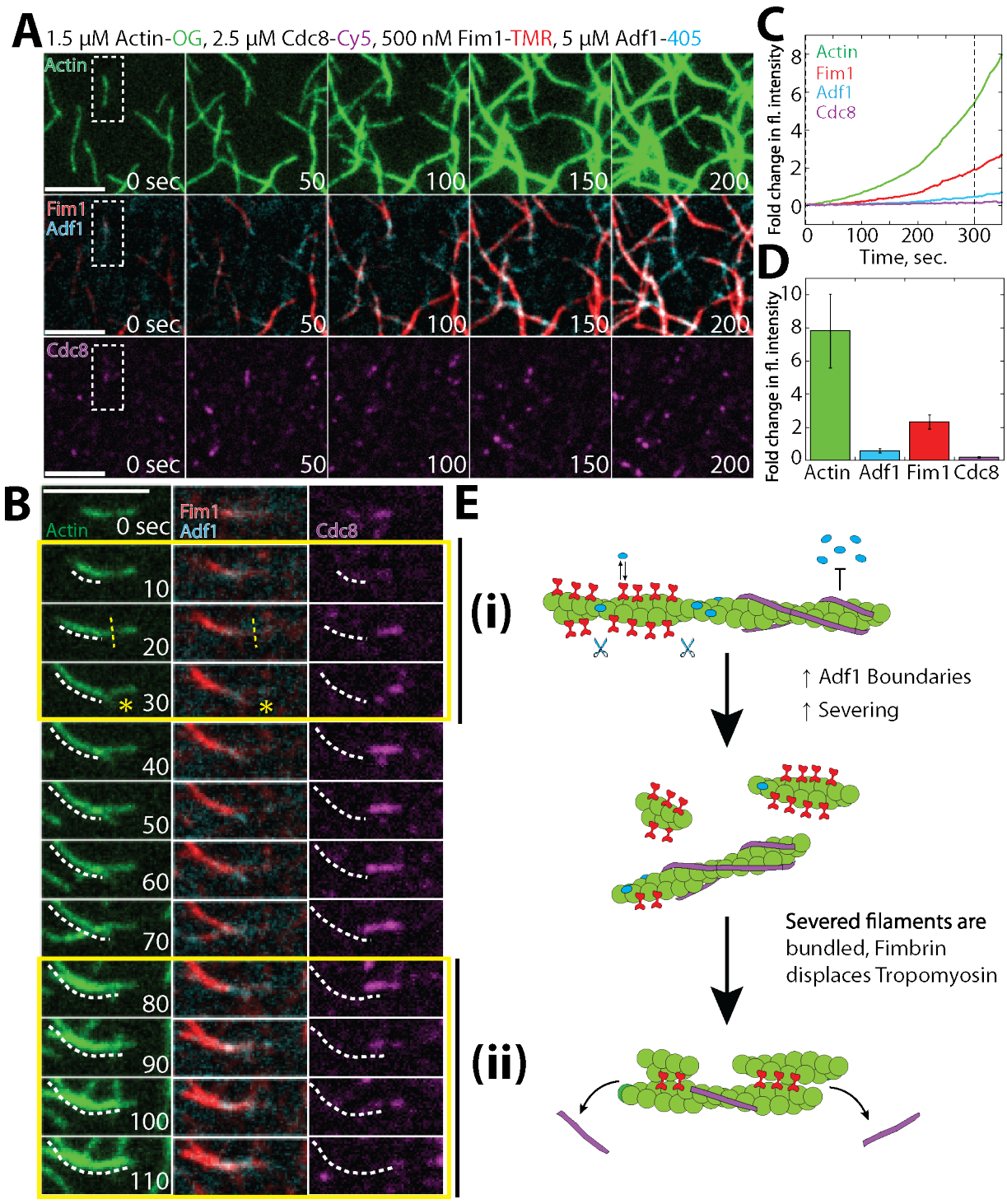

Figure 3-12: Competitive interactions between Cofilin Adf1 and Fimbrin Fim1 result in rapid displacement of Tropomyosin Cdc8 from F-actin networks.
(A-D) Four-color TIRFM of 1.5 μM Mg-ATP actin (15% Alexa 488 labeled) with 2.5 μM tropomyosin Cdc8 (Cy5-labeled), 500 nM fimbrin Fim1 (TMR-labeled), and 5 μM cofilin Adf1 (Alexa 405-labeled). **(A)** Timelapse of F-actin network generation in the presence of actin (green), fimbrin Fim1 (red), cofilin Adf1 (cyan), and tropomyosin Cdc8 (magenta). **(B)** Enlargement of the area within the dotted box in **(A)**. Fimbrin Fim1 and cofilin Adf1 synergize

Figure 3-12 (cont). to create a dense F-actin bundle (white dotted line), while tropomyosin Cdc8 associates with a single actin filament. Severing occurs at the boundary of the single actin filament and F-actin bundle **(i**, yellow asterisk**)**, creating a new elongating F-actin barbed end. The bundle extends to incorporate the single actin filament and tropomyosin Cdc8 is displaced **(ii)**. Scale bar, 5 μm. **(C)** Fold-change over time in fluorescence intensity of actin (green line), fimbrin Fim1 (red line), cofilin Adf1 (blue line), and tropomyosin Cdc8 (purple line). **(D)** Fold change in fluorescence intensity of each ABP after 300 seconds. n=2 independent experiments. **(E)** Cartoon model of events occurring in **(B).**

Section 3.4—DISCUSSION

Tropomyosin Cdc8 cooperativity

Our work demonstrates that cooperativity is a defining characteristic that is important for multiple aspects of actin network formation, organization, and ABP sorting. We show that tropomyosin Cdc8 is an actin binding protein that binds extremely cooperatively to actin filaments (Figure 3-2). Though tropomyosins from other organisms have been labeled for use in TIRFM (Hsiao et al., 2015; Schmidt et al., 2015), ours is the first study to observe two distinct tropomyosin cables associating with a single actin filament (Figure 3-3). This high degree of resolution has given us the ability to assess the roles of end-to-end and indirect interactions via the actin filament in tropomyosin cooperativity on actin filaments (Figure 3-4, 3-6).

End-to-end binding has been previously considered to be the primary source of tropomyosin's cooperativity. However, it has been suggested that other interactions between tropomyosin and the actin filament may also be involved in tropomyosin cooperativity as end-to-end attachments between tropomyosin molecules tend to be rather weak (Sousa and Farah, 2002) and the cooperativity of tropomyosin on F-actin does not scale with strength of tropomyosin end-to-end binding (Tobacman, 2008). Our findings suggest that, though end-to-end binding is a key factor in tropomyosin cooperativity, indirect interactions via the actin filament may also be important for enhancing tropomyosin coating of F-actin. Our results suggest that a small increase in indirect cooperativity (increase by a factor of 2 or smaller) would be sufficient to account for tropomyosin's high cooperativity and observed loading characteristics (Figure 3-6C). The

precise interactions within the actin filament that would allow for this cooperativity remain to be determined. However, due to the Arrhenius-type nature of chemical equilibrium, a factor of 2 in increased binding affinity corresponds to a very small increase in free-energy stabilization of -kBTln(2)~=0.3 kcal/mol. Hence, if this indirect cooperativity is due to a structural change in the actin filament, we expect that change to be quite subtle. In addition, it is possible that other factors such as long-range interactions along the actin filament also contribute to tropomyosin Cdc8's high cooperativity.

Tropomyosin cooperativity and ABP sorting

How does this high degree of cooperativity affect tropomyosin's interactions with other ABPs? The nature of tropomyosin as an elongated, end-to-end binding protein makes it an ideal F-actin 'gatekeeper'. Individual tropomyosin Cdc8 molecules associate poorly with actin filaments. However, once a tropomyosin 'seed' has been initiated, end-to-end binding and potential indirect interactions promote tropomyosin's rapid coating of actin filaments. The avidity generated from multiple actin-tropomyosin and tropomyosin-tropomyosin interactions (Milligan et al., 1990) stabilizes the actin filament and regulates the binding of other ABPs such as cofilin (Figure 3-10A,B). In addition, this large number of interactions between a tropomyosin cable and the actin filament could allow a tropomyosin cable to remain associated despite perturbations along the actin filament that may occur as a result of the association of other ABPs with the actin filament. However, these same cooperative characteristics also make tropomyosin easily removable from actin filaments once a threshold of perturbations has been bypassed; at regions of high fimbrin Fim1 association (F-actin bundles), tropomyosin's end-to-end associations allow it to rapidly peel away from those actin filaments (Figure 3-8B). In addition,

the poor ability of individual tropomyosin molecules to bind to an actin filament make it unlikely to be able to displace other ABPs once they're bound to an actin filament, resulting in tropomyosin's complete exclusion from certain F-actin networks.

Another result of tropomyosin Cdc8's high cooperativity may be that only a slight bias toward certain actin filaments could generate an 'all-or-nothing' sorting toward those networks. Several studies have suggested that the actin assembly factor may be the key to generating this initial bias. In fission yeast, altering formin localization in the cell results in the relocalization of both acetylated and unacetylated forms of tropomyosin Cdc8 (Johnson et al., 2014). This bias may be the result of formin-induced conformational changes that could be propagated down the actin filament (Bugyi et al., 2006; Papp et al., 2006). Future work will involve deciphering potential 'initiating' signals for ABP sorting and their effects on ABP cooperativity and competition.

Competition and boundary generation

Our work also addresses the importance of ABP competition in network organization and ABP sorting. An outstanding question is how cofilin, a protein that severs at low concentrations, can be present at high concentrations in the cell and yet still rapidly disassemble actin networks. Other ABPs, such as Aip1 (Nadkarni and Brieher, 2014; Gressin et al., 2015), coronin (Jansen et al., 2015), and twinfilin (Johnston et al., 2015) have been found to enhance cofilin-mediated severing via multiple mechanisms, including potential side-binding by Aip1 (Chen et al., 2015). Our study additionally implicates side-binding ABPs not involved in severing (fimbrin Fim1) as important for the enhancement of cofilin severing, likely by generating cofilin boundaries or changes in flexibility that result from fimbrin-mediated bundle formation (Figure 3-11C). The

idea of competition between cofilin and other factors as important for enhancing cofilin-mediated severing is an exciting area of investigation (Elam et al., 2013), and future work remains to determine how different ABPs regulate cofilin severing to different extents on different F-actin networks.

In addition, our study suggests an important role for cofilin not only as a disassembly factor, but also as a potent assembly factor through the creation of new barbed ends as in the model of dendritic nucleation within the lamellipodia of migrating cells (Desmarais, 2004; Ichetovkin et al., 2002). The combination of fimbrin and cofilin generates dense actin bundles composed of many more actin filaments than fimbrin alone (Figure 3-11A,B). It has been previously shown that expression of a cofilin mutant deficient in severing results in delayed patch assembly, as a lack of severing prevents the creation of new mother filaments (Chen and Pollard, 2013). Our data suggests that cofilin is additionally important for creating the bulk of filaments that compose the dense actin patch network. The creation of barbed ends via severing rather than nucleation takes advantage of the inherent polarity of an actin filament, as the newly-created barbed end at the severed site is automatically oriented in the same direction as the original barbed end. This type of mechanism could be ideal for force-generating networks such as those at endocytic actin patches or the lamellipodia. However, the proper balance of assembly vs. disassembly must be achieved for proper patch dynamics, and likely involves the concerted effort of many ABPs.

Competition and ABP sorting

Finally, our work suggests that the combined efforts of sets of ABPs can enhance or modulate effects observed for individual ABP interactions. A prime example of this has been

shown for F-actin disassembly, as multiple ABPs work together to rapidly disassemble an F-actin network (Jansen et al., 2015). We show that a similar idea holds true for ABP competition, as tropomyosin Cdc8 is rapidly displaced from actin networks created by the combined efforts of fimbrin and cofilin. Though tropomyosin Cdc8 alone is capable of preventing cofilin's associating with F-actin (Figure 3-10), fimbrin can displace tropomyosin from actin filaments (Figure 3-8), allowing cofilin severing to occur (Figure 3-12). Cofilin severing feeds back on fimbrin's bundling activity by creating small, severed filaments that can easily be incorporated into bundles (Figure 3-11), facilitating further bundling by fimbrin and resulting tropomyosin displacement (Figure 3-12). Our work has implications not only for ABP sorting, but for the formation of any organized network that contains multiple components competing for the same binding substrate. Our lab has previously shown that competition for F-actin monomers are important for generating the correct number and size of F-actin networks (Burke et al., 2014; Suarez et al., 2015). In addition, competitive interactions between DNA methylation and surrounding transcription factors have been shown to mediate transcription factor association with certain regions of the genome (Domcke et al., 2015) and competition for membrane or receptor binding has been suggested to be involved in cargo sorting in a number of contexts (Soza et al., 2004). Overall, our work and the work of others suggest that competitive interactions between individual components can have large-scale effects on cellular organization in many contexts.

CHAPTER 4: TROPOMYOSIN AND α-ACTININ COOPERATE TO COMPETE WITH FIMBRIN, DRIVING THEIR LOCALIZATION TO DIFFERENT ACTIN CYTOSKELETON NETWORKS IN FISSION YEAST

PREFACE

The work in the following chapter was performed with experimental assistance from Meghan O'Connell, Katie Homa, and Alisha Morganthaler. Meghan O'Connell assisted with the creation of fission yeast strains in Figure 4-3, assisted with the analysis and quantification in Figure 4-2, and performed the experiments and quantification for Figure 4-9. Katie Homa and Alisha Morganthaler provided experimental assistance and performed preliminary experiments that provided useful groundwork for establishing our experimental set-up, but were not included in the chapter.

Section 4.1—INTRODUCTION

We have identified competitive interactions between several ABPs (Skau and Kovar, 2010) and the molecular mechanisms behind their competition (Chapter 3). However, whether competition between ABPs is a universal mechanism affecting ABP sorting or whether these types of interactions occur only between a few ABPs remains to be determined. The fission yeast *Schizosaccharomyces pombe* has proven an ideal system for studying ABP competition as there are limited potential competitors. Although mammalian cells express hundreds of different ABPs, fission yeast has ~40 known actin interactors that facilitate the formation and organization of three F-actin networks—actin patches, actin cables, and the contractile ring.

Fimbrin Fim1 and α-actinin Ain1 are two F-actin bundling proteins with distinct cellular roles in the fission yeast cell. Fimbrin Fim1 localizes predominantly to F-actin patches, while α-actinin Ain1 localizes solely to the contractile ring. Genetic and cell biological studies have shown that altering the concentration of either in the cell can drastically impair endocytosis and cytokinesis. At actin patches, fimbrin Fim1 assists in creating a dense F-actin network that facilitates rapid internalization of endocytic vesicles (Nakano et al., 2001; Skau et al., 2011; Young, M.E., Cooper, J.A, Bridgman, P.C., 2004). *fim1-1Δ* cells show disorganized actin patches with delayed turnover that requires fimbrin Fim1's bundling activity (Skau et al., 2011; Wu et al., 2001). Overexpressing fimbrin Fim1 also results in patch defects, but additionally causes dramatic cytokinesis defects (Wu et al., 2001). The dynamic (high on-/off-rate) bundling ABP α-actinin Ain1 is involved in contractile ring formation. While *ain1-1Δ* cells have minor cytokinesis defects, overexpressing wild-type Ain1 results in dramatic cytokinesis defects (Wu et al., 2001). This phenotype is further exacerbated in a less dynamic α-actinin mutant

Ain1(R216E), with ~80% of cells displaying cytokinesis defects following expression of Ain1(R216E) from a medium-strength promoter.

In this study, we used a survey approach to identify potential ABP competitors in fission yeast. We demonstrate that fimbrin Fim1 and α-actinin Ain1 compete for association with F-actin, and that this competition mediates their associations with the proper F-actin networks. Finally, we show that contractile ring ABP tropomyosin Cdc8 enhances α-actinin Ain1-mediated bundling, allowing the combination of tropomyosin Cdc8 and α-actinin Ain1 to compete with fimbrin Fim1 for association with the contractile ring. We suggest a model by which tropomyosin Cdc8 and α-actinin Ain1 each enhance the cooperativity of the other, while preventing fimbrin Fim1 from cooperatively associating with the actin network.

Section 4.2—MATERIALS AND METHODS

Strain construction and growth

Fission yeast strains were created by genetic crossing on SPA5S plates followed by tetrad dissection on YE5S plates. Strains were screened for auxotrophic (leu, ura) or antibiotic (nat, kan) markers and maintained on YE5S plates. Glycerol stocks were created by pelleting cells and resuspending in 750 μL media and 250 μL of 50% sterile glycerol.

Cell imaging and treatment with CK-666

For live cell imaging, cells were grown in YE5S media overnight at 25°C, subcultured into EMM5S media without thiamine, and kept in log phase for 20-22 hours at 25°C. Cells were imaged directly on glass slides. Z-stacks of 10 slices, 0.5 μm apart were acquired with a 100x, 1.4 NA objective on a Zeiss Axiovert 200M equipped with a Yokogawa CSU-10 spinning-disk

unit (McBain, Simi Valley, CA) illuminated with a 50-milliwatt 473-nm DPSS laser, and a Cascade 512B EM-CCD camera (Photometrics, Tucson, AZ) controlled by MetaMorph software (Molecular Devices, Sunnyvale, CA).

Treatment with CK-666

CK-666 powder stock (Sigma, St. Louis, MO) was diluted to 10 mM in DMSO. Cells were grown as stated above, and incubated with CK-666 or an equivalent volume of DMSO (control) in a rotator at 25°C for 30 min prior to imaging. Cells were then immediately imaged as above.

Contractile ring fluorescence quantification

Contractile ring maturation was divided into three stages by measuring the distance between spindle pole bodies (SPBs, visualized by Sad1-tdTomato) and noting constriction of the contractile ring. Stage 1 cells had SPBs less than 6 μm apart, with no observable ring constriction. Stage 2 cells had SPBs greater than 6 um apart, with no observable ring constriction. Stage 3 cells had SPBs less than 9 um apart, with evident ring constriction. For cells expressing Lifeact-mCherry, mean fluorescence in the ring was traced in the actin channel, and that region of interest used in the GFP channel. For cells not expressing Lifeact-mCherry, the ring region was determined by visually examining the z-stack for the ring site. Normalized ring fluorescence was taken by drawing a region of interest (ROI) around the observed ring and around the whole cell using ImageJ. The mean fluorescence of the ring divided by the whole cell was then determined. A value of 1.00 indicates no increased fluorescence at the site of the ring,

while values >1 indicate increased fluorescence at the ring. Maximum project were used for images in figures and sum projections were used for quantification.

Tropomyosin Cdc8 antibody staining

Following standard growth and culturing protocols for live cell imaging, fission yeast cells were stained with anti-Cdc8p as performed previously (Cranz-Mileva et al., 2015). Cells were fixed in 16% formaldehyde for 5 minutes at 20°C. Cells were then washed in cold 1X PBS and resuspended in 140 µL 1.2M sorbitol. 60 µL fresh protoplasting solution (3 mg/ml zymolase 100T in 1.2M sorbitol) was added and cells were incubated for 7 minutes on a rotator at room temperature. 1 mL of 1% Triton-X was then added to the cells and incubation continued for 2 minutes. Cells were then pelleted and resuspended in 0.5 mL PBAL (10% BSA, 100 mM lysine monohydrochloride, 1 mM NaN_3, 50 ng/ml ampicillin in PBS) and incubated for 2.5 hours on a rotator at room temperature. Cells were resuspended in 100 µL of anti-Cdc8p 1:10 in PBAL (gift of Sarah Hitchcock-DeGregori) and incubated overnight at 4°C on a rotator. Following incubation with primary antibody, cells were washed 3 times with 0.5 mL PBAL and resuspended in 50 µL Alexa-Flour 555 goat anti-rabbit secondary antibody (Thermo-Fisher Scientific, Carlsbad, CA) (1:100 in PBAL) and incubated for 90 minutes at room temperature on a shaker in the dark. Cells were then washed 5 times with 0.5 mL PBAL and resuspended in 20-30 µL PBAL for imaging. Cells were stored at 4°C and imaged within 48 hours of staining.

Phallicidin staining

BODIPY-phallicidin powder was resuspended to 1 unit/µL in PEM buffer (100 mM PIPES (pH 6.9), 1 mM EGTA, 1 mM $MgSO_4$). Cells were cultured and fixed as above. Cells

were resuspended in 10 μL PEM buffer with 1 μL fresh BODIPY-phallicidin solution and incubated for 30 minutes at room temperature on a shaker in the dark. Cells were then washed with 1 mL PEM buffer and resuspended in 10 μL PEM for imaging. For cells stained with anti-Cdc8p and BODIPY-phallicidin, cells were first treated with primary and secondary antibodies, washed with PBAL, and then stained with BODIPY-phallicidin.

Protein purification

Chicken skeletal muscle actin was purified as described previously (Spudich and Watt, 1971). Fimbrin Fim1 and tropomyosin AlaSer-Cdc8 (WT and I76C mutant) were expressed in BL21-Codon Plus (DE3)-RP (Agilent Technologies, Santa Clara, CA) and purified as described previously (Skau and Kovar, 2010). Wild-type α-actinin Ain1 and mutant Ain1(R216E) were expressed in insect cells and purified as described previously (Li et al., 2016).

A_{280} of purified proteins was taken using a Nanodrop 2000c Spectrophotometer (Thermo-Scientific, Waltham, MA). Protein concentration was calculated using extinction coefficients Fim1: 55,140 M^{-1} cm^{-1}, Cdc8 (WT and I76C mutant): 2,980 M^{-1} cm^{-1}, Ain1 and Ain1(R216E): 86477 M^{-1} cm^{-1}. Proteins were labeled with TMR-6-maleimide (Life Technologies, Grand Island, NY) or Cy5-monomaleimide (GE Healthcare, Little Chalfont, UK) dyes as per manufacturer's protocols immediately following purification, and were flash-frozen in liquid nitrogen and kept at -80°C. For proteins labeled on one cysteine residue (Cdc8 I76C mutant), labeling efficiency was determined by taking the absorbance at the emission max of the dye and calculating the coupling efficiency (Kim et al., 2008).

TIRF microscopy

Time-lapse TIRFM movies were obtained using a cellTIRF 4Line system (Olympus) fitted to an Olympus IX-71 microscope with through-the-objective TIRF illumination and a iXon EMCCD camera (Andor Technology). Mg-ATP-actin (15% Alexa 488-labeled) was mixed with labeled or unlabeled actin binding proteins and a polymerization mix (10 mM imidazole (pH 7.0), 50 mM KCl, 1 mM MgCl2, 1 mM EGTA, 50 mM DTT, 0.2 mM ATP, 50 μM CaCl2, 15 mM glucose, 20 μg/mL catalase, 100 μg/mL glucose oxidase, and 0.5% (400 centipoise) methylcellulose) to induce F-actin assembly (Winkelman et al., 2014). The mixture was then added to a flow chamber and imaged at 2.5 or 5 s intervals at room temperature.

Quantification of bundling

The percentage of actin filaments bundled was quantified at similar actin filament densities (between 2095 and 2295 μm total) for each experiment. The total actin filament length in the chamber was measured manually by creating ROIs for every actin filament. ROIs for every segment of actin filament present in a bundle were then created, and the ratio of actin filament present in a bundle vs. total actin filament length was quantified.

Section 4.3—RESULTS

A survey in fission yeast identifies potential ABP competitors

We hypothesize that a series of competitive interactions between ABPs results in proper ABP sorting. If this hypothesis is true, we predicted that mislocalizing an ABP or set of ABPs from one F-actin network to another should affect the localization of ABPs typically present on the second network. Therefore, we sought to mislocalize ABPs within the fission yeast cell in order to probe any potential competitive interactions between ABPs. In order to mislocalize a set of ABPs, we depleted one F-actin network, the actin patch, from the fission yeast cell. We then examined ABP localization following actin patch depletion. When actin patches are depleted, ABPs typically associated with actin patches will be released into the cytoplasm. They are then free to remain in the cytoplasm or associate with another F-actin network: actin cables or the contractile ring. The localization of an ABP upon the removal of its primary actin network provides information into its involvement in a potential ABP hierarchy. If an actin patch ABP is an upstream 'gatekeeper' protein that typically displaces other ABPs from the actin patch, upon localization to another F-actin network, such as the contractile ring, it could displace other ABP competitors off of the contractile ring. In addition, if a patch ABP remains in the cytoplasm following patch removal, that could suggest that other ABPs are inhibiting it from associating with the contractile ring, or other mechanisms promote its association specifically with actin patches.

Actin patches were depleted using the Arp2/3 complex inhibitor CK-666 (Burke et al., 2014; Nolen et al., 2009). When fission yeast cells expressing Lifeact-GFP are treated with CK-666, we observe a depletion in actin patches and the formation of excessive actin cable and ring material (Figure 4-1A, (Burke et al., 2014)). Upon patch depletion, ABPs typically associated

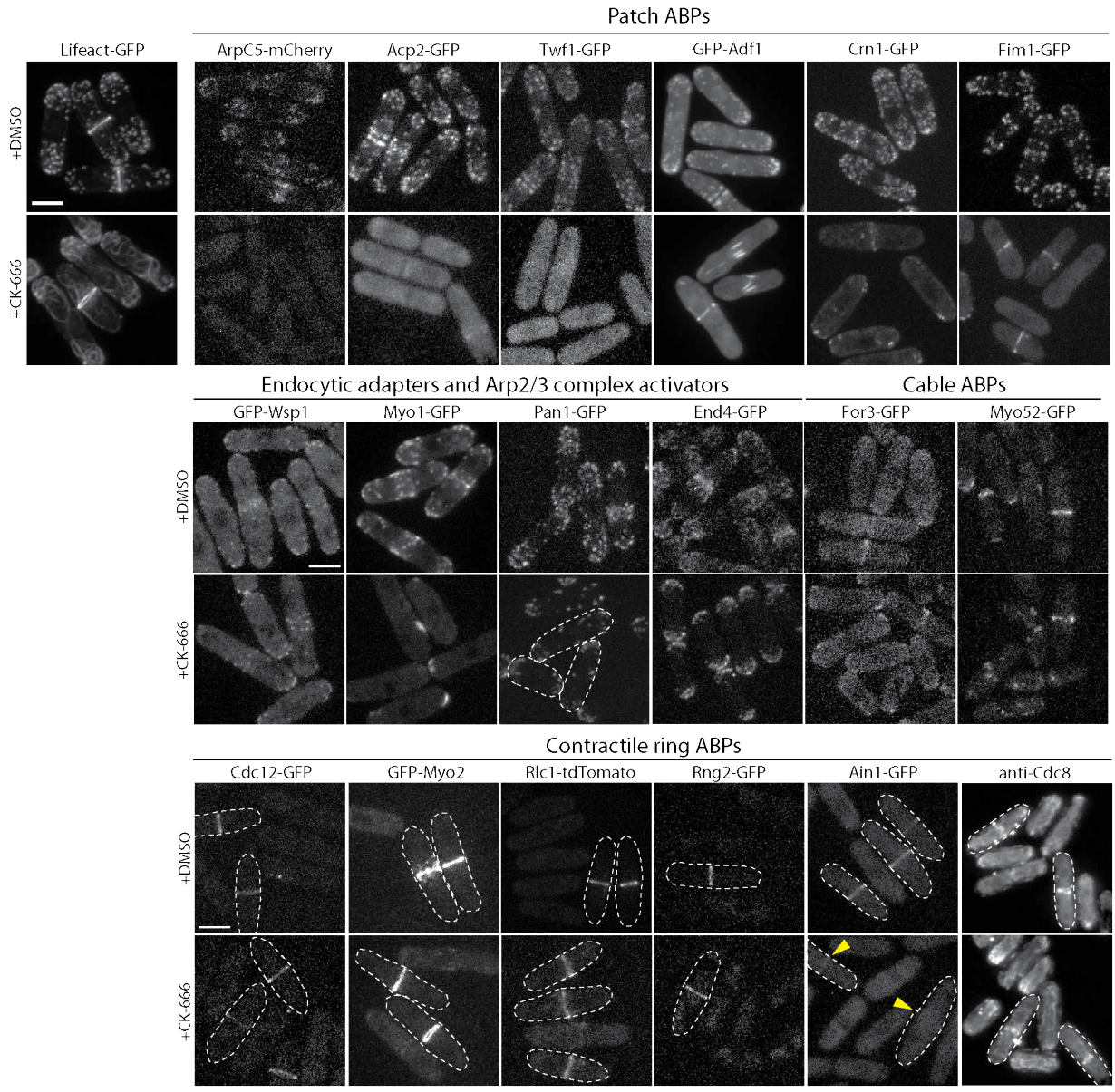

Figure 4-1: Fission yeast ABPs relocalize following treatment with Arp2/3 complex inhibitor CK-666.

Fluorescent micrographs of fission yeast cells expressing an actin marker **(A)** or ABPs that typically localize to actin patches **(B)**, endocytic adaptors **(C)**, Arp2/3 complex activators **(C)**, and ABPs that normally localize to actin cables **(D)** or the contractile ring **(E)** treated with DMSO (control) or Arp2/3 complex inhibitor CK-666. All ABPs are tagged at the endogenous locus and expressed from the endogenous promoter except for actin (Lifeact-GFP marker), cofilin GFP-Adf1 (Adh promoter), and tropomyosin Cdc8 (anti-Cdc8 antibody). Yellow arrowheads denote site of contractile ring. Dotted lines outline individual fission yeast cells for clarity.

with patches display a variety of localizations. Arp2/3 complex subunit ArpC5, capping protein Acp2, and twinfilin Twf1 all localized to the cytoplasm following patch depletion (Figure 4-1B),

and were not observed to associate with any other F-actin networks. Arp2/3 complex activators Wsp1 and Myo1 and endocytic adapters End1 and Pan1 maintained cortical localization following patch depletion (Figure 4-1C), but did not associate with any visible F-actin. On the other hand, three patch ABPs, fimbrin Fim1 (Figure 4-2A), coronin Crn1, and cofilin Adf1, relocalized to the contractile ring (Figure 4-1B) following patch depletion. Interestingly, all three ABPs that relocalize to the contractile ring following CK-666 treatment are known to localize in small amounts to the contractile ring under normal circumstances (Nakano et al., 2001; Nakano and Mabuchi, 2006b; Pelham and Chang, 2001), perhaps suggesting that each of these ABPs has an initial preference for actin patches, but when patches are removed, will localize to any available F-actin.

F-actin crosslinking proteins Fimbrin Fim1 and α-actinin Ain1 compete at the contractile ring and actin patches

The majority of contractile ring ABPs retain their localization following CK-666 treatment (Figure 4-1E). However, α-actinin Ain1 is depleted from the contractile ring following CK-666 treatment (Figure 4-2B, Figure 4-1E), suggesting that another ABP may be competing it off of the contractile ring. Fimbrin Fim1, coronin Crn1, and cofilin Adf1 were prime candidates as they strongly localize to the contractile ring following CK-666 treatment. As fimbrin Fim1 and α-actinin Ain1 are both actin crosslinking proteins, we hypothesized that fimbrin Fim1 may be associating with the contractile ring and competitively displacing α-actinin Ain1. In order to test this hypothesis, we generated a *fim1-1Δ*, Ain1-GFP strain in order to observe α-actinin Ain1 localization in the absence of its putative competitor. In a *fim1-1Δ* background, Ain1-GFP was not displaced from the contractile ring following CK-666 treatment, suggesting that fimbrin

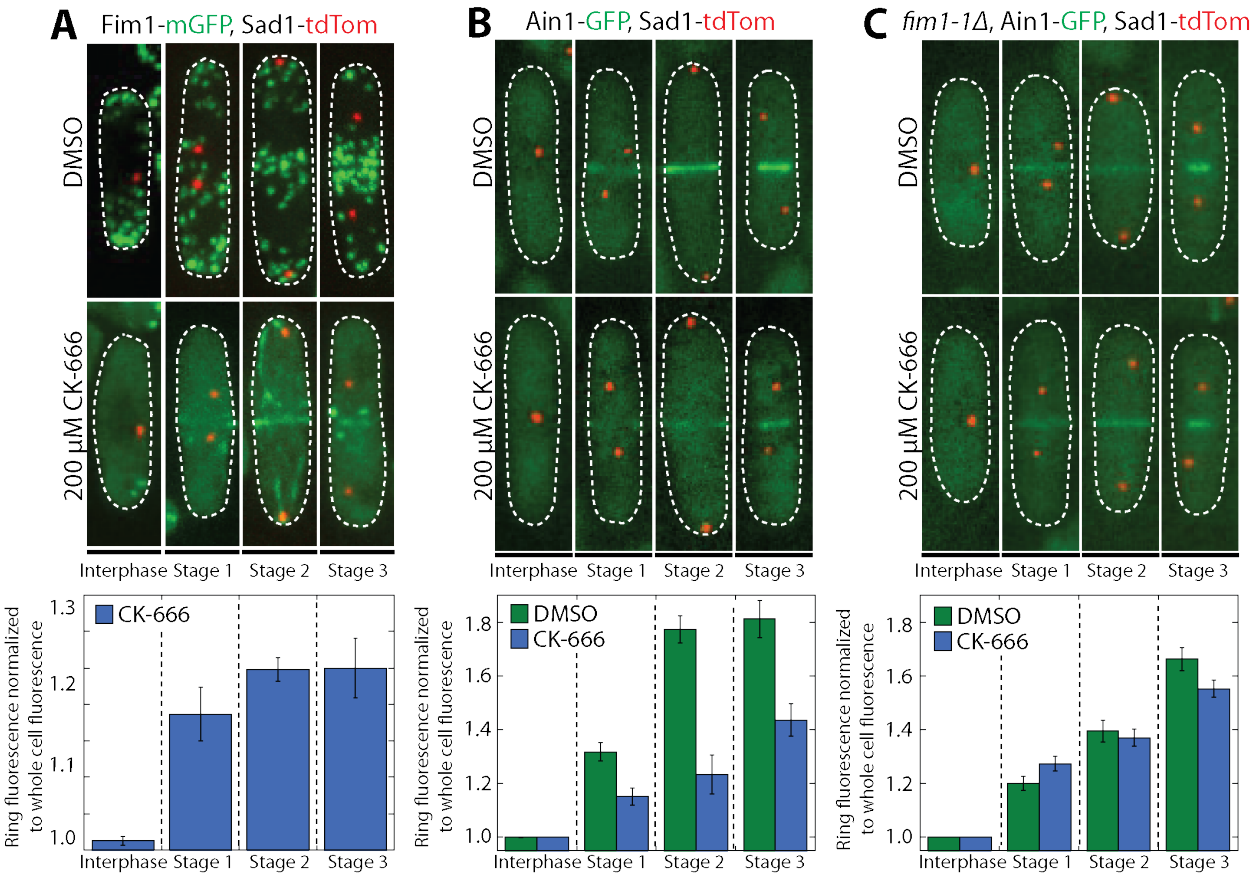

Figure 4-2: Fimbrin Fim1 displaces α-actinin Ain1 from the contractile ring following CK-666 treatment.
(A-C) (Top) Fission yeast cells expressing spindle pole body marker Sad1-tdTomato and Fim1-mGFP **(A)**, Ain1-GFP **(B)**, or Ain1-GFP in a *fim1-1Δ* background **(C)**. **(Bottom)** Mean Fim1-mGFP **(A)** or Ain1-GFP **(B,C)** ring fluorescence normalized to whole cell fluorescence was quantified for cells in interphase, stage 1 (ring formation), stage 2 (ring dwell), or stage 3 (ring constriction) following treatment with DMSO (control) or CK-666. Error bars=s.e. n≥10 cells.

Fim1 and α-actinin Ain1 are competitors (Figure 4-2C). Localization of fimbrin Fim1 to the contractile ring and displacement of α-actinin Ain1 from the contractile ring occurred in each stage of contractile ring formation (Figure 4-2).

If competition between fimbrin Fim1 and α-actinin Ain1 for association with F-actin is a primary driver of their sorting, we expected to observe competition at both the contractile ring and at actin patches. However, in a *fim1-1Δ*, Ain1-GFP strain, no Ain1-GFP is observed at actin patch sites (Figure 4-2C, Figure 4-3A). Though this finding could suggest that fimbrin Fim1 and

α-actinin Ain1 competition may be limited to contractile ring, perhaps as a result of additional competitive interactions with other ABPs, we suspected that the low number of α-actinin Ain1 polypeptides in the cell (3,600±500; Wu and Pollard, 2005) and a high density of F-actin at patch sites (5,000-7,000 in each of 30-50 actin patches (Sirotkin et al., 2010; Wu and Pollard, 2005) may dilute the Ain1-GFP signal enough that it is not visible.

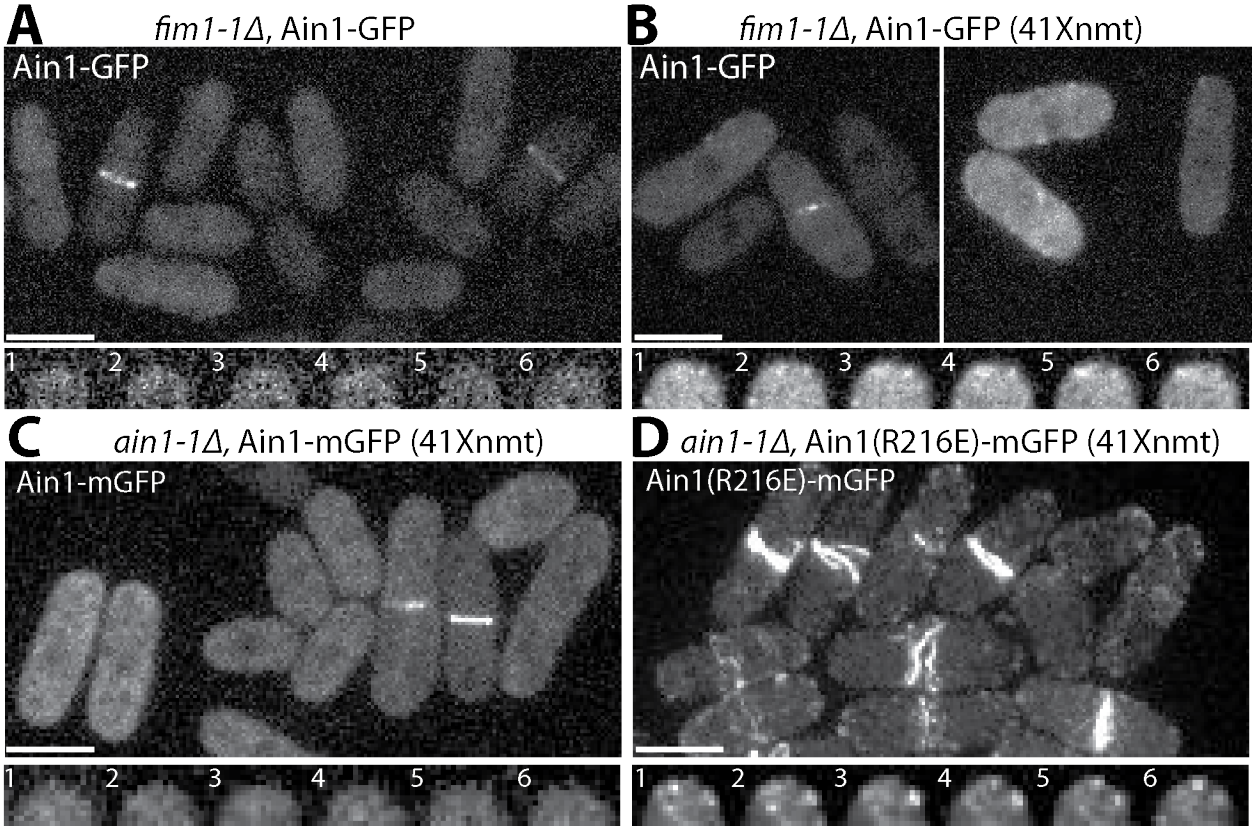

Figure 4-3: Fimbrin Fim1 and α-actinin Ain1 compete at the contractile ring and at actin patches.
(A-B, Top panels) Fluorescence micrographs of fission yeast in a *fim1-1Δ* background expressing GFP-tagged α-actinin Ain1 at endogenous levels **(A)** or overexpressed from the 41xnmt promoter for 20 hours **(B). (Bottom panels)** Timelapse of a cell end taken from a single plane over time. Time in sec. **(C-D)** Fluorescence micrographs of fission yeast in an *ain1-1Δ* background overexpressing GFP-tagged wild-type α-actinin Ain1 **(C)** or less-dynamic mutant α-actinin Ain1(R216E) **(D)** from the 41xnmt promoter.

If our inability to see Ain1-GFP is due to low signal, increasing the concentration of Ain1-GFP should allow us to observe Ain1-GFP at actin patches, but only in a *fim1-1Δ* background. In a

fim1-1Δ background, Ain1-mGFP overexpressed under the 41xnmt promoter can be observed at actin patch sites (Figure 4-3B). Importantly, similarly overexpressed Ain1-mGFP is not observed at actin patch sites in a strain expressing endogenous fimbrin Fim1, demonstrating that fimbrin Fim1 and α-actinin Ain1 compete at actin patches (Figure 4-3C).

Fimbrin Fim1 and α-actinin Ain1 dynamics on F-actin determine their ability to compete in vitro and in vivo

A series of mutational studies followed by cryo-EM images of fimbrin and α-actinin from several organisms have demonstrated that they bind to the same site on an actin filament (Galkin et al., 2010; Holtzman et al., 1994; Honts et al., 1994; McGough et al., 1994; Galkin et al., 2008), suggesting that competition between fimbrin and α-actinin in fission yeast may be via competition for binding to the same site on F-actin. Though bind to the same site on an actin filament, fimbrin Fim1 and α-actinin Ain1 have very different dynamics on single actin filaments and F-actin bundles. Fimbrin Fim1 is relatively stable on single filaments (k_{off}= 0.043±0.001 s^{-1}) and very stable on F-actin bundles (k_{off}=0.023±0.003 s^{-1}). α-actinin Ain1, on the other hand, is not observed to bind to single filaments and is extremely dynamic on F-actin bundles (k_{off}=3.33 s^{-1} on two-filament and three-filament bundles). We suspected that the difference in dynamics explained fimbrin Fim1's ability to outcompete α-actinin Ain1, as fimbrin Fim1 simply remained on actin filaments for a longer period of time, blocking α-actinin Ain1's access. In order to test this hypothesis, we used an α-actinin Ain1 mutant, Ain1(R216E), that is less dynamic on F-actin bundles (k_{off}=0.67 s^{-1} and k_{off}=0.33 s^{-1} on two- and three-filament bundles, respectively) (Li et al., 2016) and observed its ability to compete with fimbrin Fim1 in fission yeast cells and using in vitro TIRF microscopy.

In order to investigate the mechanism of competition, we utilized multi-color TIRF microscopy to visualize fluorescently labeled fimbrin Fim1 in the presence or absence of unlabeled wild-type α-actinin Ain1 on actin filaments. 50 nM of Fimbrin Fim1 alone fully decorated actin bundles (Figure 4-4A). In the presence of 1 μM Ain1 or Ain1(R216E), less fimbrin Fim1 is localized to F-actin bundles than when fimbrin Fim1 is present alone (Figure 4-4A,B), though no difference is observed between wild-type Ain1 and mutant Ain1(R216E).

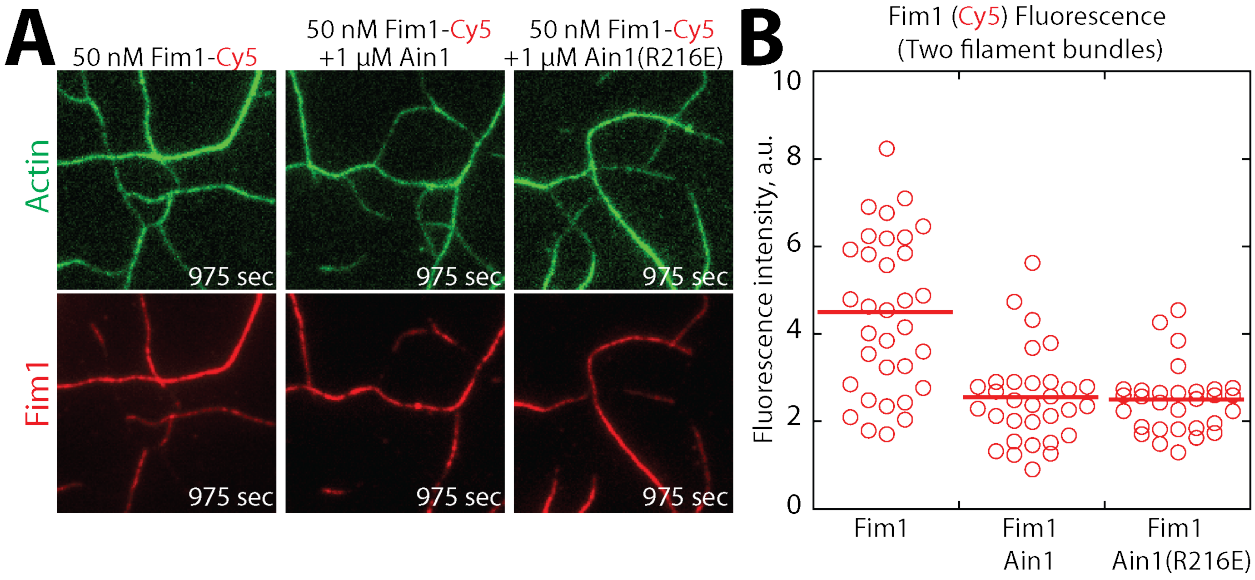

Figure 4-4: Fimbrin Fim1 and α-actinin Ain1 compete for association with F-actin. **(A-B)** Two-color TIRFM of 1.5 μM Mg-ATP actin (15% Alexa 488-labeled) with 50 nM fimbrin Fim1 (Cy5-labeled) alone (left) or with 1 μM wild-type Ain1 (middle) or 1 μM mutant Ain1(R216E) (right). **(B)** Dot plots of the amount of Fim1-Cy5 fluorescence on two-filament bundles in the absence or presence of Ain1 or Ain1(R216E). n≥30 measurements.

Interestingly, in fission yeast cells expressing endogenous fimbrin Fim1, overexpressed mutant Ain1(R216E)-mGFP localizes to actin patches (Figure 4-3D) while overexpressed wild-type Ain1-mGFP does not (Figure 4-3C), suggesting that a more stable α-actinin is better able to compete with fimbrin at actin patches despite no observed difference in vitro.

At low concentrations of labeled fimbrin Fim1 (5 nM) and high concentrations of unlabeled α-actinin Ain1 (400 nM), we can observe a self-sorting phenomenon, whereby fimbrin

Fim1 sorts to specific two-filament bundles, but is excluded from other two-filament bundles, presumably by α-actinin Ain1 (Figure 4-5). The observation of bundling proteins self-segregating to different bundled regions has been previously noted for actin bundling proteins fascin and human α-actinin 4 (Winkelman et al., 2016). However, we see less distinct segregation between Fim1 and Ain1. As we hypothesize that this self-sorting behavior is the result of compact bundlers segregating to different bundled regions than wider bundlers, we suspect that the smaller difference in bundle spacing between Fim1 and Ain1 (~12 nm/~20 nm for S. pombe Fim1/Ain1 compared to ~8 nm/~40 nm for fascin/HsACTN4) (Hanein et al., 1998) may result in less stringent boundary denotations.

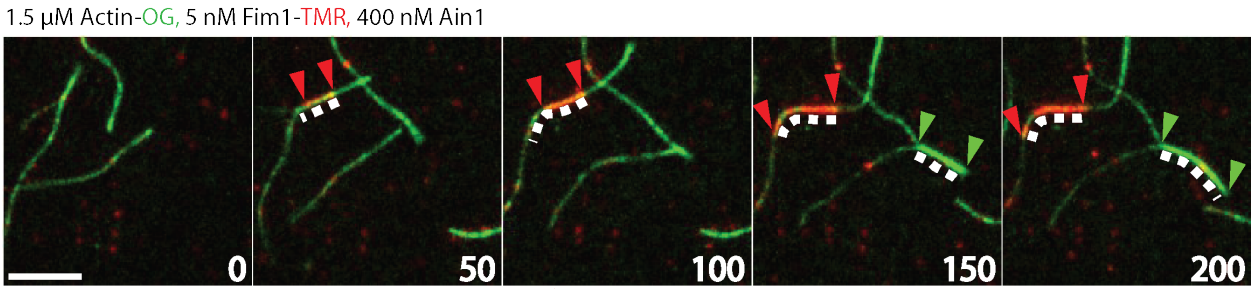

Figure 4-5: Fimbrin Fim1 and α-actinin Ain1 self-sort to distinct two-filament bundles *in vitro.*
(A-B) Two-color TIRFM of 1.5 μM Mg-ATP actin (15% Alexa 488-labeled) with fimbrin Fim1 (TMR-labeled) and wild-type α-actinin Ain1 (unlabeled).

Tropomyosin Cdc8 and α-actinin Ain1 do not compete on actin filaments

We have demonstrated that fimbrin Fim1 and α-actinin Ain1 compete for binding to F-actin, and that fimbrin Fim1's stable association with F-actin bundles allows it to prevent association of α-actinin Ain1 with actin patches. However, the number of fimbrin Fim1 polypeptides in the cell is ~20 times the number of α-actinin dimers (Wu and Pollard, 2005) raising the question as to how α-actinin is capable of preventing fimbrin Fim1 from associating

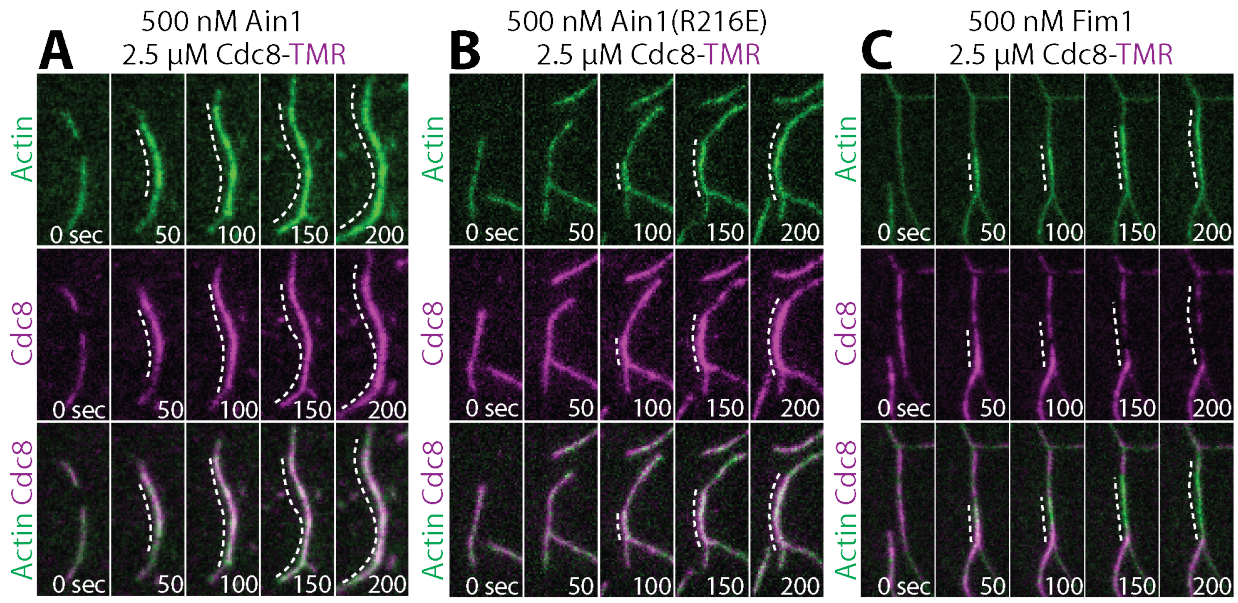

Figure 4-6: α-actinin Ain1 does not displace tropomyosin Cdc8 from F-actin bundles. **(A-C)** Two-color TIRFM of 1.5 µM Mg-ATP actin (15% Alexa 488-labeled) with tropomyosin Cdc8 (TMR-labeled) and 500 nM **(A)** wild-type α-actinin Ain1 (unlabeled), **(B)** less dynamic bundling mutant α-actinin Ain1(R216E), or **(C)** fimbrin Fim1 (unlabeled). Dotted lines denote bundled region.

with the contractile ring under normal circumstances. We hypothesized that another ABP may work together with α-actinin to prevent fimbrin association with the contractile ring. We investigated the role of tropomyosin Cdc8, a side-binding protein that associates with the contractile ring, in this competition. Fimbrin has been shown to displace tropomyosin from F-actin bundles (Figure 3-8, Skau and Kovar, 2010). As multiple fimbrin and α-actinin isoforms have been demonstrated to bind to the same site on F-actin, we wondered if α-actinin Ain1 would displace tropomyosin Cdc8 from a bundled network similarly to fimbrin Fim1. In vitro, we observe no displacement of Cdc8 from Ain1-bundled networks (Figure 4-6A), demonstrating that Ain1 and Cdc8 are capable of co-existing on the same F-actin network, as they do in vivo at the contractile ring. In addition, we find that Cdc8 greatly enhances the bundling ability of Ain1 (Figure 4-7A,B). The presence of 500 nM tropomyosin Cdc8 is capable of increasing α-actinin-mediated bundling 10-fold over α-actinin alone (Figure 4-7B).

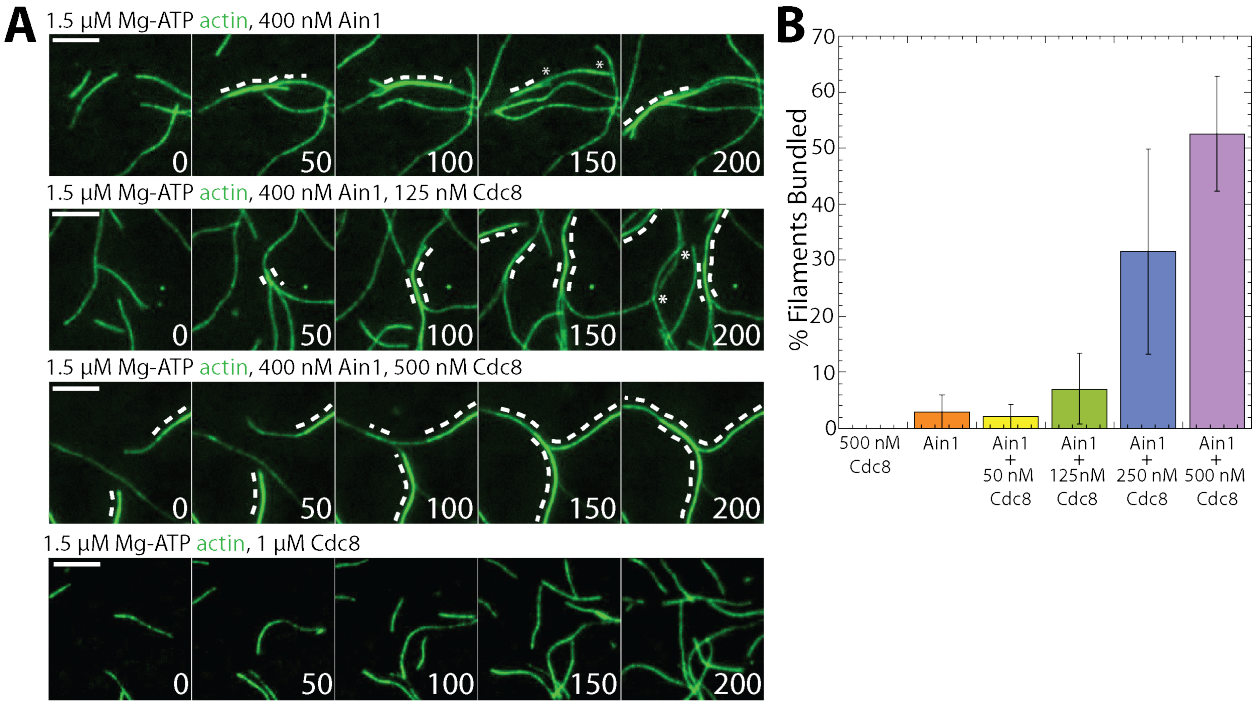

Figure 4-7: Tropomyosin Cdc8 increases α-actinin Ain1-mediated bundling.
(A) TIRFM of 1.5 µM Mg-ATP actin (15% Alexa 488-labeled) in the presence of α-actinin Ain1 and a range of concentrations of tropomyosin Cdc8. Dotted lines indicate the bundled region. Scale bar, 5 µm. Time in sec. **(B)** Quantification of percent of F-actin bundled under 400 nM α-actinin Ain1 and a range of concentrations of tropomyosin Cdc8.

Tropomyosin Cdc8 and α-actinin Ain1 cooperate to displace fimbrin Fim1 from actin filaments

We have demonstrated that fimbrin Fim1 is a better competitor than either α-actinin Ain1 or tropomyosin Cdc8 alone. However, we have also shown that tropomyosin Cdc8 enhances the bundling ability of α-actinin Ain1, suggesting that tropomyosin Cdc8 could potentially work with α-actinin Ain1 to prevent fimbrin Fim1 association with F-actin at the contractile ring. In order to determine if α-actinin Ain1 and tropomyosin Cdc8 could work together to inhibit fimbrin Fim1 association with actin filaments, we performed three-color TIRF microscopy with labeled ABPs and quantified fimbrin Fim1 association with F-actin in the presence of tropomyosin Cdc8 and/or α-actinin Ain1. When fimbrin Fim1 is the only ABP present, it fully

coats actin bundles (Figure 4-4A). In the presence of either tropomyosin Cdc8 (Figure 4-8A,C) or α-actinin Ain1 (Figure 4-4A,B) alone, less fimbrin Fim1 is associated with two-filament bundles, demonstrating that though fimbrin Fim1 is a better competitor than α-actinin Ain1 or tropomyosin Cdc8 alone, both compete to different extents with fimbrin Fim1 for association with F-actin.

In the presence of fimbrin Fim1 alone, tropomyosin Cdc8 is displaced from actin filaments in a cooperative way, with segments of F-actin completely devoid of tropomyosin Cdc8, concurrent with regions of high fimbrin Fim1 localization (Figure 4-8A, yellow boxes). In the presence of fimbrin Fim1 and α-actinin Ain1, less tropomyosin Cdc8 is displaced from F-actin. We speculate that, though Ain1 alone is a poor competitor with Fim1, its competition for the same binding site as Fim1 allows it to prevent long stretches of Fim1 from forming that might displace tropomyosin Cdc8. The inability of Fim1 to cooperatively associate on F-actin along with Cdc8's ability to compete it off of actin filaments result in Fim1 poorly associating with F-actin in the presence of both Cdc8 and Ain1.

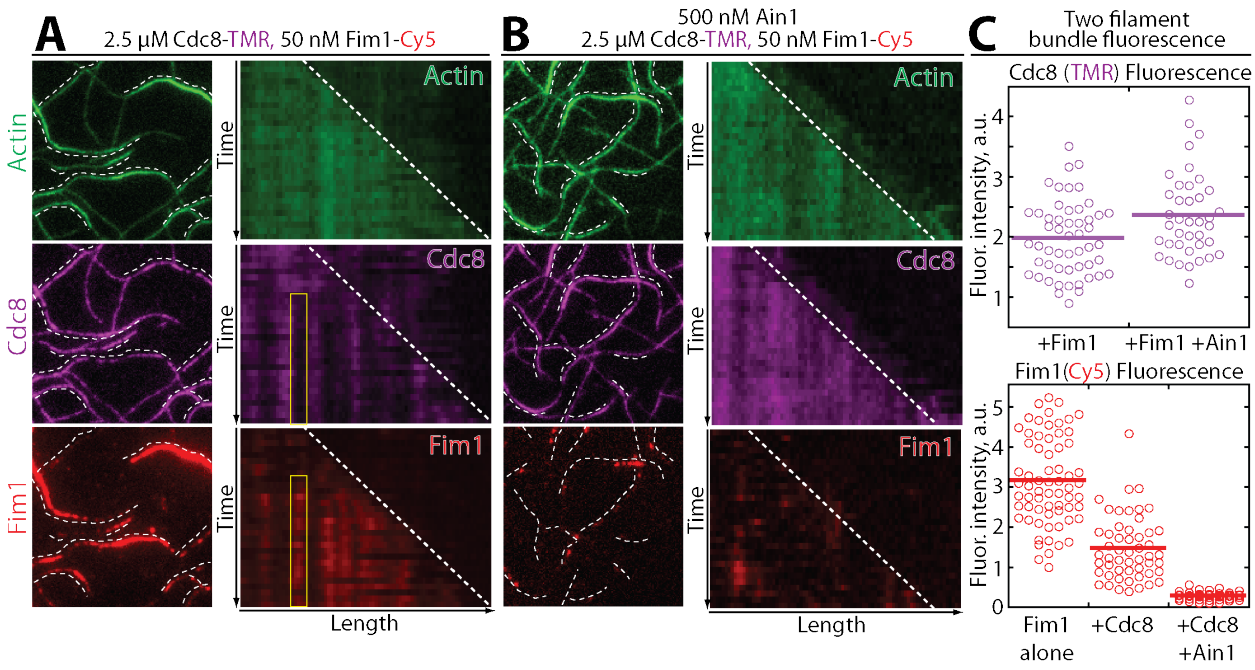

Figure 4-8: Tropomyosin Cdc8 and α-actinin Ain1 cooperate to compete with fimbrin Fim1 for association with actin filaments.
(A-C) Three-color TIRFM of 1.5 μM Mg-ATP actin (15% Alexa 488-labeled) with 50 nM fimbrin Fim1 (Cy5-labeled) and 2.5 μM tropomyosin Cdc8 (TMR-labeled) in the **(A)** absence or **(B)** presence of 500 nM α-actinin Ain1. Kymographs of actin, fimbrin Fim1, and tropomyosin Cdc8 during bundle formation. Dotted lines indicate bundled regions. **(C)** Dot plots of the amount of Cdc8-TMR (top) or Fim1-Cy5 fluorescence (bottom) on two-filament bundles in the presence of tropomyosin Cdc8 and fimbrin Fim1 or tropomyosin Cdc8, fimbrin Fim1, and α-actinin Ain1. n≥30 measurements.

Section 4.4—DISCUSSION

Fimbrin Fim1 association with the contractile ring is prevented by several mechanisms

Our model is that in a wild-type cell, fimbrin Fim1's association with the contractile ring is inhibited by 1) its preferred association with actin patches and 2) synergistic activities between tropomyosin Cdc8 and α-actinin Ain1 that inhibit fimbrin Fim1 from associating with the contractile ring. We suspect that Fim1 preferentially associates with actin patches over other F-actin networks. If that is the case, actin patches could act as a 'sink' for Fim1, harboring Fim1 from associating with other F-actin networks. This preference of Fim1 for actin patches could result from an architectural preference for branched filaments or a particular twist or

conformational change on Arp2/3 complex-assembled F-actin. Alternatively, other upstream ABPs could recruit Fim1 to actin patches by other mechanisms.

However, a sink model cannot fully account for Fim1 localization given the Fim1 concentration in the cell. If we assume that there are 50 patches per fission yeast cell (Sirotkin et al., 2010) and ~500 fimbrin Fim1 polypeptides in each actin patch (Wu and Pollard, 2005), at most ~25,000 fimbrin Fim1 polypeptides are associated with actin patches. That leaves 61,500 fimbrin Fim1 polypeptides within the cytoplasm and with access to F-actin networks such as the contractile ring. Therefore, other mechanisms must be in place to prevent Fim1 association with other F-actin networks.

Fimbrin Fim1 and α-actinin Ain1 as competitors

In vitro, we found that α-actinin Ain1 is a competitor with Fim1. We observe that Fim1 fluorescence is decreased on two-filament bundles in the presence of wild-type Ain1 and mutant Ain1(R216E) (Figure 4-4). Though we initially speculated that the residence time of an ABP on actin bundles would be important for their ability to compete, and that Fim1 was capable of outcompeting Ain1 as a result of its longer dwell time on F-actin bundles, an Ain1(R216E) mutant with increased residence time showed no increased ability to compete with Fim1 in vitro. However, the residence time of this Ain1(R216E) mutant is still much shorter than Fim1, suggesting that dynamics may still play a role in ABP competition. It is possible that slight differences in dynamics have a bigger effect in a cellular context, as overexpressed wild-type Ain1 does not localize to actin patches in the presence of fimbrin, while overexpressed mutant Ain1(R216E) does.

Tropomyosin Cdc8 enhances α-actinin Ain1-mediated bundling of F-actin

We demonstrated that increasing concentrations of tropomyosin Cdc8 enhance F-actin bundling in the presence of α-actinin Ain1 (Figure 4-7). Our initial hypothesis was that the presence of tropomyosin Cdc8 enhanced the residence time of Ain1 on F-actin. However, preliminary single molecule experiments have demonstrated that the run time was similar for Ain1 on Cdc8-coated and uncoated actin filaments (data not shown). Therefore, we hypothesize that the change in persistence length that occurs as a result of tropomyosin Cdc8 association with F-actin may make the filaments more likely to be bundled, as they are more rigid and incorporation of a part of the filament into a bundle may force the rest of the filament into the bundle. In the future, we can use small amounts of phalloidin to alter the persistence length of F-actin and test this hypothesis. Additionally, modeling of contractile ring formation in the presence of Ain1 has demonstrated how Ain1 dynamics affect contractile ring formation (Li et al., 2016). By altering the persistence length of the modeled actin filaments in a simulated system, we can also determine the affect of filament persistence length on F-actin bundling.

Tropomyosin Cdc8 and α-actinin Ain1 work together to compete with fimbrin Fim1 at the contractile ring

Despite the ability of fimbrin Fim1 to actively displace tropomyosin Cdc8 from F-actin bundles (Figure 3-8, Figure 4-6), Cdc8 is also capable of inhibiting Fim1 association with F-actin (Figure 4-8). Together, we observe that Ain1 and Cdc8 are capable of displacing Fim1 from F-actin bundles to a significantly greater degree than either alone. It should be noted that though Ain1 and Cdc8 work together to compete with Fim1, this competition is only obvious at low concentrations of Fim1 (Figure 4-8). Similarly, in the cell, though tropomyosin Cdc8 and α-

actinin Ain1 could prevent access of a portion of Fim1 polypeptides to contractile ring F-actin, the potent F-actin binding and bundling capabilities of Fim1 make it seem unlikely that Cdc8 and Ain1 would be able to prevent association of all cytoplasmic Fim1. Therefore, we suspect that there are potentially other ABPs or sets of ABPs at the contractile ring that inhibit Fim1 association. Additionally, recent work in budding yeast has demonstrated that fimbrin Sac6 is phosphorylated at different stages of the cell cycle, and that this phosphorylation affects its ability to bundle F-actin (Miao et al., 2016). It is possible that a similar post-translational modification might affect fission yeast Fim1, and that a portion of the large pool of Fim1 within the cytoplasm might be in an inactive or less active state. Future work will seek to determine whether Fim1 and other ABPs are post-translationally modified and how these modifications affect their ability to compete with other ABPs and sort to the correct F-actin network.

Other factors in proper ABP sorting

There are still several findings that cannot be explained solely by competition. We have shown that tropomyosin Cdc8 remains associated with the contractile ring following CK-666 treatment, when fimbrin Fim1 relocalizes to the contractile ring and displaces α-actinin Ain1 (Figure 4-1, Figure 4-9). As fimbrin Fim1 and tropomyosin Cdc8 are known competitors, why isn't tropomyosin Cdc8 also displaced from the contractile ring when excessive fimbrin Fim1 associates with the contractile ring? There are obviously other factors at play that keep tropomyosin Cdc8 at the contractile ring. These factors could be a preferred association of tropomyosin Cdc8 with formin-assembled filaments or other ABPs that stabilize tropomyosin Cdc8 specifically with contractile ring F-actin.

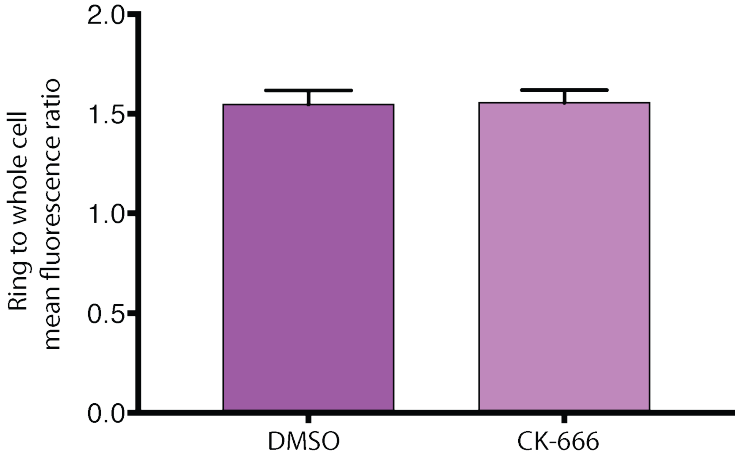

Figure 4-9: Tropomyosin Cdc8 does not leave the contractile ring following CK-666 treatment.
Mean anti-Cdc8 ring fluorescence normalized to total cell fluorescence. Error bars=s.e., n≥10 cells.

Additionally, we found that in a *fim1-1Δ* background, the amount of Ain1-GFP is the same on the contractile ring in DMSO or CK-666 treated cells. However, the total amount of Ain1-GFP localized to the contractile ring is lower in a *fim1-1Δ* background than in a wild-type background (Figure 4-2C). These findings are puzzling, as at face value they seem to suggest that Fim1 somehow enhances association of Ain1 with the contractile ring. However, we speculate that multiple competitive interactions may cause this phenotype. For example, in a *fim1-1Δ* background, tropomyosin Cdc8 localizes to actin patches (Skau and Kovar, 2010). Cdc8's association with actin patches could inhibition cofilin Adf1 from associating with actin patches, displacing it to the contractile ring, where it could displace Ain1 by competition for binding sites. Additionally, other ABPs that we have not studied closely may also localize to different networks in a *fim1-1Δ* background, affecting Ain1 localization. Future work will involve investigating these potential ABP localizations in vivo. In particular, another survey could be performed in which one ABP is deleted from the genome (*fim1-1Δ,* for example), and the localization of every other ABP-GFP is examined following the disruption of a single ABP. This survey could then be completed for other ABP knockouts. This systematic approach would certainly yield interesting information regarding other competitive interactions between ABPs in vivo.

CHAPTER 5: CONCLUSIONS, IMPLICATIONS, AND FUTURE DIRECTIONS

Section 5.1—ACTIN BINDING PROTEINS COMPETE BY PASSIVE AND ACTIVE MECHANISMS

Passive competition

We have identified several ABPs that have competitive interactions and determined the molecular mechanisms behind their competition. These competitive mechanisms can be divided generally into two types: passive or active modes of competition. In passive competition, one ABP competes with another ABP by blocking its ability to bind (Figure 5-1A). In instances of passive competition, the most successful competitor will 1) associate with an actin filament first and 2) remain associated with an actin filament for the longest amount of time. Therefore, the k_{on} and k_{off} of two ABPs can provide some indication as to their ability to compete. We identified fission yeast fimbrin Fim1 and α-actinin Ain1 as competitors. Fim1 and Ain1 are believed to associate with the same site on F-actin, but Fim1 has a longer residence time on two-filament actin bundles than Ain1 (residence time=~43.4 sec for Fim1 vs. 0.3 sec for Ain1), likely affecting its ability to remain associated with F-actin and outcompete Ain1 both in vivo (Figure 4-2, 4-3) and in vitro (Figure 4-4). We utilized a less dynamic Ain1 mutant Ain1(R216E) in order to test our hypothesis that residence time on F-actin bundles affected an ABP's ability to compete. We found that Ain1 and Ain1(R216E) similarly displaced Fim1 from two-filament bundles in vitro, though in vivo an overexpressed Ain1(R216E) was capable of localizing to patches, while Ain1 was not. This data suggests that ability to reside on actin bundles may affect ability to compete. However, though Ain1(R216E) has a slightly longer residence time (residence time=1.5±0.3 sec), than Ain1 (residence time=0.3±0.04 sec), it still has a considerably

lower residence time than Fim1 (residence time=~43.4 sec), potentially explaining its poor ability to compete in vitro.

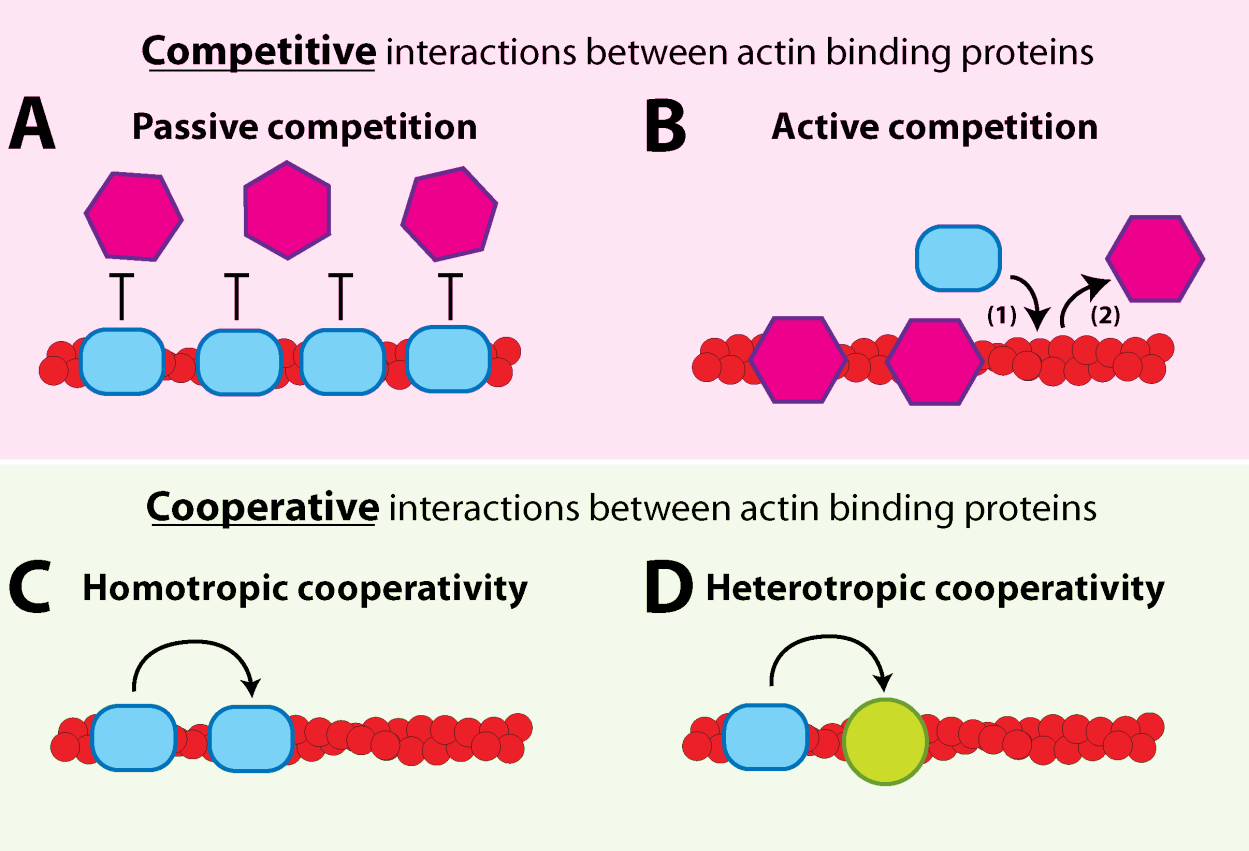

Figure 5-1: Mechanisms of competition and cooperativity between ABPs.
(A) Passive competition involves an ABP (blue oval) associating with an actin filament and preventing the association of another ABP (magenta hexagon) with that filament. **(B)** Active competition involves the competing ABP (blue oval) associating directly with another ABP (magenta hexagon) or indirectly via the actin filament (1). This action then results in the removal of the first ABP from the actin filament (2). **(C)** Homotropic cooperativity involves one type of ABP (blue oval) recruiting the same type of ABP to the actin filament. **(D)** Heterotropic cooperativity involves one type of ABP (blue oval) recruiting a second type of ABP (green circle) to the actin filament.

Fission yeast fimbrin Fim1 and cofilin Adf1 also likely compete by binding to the same (or similar) site on F-actin. However, whereas Fim1 and α-actinin Ain1 bind to the same site and are thought to make the same slight change in the actin filament, Fim1 and Adf1 make distinctly different conformational changes to the actin filament (Hanein et al. 1997; Galkin et al. 2011),

adding an additional layer of complexity to their competition. Indeed, we suspect that the difference in conformational change results in local alterations in flexibility that increase the rate of Adf1-mediated severing in the presence of Fim1.

Finally, passive competition is evident in tropomyosin Cdc8's inhibition of initial cofilin Adf1 association with F-actin. We observe that tropomyosin Cdc8 prevents only the initial association of cofilin Adf1 with F-actin (Figure 3-10), as once cofilin Adf1 associates with F-actin, it cannot be displaced by tropomyosin Cdc8 (Figure 3-10D,F). Certain properties of Cdc8 may explain its role as a passive competitor. Individual Cdc8 molecules poorly associate with actin filaments, and Cdc8 molecules primarily associate with F-actin by elongating already-present Cdc8 cables. This poor ability to associate suggests that Cdc8 would likely be unable to compete with an ABP already present on an actin filament. Additionally, the cable-like properties of Cdc8 and the multiple interactions between a Cdc8 strand and the actin filament could allow a Cdc8 cable to remain associated despite perturbations along the actin filament that may occur as a result of the association of other ABPs with the actin filament. Cdc8 would be a particularly successful competitor against an ABP like Adf1 that is delayed in its association with F-actin as a result of its preference for ADP-actin. Cdc8 can arrive first, and block binding of Adf1. When ATP hydrolysis and phosphate release occurs, slight conformational changes in the actin filament or tropomyosin binding site may change, enhancing the ability of Adf1 to associate with the actin filament. Adf1 could then twist the actin filament, enhancing the ability of other Adf1 molecules to bind while displacing Cdc8 from the actin filament.

Active competition

As opposed to passive competition, in which ABPs are competing for open binding sites, active competition involves the active displacement of an ABP already present on an actin filament (Figure 5-1B). Active competition, therefore, would necessitate either a direct ABP-ABP interaction, or a conformational or architectural change to the actin filament. The most obvious example of active displacement that we observed is in displacement of tropomyosin Cdc8 from F-actin bundles by fimbrin Fim1. We observe that when both Cdc8 and Fim1 are present in the chamber, Cdc8 localizes to single actin filaments. However, once Fim1 bundles two filaments together, Cdc8 is rapidly displaced from the bundled region. This displacement could potentially be the result of the creation of a tight bundle that is unfavorable to Cdc8 localization. However, we suspect that the displacement of Cdc8 is instead due to the presence of excess Fim1 at bundled regions. Fim1 localizes more strongly to bundled regions than to single filaments, and other fimbrins are known to make slight conformational changes in the actin filament upon binding (Hanein et al., 1997). We suspect that on single filaments, few Fim1 molecules are associated and the degree of conformational change in the actin filament is small and easily resisted by the cable-like Cdc8. However, at a bundled region, more Fim1 is associated (as Fim1 is likely cooperative at bundled regions) and a threshold in conformational changes is bypassed which results in Cdc8 displacement from those actin filaments. This hypothesis is supported by the delay in Cdc8 displacement following Fim1-mediated bundling (Figure 3-8). It is possible that Cdc8 displacement is initiated at 'weak points' or gaps in the Cdc8 cable that result in Cdc8's cooperative displacement from the actin filament. Though cryo-EM structures of mammalian fimbrin and tropomyosin associated with actin show that their binding sites do not overlap (Figure 1-5), the exact residues that both fission yeast Cdc8 and

Fim1 interact with on an actin filament are unclear, and whether any potential conformational changes by Fim1 would displace the Cdc8 binding interface still remain to be determined.

It should be stated that in competition between two ABPs, A and B, it is possible for A to compete with B via a passive mechanism, while B utilizes active competition to compete with A. Indeed, this is similar to what we observe for competition between tropomyosin Cdc8 and cofilin Adf1. As mentioned in the above section, Cdc8 prevents Adf1 association with the actin filament by blocking its initial association. However, once Adf1 does associate with an actin filament, it begins to displace Cdc8 in an active, cooperative way (Figure 3-10F), likely by altering the conformation of the actin filament. Budding yeast cofilin Cof1 has been shown to displace budding yeast tropomyosin Tpm1 by a direct interaction (Fan et al., 2008), presenting another potential mechanism for displacement of Cdc8 by Adf1.

Finally, though fimbrin Fim1 and cofilin Adf1 competition for the same binding site might indicate passive competition, there is also a potential aspect of active competition as a result of the different conformational changes that each make to the actin filament. It will be interesting to determine how Adf1 competes with contractile ring ABPs such as Ain1 and myosin-II Myo2 and how those interactions affect the degree of Adf1-mediated severing at the contractile ring.

Section 5.2—COOPERATIVITY OCCURS BETWEEN ACTIN BINDING PROTEINS OF THE SAME AND DIFFERENT TYPES

Homotropic cooperativity

Homotropic cooperativity, or positive cooperativity between ABPs the same type is a common and important feature amongst many different types of ABPs (Figure 5-1C). This type

of positive cooperativity can be established by 1) direct physical interactions between individual proteins, 2) an architectural feature such as the formation of an F-actin bundle that recruits specific ABPs (Winkelman et al., 2016), or 3) a change in the conformation of an actin filament that propagates the creation of favorable binding sites (McGough et al., 1997). Tropomyosin's characteristic end-to-end binding provides us with a model of cooperative behavior that occurs by direct physical interactions between ABPs as well as potential indirect interactions via a conformational change in the actin filament. By directly visualizing tropomyosin Cdc8 behavior on actin filaments, we found that tropomyosin cables do appear to extend along actin filaments in a cooperative fashion. Additionally, the use of mathematical modeling to describe tropomyosin behavior suggests that an additional factor of indirect cooperativity via potential conformational changes in the actin filament may additionally be involved in the higher degree of cooperativity observed for tropomyosin binding. Despite being able to directly visualize tropomyosin association with F-actin, there are still many components of the interaction between tropomyosin and F-actin that are not well understood.

An obvious future direction is to probe the nature of any actin filament conformational changes that occur as a result of tropomyosin binding to an actin filament. It has been well-documented that tropomyosins alter the persistence length of actin filaments (Gittes et al., 1993; Loong et al., 2012). Therefore, it is reasonable to suggest that tropomyosin could exert some type of change onto an actin filament that may influence the conformation of the filament. The cryo-electron microscopy structure of mouse tropomyosin on an actin filament shows little change in the structure of a tropomyosin-coated actin filament compared to an uncoated actin filament (Ecken et al., 2014). This high-resolution structure is at 3.7 Å for F-actin and 6.5 Å for tropomyosin. However, the possibility still remains that minute changes in the actin filament

structure are capable of facilitating changes that affect tropomyosin cooperativity. Additionally, this change could be in actin filament curvature or rigidity rather than twist. Tropomyosin could affect the persistence length or rigidity of F-actin at the site it binds. This rigidity could potentially be propagated slightly further up or down the actin filament, promoting the association of more tropomyosin molecules with an actin filament as a result of its increase in rigidity.

Including our study, four tropomyosin isoforms have been labeled and visualized using TIRF microscopy (Hsiao et al., 2015; Schmidt et al., 2015). Though several general characteristics are consistent amongst these tropomyosins studied so far (poor initial association with F-actin, cables spread from initial binding events), other characteristics vary remarkably (degree of cooperativity, site of initial 'seed' association on the filament, rate of binding, rate of cable extension). Differences amongst tropomyosins likely affect their functionality in the cell. Unlike fission yeast, which expresses a single tropomyosin isoform, mammalian cells express over 40 tropomyosin isoforms. Characteristics such as the ability of single tropomyosins to initially associate with F-actin, cooperativity, end-to-end binding, conformational changes in the actin filament, and where tropomyosin prefers to bind on the actin filament (near barbed vs. pointed end) likely vary amongst these tropomyosin isoforms, and could contribute to how different tropomyosins sort to different actin networks as well as their interactions with other ABPs.

Furthermore, other untested features may also be important for how tropomyosin associates with F-actin and potentially regulates the association of other ABPs. For example, we did not investigate whether tropomyosin Cdc8 preferentially bound to actin filament regions of specific curvature or flexibility. Additionally, we did not investigate any potential preference for

tropomyosin binding dependent on the ATP state of F-actin, though we think that this is unlikely as we see no bias in tropomyosin binding to the older, pointed end of actin filaments (Figure 3-4A). Therefore, other changes in actin filament conformation or other changes that are not visible at our current resolution may also effect tropomyosin association with single actin filaments.

Heterotropic cooperativity

Cooperativity is typically thought of in the context of ABPs of the same type. However, work from several groups has suggested that heterotropic cooperativity, that is, where an ABP of one type can influence the association of a second ABP of a different type, may additionally affect how ABPs associate with an actin filament (Figure 5-1D). In the context of ABP association with F-actin, heterotropic cooperativity is likely achieved by mechanisms similar to homotropic cooperativity.

In the simplest mode of positive heterotropic cooperativity, the association of one ABP with an actin filament positively regulates the ability of a second ABP to associate with the actin filament. This type of association has been previously suggested for cofilin and α-actinin. Human non-muscle cofilin was shown to enhance the bundling ability of rabbit muscle α-actinin, the model being that cofilin binding shortens the actin filament period, increasing the number of α-actinin binding sites per unit length (Bonet et al., 2009). However, α-actinin and cofilin have partially overlapping binding sites (as with fimbrin and cofilin, below), suggesting potential competition for binding sites and complicating any potential increase in α-actinin binding sites.

In the simplest mode of negative heterotropic cooperativity, the association of one ABP with an actin filament negatively regulates the ability of a second ABP to associate with the actin filament. This type of negative regulation has been observed in vitro between actin bundling

proteins fascin and α-actinin. Fascin creates compact actin bundles (8 nm between actin filaments), while α-actinin creates more widely-spaced bundles (35 nm). These ABPs were found to self-sort to bundled regions with different spacing, suggesting that α-actinin was inhibited from associating with fascin-bound regions and vice versa, as a result of spacing in actin bundles (Winkelman et al., 2016).

Section 5.3—COMPETITION AND COOPERATIVITY ARE LINKED

In a cell, "simple" modes of positive or negative heterotropic cooperativity are likely more complicated, as many different types of ABPs are all competing for association with the same actin filaments. Therefore, in many instances, competition and cooperativity are interlinked. Indeed, positive heterotropic cooperativity could be achieved either by enhancing the ability of an ABP to associate with an actin filament or by preventing that ABP's competitor from associating with that region. In the above example, fimbrin, another ABP that creates compact bundles, was found to associate with fascin-bundled regions, with the model being that fascin creates compact bundled regions that positively recruit other compact ABPs. However, an additional interpretation could be that fascin excludes fimbrin's competitor α-actinin, allowing fimbrin to associate with those regions not bound by α-actinin. Clearly, models of competition and cooperativity are complicated, and the coalescence of these distinct interactions is likely important for generating the 'all-or-nothing' sorting frequently observed in cells.

Our results suggest, though they do not prove, that some type of heterotropic cooperativity exists between α-actinin Ain1 and tropomyosin Cdc8 in fission yeast. We found that α-actinin does not displace tropomyosin Cdc8 from F-actin bundles (Figure 4-6). Additionally, we observe that Cdc8 enhances Ain1-mediated bundling (Figure 4-7). However, neither of these findings alone is absolutely indicative of heterotropic cooperativity as defined

above, as we have not demonstrated that Cdc8 binding promotes Ain1 binding or that Ain1 binding promotes Cdc8 binding. In fact, we found that the residence time of single Ain1 molecules was the same on tropomyosin-coated or uncoated F-actin. If tropomyosin Cdc8 does not promote association of Ain1 with actin filaments, inhibiting fimbrin Fim1 from binding to those filaments, how else could Cdc8 and Ain1 work together to inhibit Fim1 from associating with F-actin?

We hypothesize that in this case, tropomyosin Cdc8 and α-actinin Ain1 compete with fimbrin Fim1 by preventing fimbrin Fim1 from being cooperative. As mentioned above, we hypothesize that fimbrin Fim1 displaces tropomyosin Cdc8 via multiple conformational changes within a single stretch of the actin filament. In order to exert multiple conformational changes along an entire stretch of F-actin, fimbrin Fim1 must be continuously bound along that stretch. As Ain1 and Fim1 are thought to compete for the same binding site, the presence of Ain1 makes it more difficult for a long stretch of Fim1 to form along the actin filament, resulting in fewer persistent conformational changes, allowing Cdc8 to remain bound to the actin filament and compete with Fim1. There are other potential mechanisms that may explain this competition. It may be that Cdc8 and Ain1 alone can each compete a small amount with Fim1, and that the additive effects of their individual interactions result in more visible Fim1 inhibition. Alternatively, fission yeast Ain1 may affect no change or a different conformational change on the actin filament compared to other α-actinins, resulting in no displacement of tropomyosin Cdc8.

Section 5.4—FUTURE DIRECTIONS

Further investigation of key ABPs involved in ABP sorting

This work has identified multiple ABPs that affect the interactions of other ABPs with F-actin, and has determined several mechanisms by which ABPs compete and cooperate with each other. In addition, we have discovered that these cooperative and competitive interactions are involved in ABP sorting on a cellular scale. However, many questions remain as to how ABP sorting is established and executed for the entire cellular set of ABPs. We performed a preliminary survey in an attempt to determine which ABPs may have competitive interactions with each other (Figure 4-1). We found a variety of interesting ABP relocalizations following CK-666 treatemnt, many of which have potential for follow-up studies. In particular, we found that in addition to fimbrin Fim1, ADF/cofilin Adf1 and coronin Crn1 also relocalize to the contractile ring following CK-666 treatment (Figure 4-1). Interestingly, all three of these ABPs have been implicated in localizing to the contractile ring in small amounts under normal circumstances. This finding suggests that actin patches are potentially acting as a 'sink' for certain ABPs, but that following patch removal, the cytoplasmic concentration increases and they are more able to compete with contractile ring ABPs and associate with that network. Therefore, it would be interesting to use a similar combination of in vitro biochemistry and live fission yeast cell imaging to determine if fimbrin Fim1, ADF/cofilin Adf1, and coronin Crn1 compete with contractile ring ABPs by similar mechanisms, and if the combination of tropomyosin Cdc8 and **α**-actinin Ain1 is similarly able to prevent ADF/cofilin Adf1 and coronin Crn1 association with the contractile ring.

ADF/cofilin Adf1 is an interesting candidate of study for other reasons as well. Adf1-mediated severing is clearly important and well-understood for actin patch disassembly.

However, its role in contractile ring assembly and disassembly, though important, is less well-defined (Chen and Pollard, 2011). Therefore, the role of Adf1-mediated severing at the contractile ring and how its severing is regulated by other associated ABPs remains to be determined. We found that Fim1/Adf1 competition competing for F-actin binding sites enhances Adf1 severing, as the presence of Fim1 creates Adf1 boundaries (Figure 3-11). The addition of other ABPs, specifically contractile ring components such as myosin-II Myo2 and α-actinin Ain1 to Adf1-coated actin filaments in vitro would allow us to determine how ABPs associated with the contractile ring affect Adf1-mediated severing. I hypothesize that as Ain1 binds to the same site on F-actin as Fim1, but is more dynamic, that perhaps it would enhance Adf1 severing to a lesser extent, or not at all, as it may not be present on actin filaments for long enough to create boundaries of differing Adf1-concentration and/or flexibility (McCullough et al., 2008; Suarez et al., 2011). Skeletal muscle myosin S1 has been shown to enhance ADF/cofilin-mediated severing (Elam et al., 2013). Therefore, it will be interesting to determine whether myosin-II has a similar effect, and whether this enhancement in severing is negated by the presence of other contractile ring ABPs such as tropomyosin Cdc8 and Ain1. Furthermore, at actin patch sites in fission yeast and budding yeast, it is known that other actin disassembly proteins such as coronin Crn1, actin-interacting protein Aip1, twinfilin Twf1, and adenylyl-cyclase associated protein CAP assist ADF/cofilin in rapidly disassembling F-actin at patch sites. However, how these ABPs are involved in actin disassembly at the contractile ring and whether their activities are regulated by competition with other contractile ring ABPs remains to be determined.

Future exploration into the mechanism behind tropomyosin Cdc8 competition with other ABPs will also yield insight into how physical characteristics such as cooperativity influence the ability of an ABP to compete with other ABPs. Tropomyosin is a particularly good candidate for

this study as there is a wealth of information on its interactions with the actin filament. We could engineer regions of the tropomyosin Cdc8 protein in order to determine how its properties are altered, and how those changes affect its ability to compete with other ABPs. For example, muscle tropomyosin that is less able to associate end-to-end is still cooperative (Willadsen et al. 1992). Using in vitro TIRF microscopy, we could determine the mechanism of this mutant's cooperativity on actin, perhaps further elucidating how indirect interactions between tropomyosin molecules via alterations in the actin filament may affect tropomyosin's cooperativity. Additionally, similar mutations could be made in the fission yeast tropomyosin Cdc8 to ask similar questions. Furthermore, as mammalian cells express ~40 tropomyosin isoforms, different tropomyosin isoforms could be purified, labeled with different fluorophores, and visualized simultaneously in TIRF in order to determine whether these isoforms segregate to different actin filaments.

Additionally, interactions between tropomyosin and other ABPs can be investigated using our high-resolution TIRF imaging. Tropomodulin is a protein that associates with the pointed end of F-actin in the Z-disk of muscle cells and is believed to template tropomyosin association with F-actin. By labeling both tropomodulin and tropomyosin, we can determine the mechanism by which tropomodulin templates tropomyosin. As initial tropomyosin molecules poorly associate with F-actin, tropomodulin could enhance initial binding by directly associating with tropomyosin, allowing tropomyosin's cooperativity to then promote the rapid coating of actin filaments within the Z-disk. Additionally, tropomodulin could potentially affect tropomyosin loading indirectly by altering the conformation of an actin filament such that tropomyosin can more easily associate. Our in vitro TIRF assays combined with similar mathematical models as described in Chapter 3 can help to distinguish between these different

modes of enhancement of tropomyosin loading on F-actin by tropomodulin. Tropomyosin is also known to enhance or inhibit the activities of different myosins, depending on the isoform (Clayton et al., 2010). Using our set-up, we could additionally label myosin molecules in order to determine how tropomyosin affects the run length or speed of myosin molecules as well as determine whether the presence of different myosin isoforms enhance or inhibit the ability of tropomyosin to associate with an actin filament.

The effect of post-translational modifications on ABPs

As the majority of our experiments have been performed with recombinant proteins purified from *E. coli*, it is possible that our experiments fail to take into account other effects on these ABPs, such a post-translational modifications. Recently, budding yeast fimbrin Sac6 was shown to be post-translationally modified, and this modification was shown to regulate the ability of Sac6 to bind to F-actin (Miao et al. 2016). Additionally, ADF/cofilin phosphorylation has been demonstrated to regulate its functionality in vivo (Bravo-Cordero et al., 2013). Similar modifications may exist for fission yeast fimbrin Fim1 or cofilin Adf1 that regulate their activity. A simple, straightforward way of initially assessing whether post-translational modification or other cellular factors may affect the activity of these ABPs is to purify them directly from fission yeast and assay their activity using bulk biochemistry or in vitro TIRF microscopy assays. If a difference in activity is seen, running a phosphogel or mobility shift gel assay in conjunction with later mass spec of the protein could assist in determining whether the protein is modified by phosphorylation and at what residues. Those residues could then be mutated in vitro and in vivo and whether the modification affects ABP sorting could be investigated.

Additionally, fission yeast tropomyosin Cdc8, like many tropomyosins, is acetylated on its N-terminus (Skoumpla et al. 2007), and this acetylation has been shown to enhance the ability of tropomyosin Cdc8 to associate with F-actin. However, whether this modification affects Cdc8's initial ability to bind to F-actin and/or its cooperativity on F-actin, and how this modification affects its ability to sort to different F-actin networks in the fission yeast cell (Coulton et al. 2010, Johnson et al. 2014), remain to be determined. In particular, it would be interesting to determine whether unacetylated Cdc8 competes or cooperates to different extents with the other ABPs we have worked with (α-actinin, cofilin, fimbrin), and whether alterations in its competitive interactions with these ABPs mediates its sorting.

Assembly factor involvement in defining the ABP composition of an F-actin network

Of primary interest is whether competitive interactions between ABPs are organized as a hierarchy or as a web of interactions. In the hierarchy model, upstream ABPs will be recruited to an F-actin network. These upstream ABPs will then recruit certain downstream ABPs while preventing the association of others, resulting in the association of the correct set of ABPs to the network. In the web model, many small interactions amongst different ABPs as well as potential small biases in ABPs toward F-actin synthesized by a specific assembly factor coalesce to generate proper sorting of ABPs to the correct F-actin network. In either model, a key question concerns the role of the assembly factor or other upstream signals in setting up a 'hierarchy' or affecting recruitment of ABPs to a specific F-actin network. It will be interesting to investigate which, if any, ABPs have preferences for actin polymerized by a specific assembly factor, and whether competitive interactions are necessary for these preferences to be exposed. The detailed mechanisms can be investigated by using multi-color TIRF microscopy with labeled ABPs and

assembly factors. However, utilizing a combination of biochemistry and cell biology will be most effective in addressing this question.

One key future project would involve moving different nucleation factors to different regions of the cell and determining whether the same set of ABPs localizes to a formin- or Arp2/3 complex-assembled filament synthesized in a non-standard region of the cell. In a previous study, the formins For3 and Cdc12 were moved to different locations in the fission yeast cell by creating formin fusions with proteins that localize to cell pole or contractile ring sites. It was demonstrated that unacetylated and acetylated tropomyosin Cdc8 correctly localized to actin synthesized by their native formin, regardless of its localization (Johnson et al. 2014). A similar system could be used to target For3 and Cdc12 as well as the Arp2/3 complex to different sites in the cell and examine the ABPs that localize to F-actin synthesized by these assembly factors. This strategy could yield information regarding whether certain ABPs only localize to actin networks formed in distinct regions of the cell (perhaps suggesting the presence of a spatial regulatory factor) or whether the assembly factor itself is sufficient to mediate the recruitment of the proper set of ABPs.

As moving actin assembly factors in the cell often has deleterious effects on cell viability, a second strategy to answer a similar question is to perform a variant of the CK-666 survey initially used to identify competitive ABPs (Figure 4-1). In this survey, two actin assembly factors are depleted such that all of the actin in the fission yeast cell is made by a distinct assembly factor. *Cdc12-112* or *for3Δ* cells could be treated with CK-666 to deplete Arp2/3 complex-mediated actin, such that all F-actin is made by the remaining assembly factor (Burke et al. 2014). Then, a similar survey could be performed to determine which ABPs localize to F-actin only made by Cdc12 or For3. A more detailed analysis could also determine whether a

specific ABP's localization occurs on all F-actin synthesized by that assembly factor or only to a subset (F-actin near the cortex, F-actin at the contractile ring, etc.) in order to yield insight into how ABPs localize to distinct F-actin networks.

ABP competition at the cellular level

Though this work focused on key ABPs involved in ABP sorting, there are likely additional ABPs that are also crucial for actin cytoskeleton self-organization. Further surveys and systems level experiments could assist in identifying other ABPs or other cellular factors important for proper ABP sorting and actin network organization. A remaining survey that could yield insight into competitive interactors is to systematically knockout (or knock down) every ABP in fission yeast and examine the localization of every other ABP-GFP when a single ABP is removed from the cell. For example, a *fim1Δ* strain could be made and crossed with strains expressing a different GFP-tagged ABP. Then, the localization of each ABP in the absence of Fim1 could be determined. Though this is a time-consuming project, it would likely yield great insight into which ABPs affect each other's localizations.

A second project could involve treating fission yeast cells with latrunculin A. Latrunculin A binds to actin monomer, preventing it from polymerizing and eventually resulting in depolymerization of all F-actin in the cell. When latrunculin A is then washed out, the actin networks rebuild themselves. Examining the reassembly of the different F-actin networks as well as the timed localization of different ABPs to those networks could yield insight into order of recruitment of ABPs to an F-actin network.

Finally, mathematical modeling will likely be important to determine the influence of each of these factors (ABP dynamics, competitive interactions, preference for assembly factor,

age of F-actin) on ABP sorting. It seems possible that in the future, by understanding distinct parameters for each ABP, we could potentially recapitulate ABP sorting in silico, and gain further insight into which parameters are important for ABP sorting in vivo. Future work will involve utilizing a combination of single molecule biochemistry, live cell imaging, and mathematical modeling to determine which ABP characteristics and parameters are important for ABP sorting.

REFERENCES

Andrianantoandro, E., and Pollard, T.D. (2006). Mechanism of actin filament turnover by severing and nucleation at different concentrations of ADF/cofilin. Molecular Cell *24*, 13–23.

Avasthi, P., Onishi, M., Karpiak, J., Yamamoto, R., Mackinder, L., Jonikas, M.C., Sale, W.S., Shoichet, B., Pringle, J.R., and Marshall, W.F. (2014). Actin Is Required for IFT Regulation in Chlamydomonas reinhardtii. Current Biology *24*, 2025–2032.

Balasubramanian, M.K., Helfman, D.M., and Hemmingsen, S.M. (1992). A new tropomyosin essential for cytokinesis in the fission yeast S. pombe. Nature *360*, 84–87.

Bamburg, J.R., and Bray, D. (1987). Distribution and cellular localization of actin depolymerizing factor. The Journal of Cell Biology *105*, 2817–2825.

Barua, B., Fagnant, P.M., Winkelmann, D.A., Trybus, K.M., and Hitchcock-DeGregori, S.E. (2013). A periodic pattern of evolutionarily conserved basic and acidic residues constitutes the binding interface of actin-tropomyosin. J. Biol. Chem. *288*, 9602–9609.

Bernstein, B.W., and Bamburg, J.R. (1982). Tropomyosin binding to F-actin protects the F-actin from disassembly by brain actin-depolymerizing factor (ADF). Cell Motil. *2*, 1–8.

Bestul, A.J., Christensen, J.R., Grzegorzewska, A.P., Burke, T.A., Sees, J.A., Carroll, R.T., Sirotkin, V., Keenan, R.J., and Kovar, D.R. (2015). Fission yeast profilin is tailored to facilitate actin assembly by the cytokinesis formin Cdc12. Mol. Biol. Cell *26*, 283–293.

Blanchoin, L., Boujemaa-Paterski, R., Sykes, C., and Plastino, J. (2014). Actin dynamics, architecture, and mechanics in cell motility. Physiol. Rev. *94*, 235-263.

Bombardier, J.P., Eskin, J.A., Jaiswal, R., Corrêa, I.R., Xu, M.-Q., Goode, B.L., and Gelles, J. (2015). Single-molecule visualization of a formin-capping protein "decision complex" at the actin filament barbed end. Nat Commun *6*, 8707.

Bonet, C., Maciver, S.K., and Mozo-Villarías, A. (2009). The regulatory action of α-actinin on actin filaments is enhanced by cofilin. Eur Biophys J *39*, 1143–1153.

Bravo-Cordero, J.J., Magalhaes, M.A.O., Eddy, R.J., Hodgson, L., and Condeelis, J. (2013). Functions of cofilin in cell locomotion and invasion. Nat. Rev. Mol. Cell. Biol. *14*, 405-415.

Bugyi, B., Papp, G., Hild, G., Lorinczy, D., Nevalainen, E.M., Lappalainen, P., Somogyi, B., and Nyitrai, M. (2006). Formins regulate actin filament flexibility through long range allosteric interactions. J. Biol. Chem. *281*, 10727–10736.

Burke, T.A., Christensen, J.R., Barone, E., Suarez, C., Sirotkin, V., and Kovar, D.R. (2014). Homeostatic Actin Cytoskeleton Networks Are Regulated by Assembly Factor Competition for Monomers. Current Biology *24*, 579–585.

Cameron, L.A., Footer, M.J., van Oudenaarden, A., and Theriot, J.A. (1999). Motility of ActA

protein-coated microspheres driven by actin polymerization. Proc Natl Acad Sci USA *96*, 4908–4913.

Carlsson, L., Nystrom, L.E., Sundkvist, I., Markey, F., and Lindberg, U. (1977). Actin polymerizability is influenced by profilin, a low molecular weight protein in non-muscle cells. Journal of Molecular Biology *115*, 465–483.

Chalkia, D., Nikolaidis, N., Makalowski, W., Klein, J., and Nei, M. (2008). Origins and evolution of the formin multigene family that is involved in the formation of actin filaments. Mol Biol Evol *25*, 2717–2733.

Chen, Q., and Pollard, T.D. (2011). Actin filament severing by cofilin is more important for assembly than constriction of the cytokinetic contractile ring. The Journal of Cell Biology *195*, 485–498.

Chen, Q., and Pollard, T.D. (2013). Actin filament severing by cofilin dismantles actin patches and produces mother filaments for new patches. Current Biology : CB *23*, 1154–1162.

Chen, Q., Courtemanche, N., and Pollard, T.D. (2015). Aip1 promotes actin filament severing by cofilin and regulates constriction of the cytokinetic contractile ring. J. Biol. Chem. *290*, 2289–2300.

Clayton, J.E., Sammons, M.R., Stark, B.C., Hodges, A.R., and Lord, M. (2010). Differential regulation of unconventional fission yeast myosins via the actin track. Current Biology : CB *20*, 1423–1431.

Collins, A., Warrington, A., Taylor, K.A., and Svitkina, T. (2011). Structural organization of the actin cytoskeleton at sites of clathrin-mediated endocytosis. Current Biology : CB *21*, 1167–1175.

Coulton, A.T., East, D.A., Galinska-Rakoczy, A., Lehman, W., and Mulvihill, D.P. (2010). The recruitment of acetylated and unacetylated tropomyosin to distinct actin polymers permits the discrete regulation of specific myosins in fission yeast. J. Cell. Sci. *123*, 3235–3243.

Cranz-Mileva, S., MacTaggart, B., Russell, J., and Hitchcock-DeGregori, S.E. (2015). Evolutionarily conserved sites in yeast tropomyosin function in cell polarity, transport and contractile ring formation. Biology Open *4*, 1040–1051.

Cranz-Mileva, S., Pamula, M.C., Barua, B., Desai, B., Hong, Y.H., Russell, J., Trent, R., Wang, J., Walworth, N.C., and Hitchcock-DeGregori, S.E. (2013). A Molecular Evolution Approach to Study the Roles of Tropomyosin in Fission Yeast. PLoS ONE *8*, e76726.

Dayel, M.J., and Mullins, R.D. (2004). Activation of Arp2/3 Complex: Addition of the First Subunit of the New Filament by a WASP Protein Triggers Rapid ATP Hydrolysis on Arp2. PLoS Biol *2*, e91–10.

Desmarais, V. (2004). Synergistic interaction between the Arp2/3 complex and cofilin drives stimulated lamellipod extension. J. Cell. Sci. *117*, 3499–3510.

DesMarais, V., Ichetovkin, I., Condeelis, J., and Hitchcock-DeGregori, S.E. (2002). Spatial regulation of actin dynamics: a tropomyosin-free, actin-rich compartment at the leading edge. J. Cell. Sci. *115*, 4649–4660.

Detmers, P.A., Carboni, J.M., and Condeelis, J. (1985). Localization of actin in Chlamydomonas using antiactin and NBD-phallacidin. Cell Motil. *5*, 415–430.

Detmers, P.A., Goodenough, U.W., and Condeelis, J. (1983). Elongation of the fertilization tubule in Chlamydomonas: new observations on the core microfilaments and the effect of transient intracellular signals on their structural integrity. The Journal of Cell Biology *97*, 522–532.

Domcke, S., Bardet, A.F., Ginno, P.A., Hartl, D., Burger, L., and Schübeler, D. (2015). Competition between DNA methylation and transcription factors determines binding of NRF1. Nature *528*, 575–579.

Ecken, von der, J., Müller, M., Lehman, W., Manstein, D.J., Penczek, P.A., and Raunser, S. (2014). Structure of the F-actin--tropomyosin complex. Nature 1–17.

Elam, W.A., Kang, H., and La Cruz, De, E.M. (2013). Competitive displacement of cofilin can promote actin filament severing. Biochemical and Biophysical Research Communications *438*, 728–731.

Fan, X., Martin-Brown, S., Florens, L., and Li, R. (2008). Intrinsic capability of budding yeast cofilin to promote turnover of tropomyosin-bound actin filaments. PLoS ONE *3*, e3641.

Feng, Y., Ngu, H., Alford, S.K., Ward, M., Yin, F., and Longmore, G.D. (2013). α-actinin1 and 4 tyrosine phosphorylation is critical for stress fiber establishment, maintenance and focal adhesion maturation. Experimental Cell Research *319*, 1124–1135.

Friedmann, I., Colwin, A.L., and Colwin, L.H. (1968). Fine-structural aspects of fertilization in Chlamydomonas reinhardi. J. Cell. Sci. *3*, 115–128.

Galkin, V.E., Orlova, A., Cherepanova, O., Lebart, M.C., and Egelman, E.H. (2008). High-resolution cryo-EM structure of the F-actin-fimbrin/plastin ABD2 complex. Proceedings of the National Academy of Sciences of the United States of America *105*, 1494–1498.

Galkin, V.E., Orlova, A., Salmazo, A., Djinović-Carugo, K., and Egelman, E.H. (2010). Opening of tandem calponin homology domains regulates their affinity for F-actin. Nat Struct Mol Biol *17*, 614–616.

Galkin, V.E., Orlova, A., Kudryashov, D.S., Solodukhin, A., Reisler, E., Schroder, G.F., and Egelman, E.H. (2011). Remodeling of actin filaments by ADF/cofilin proteins. Proc. Natl. Acad. Sci. USA. *108*, 20568-20572.

Gittes, F., Mickey, B., Nettleton, J., and Howard, J. (1993). Flexural rigidity of microtubules and actin filaments measured from thermal fluctuations in shape. The Journal of Cell Biology *120*, 923–934.

Goldschmidt-Clermont, P.J., Furman, M.I., Wachsstock, D., Safer, D., Nachmias, V.T., and Pollard, T.D. (1992). The control of actin nucleotide exchange by thymosin beta 4 and profilin. A potential regulatory mechanism for actin polymerization in cells. Molecular Biology of the Cell *3*, 1015–1024.

Goldstein, B., and Macara, I.G. (2007). The PAR Proteins: Fundamental Players in Animal Cell Polarization. Developmental Cell *13*, 609–622.

Goley, E.D., Rodenbusch, S.E., Martin, A.C., and Welch, M.D. (2004). Critical Conformational Changes in the Arp2/3 Complex Are Induced by Nucleotide and Nucleation Promoting Factor. Molecular Cell *16*, 269–279.

Goode, B.L., and Eck, M.J. (2007). Mechanism and function of formins in the control of actin assembly. Annu Rev Biochem *76*, 593–627.

Goodenough, U.W., and Weiss, R.L. (1975). Gametic differentiation in Chlamydomonas reinhardtii. III. Cell wall lysis and microfilament-associated mating structure activation in wild-type and mutant strains. The Journal of Cell Biology *67*, 623–637.

Graceffa, P., and Dominguez, R. (2003). Crystal structure of monomeric actin in the ATP state. Structural basis of nucleotide-dependent actin dynamics. J.Biol. Chem. *278*, 34172-34180.

Gressin, L., Guillotin, A., Guérin, C., Blanchoin, L., and Michelot, A. (2015). Architecture Dependence of Actin Filament Network Disassembly. Current Biology *25*, 1437–1447.

Gunning, P.W., Hardeman, E.C., Lappalainen, P., and Mulvihill, D.P. (2015). Tropomyosin - master regulator of actin filament function in the cytoskeleton. J. Cell. Sci. *128*, 2965–2974.

Hall, A. (1998). Rho GTPases and the Actin Cytoskeleton. Science *279*, 509–514.

Hanein, D., Matsudaira, P., and DeRosier, D.J. (1997). Evidence for a conformational change in actin induced by fimbrin (N375) binding. The Journal of Cell Biology *139*, 387–396.

Hanein, D., Volkmann, N., Goldsmith, S., Michon, A.M., Lehman, W., Craig, R., DeRosier, D., Almo, S., and Matsudaira, P. (1998). An atomic model of fimbrin binding to F-actin and its implications for filament crosslinking and regulation. Nat Struct Biol *5*, 787–792.

Hanson, J., and Lowy, J. (1964). The structure of actin filaments and the origin of the axial periodicity in the I-substance of vertebrate striated muscle. Proc. R. Soc. Lond., B, Biol. Sci. *160*, 449–460.

Harper, J.D., McCurdy, D.W., Sanders, M.A., Salisbury, J.L., and John, P.C. (1992). Actin dynamics during the cell cycle in Chlamydomonas reinhardtii. Cell Motil. Cytoskeleton *22*, 117–126.

Hayakawa, K., Sakakibara, S., Sokabe, M., and Tatsumi, H. (2014). Single-molecule imaging and kinetic analysis of cooperative cofilin–actin filament interactions. Proc Natl Acad Sci USA *111*, 9810–9815.

Heald, R., Tournebize, R., Blank, T., Sandaltzopoulos, R., Becker, P., Hyman, A., and Karsenti, E. (1996). Self-organization of microtubules into bipolar spindles around artificial chromosomes in *Xenopus* egg extracts. Nature *382*, 420–425.

Holtzman, D.A., Wertman, K.F., and Drubin, D.G. (1994). Mapping actin surfaces required for functional interactions in vivo. The Journal of Cell Biology *126*, 423–432.

Honts, J.E., Sandrock, T.S., Brower, S.M., O'Dell, J.L., and Adams, A.E. (1994). Actin mutations that show suppression with fimbrin mutations identify a likely fimbrin-binding site on actin. The Journal of Cell Biology *126*, 413–422.

Hotulainen, P., and Lappalainen, P. (2006). Stress fibers are generated by two distinct actin assembly mechanisms in motile cells. The Journal of Cell Biology *173*, 383–394.

Hsiao, J.Y., Goins, L.M., Petek, N.A., and Mullins, R.D. (2015). Arp2/3 Complex and Cofilin Modulate Binding of Tropomyosin to Branched Actin Networks. Current Biology *25*, 1573–1582.

Ichetovkin, I., Grant, W., and Condeelis, J. (2002). Cofilin produces newly polymerized actin filaments that are preferred for dendritic nucleation by the Arp2/3 complex. Current Biology *12*, 79–84.

Jansen, S., Collins, A., Chin, S.M., Ydenberg, C.A., Gelles, J., and Goode, B.L. (2015). Single-molecule imaging of a three-component ordered actin disassembly mechanism. Nat Commun *6*, 7202.

Johnson, M., East, D.A., and Mulvihill, D.P. (2014). Formins Determine the Functional Properties of Actin Filaments in Yeast. Current Biology 1–6.

Johnston, A.B., Collins, A., and Goode, B.L. (2015). High-speed depolymerization at actin filament ends jointly catalysed by Twinfilin and Srv2/CAP. Nat. Cell Biol. *17*, 1504–1511.

Kaiser, D.A., Vinson, V.K., Murphy, D.B., and Pollard, T.D. (1999). Profilin is predominantly associated with monomeric actin in Acanthamoeba. J. Cell. Sci. *112 (Pt 21)*, 3779–3790.

Kaplan, E.L., and Meier, P. (1958). Nonparametric estimation from incomplete observations. Journal of the American Statistical Association *53*, 457–481.

Karsenti, E. (2008). Self-organization in cell biology: a brief history. Nat Rev Mol Cell Biol *9*, 255–262.

Kato-Minoura, T.E.A. (1998). Highly Divergent Actin Expressed in a Chlamydomonas Mutant Lacking the Conventional Actin Gene. 1–6.

Khurana, S., and George, S.P. (2014). The role of actin bundling proteins in the assembly of filopodia in epithelial cells. Cell Adhesion & Migration *5*, 409–420.

Kim, Y., Ho, S.O., Gassman, N.R., Korlann, Y., Landorf, E.V., Collart, F.R., and Weiss, S.

(2008). Efficient Site-Specific Labeling of Proteins via Cysteines. Bioconjugate Chem. *19*, 786–791.

Kollmar, M., Lbik, D., and Enge, S. (2012). Evolution of the eukaryotic ARP2/3 activators of the WASP family: WASP, WAVE, WASH, and WHAMM, and the proposed new family members WAWH and WAML. BMC Research Notes *5*, 88.

Kovar, D.R., Harris, E.S., Mahaffy, R., Higgs, H.N., and Pollard, T.D. (2006). Control of the assembly of ATP- and ADP-actin by formins and profilin. Cell *124*, 423–435.

Kovar, D.R., Kuhn, J.R., Tichy, A.L., and Pollard, T.D. (2003). The fission yeast cytokinesis formin Cdc12p is a barbed end actin filament capping protein gated by profilin. The Journal of Cell Biology *161*, 875–887.

Kovar, D.R., Yang, P., Sale, W.S., Drobak, B.K., and Staiger, C.J. (2001). Chlamydomonas reinhardtii produces a profilin with unusual biochemical properties. J. Cell. Sci. *114*, 4293–4305.

Kuhn, T.B., and Bamburg, J.R. (2008). Tropomyosin and ADF/cofilin as collaborators and competitors. Adv Exp Med Biol *644*, 232–249.

Kurahashi, H., Imai, Y., and Yamamoto, M. (2002). Tropomyosin is required for the cell fusion process during conjugation in fission yeast. Genes Cells *7*, 375–384.

Kurisu, S., and Takenawa, T. (2009). The WASP and WAVE family proteins. Genome Biol. *10*, 226.

De La Cruz, E.M. (2009). How cofilin severs an actin filament. Biophys Rev *1*, 51–59.

De La Cruz, E.M. (2005). Cofilin Binding to Muscle and Non-muscle Actin Filaments: Isoform-dependent Cooperative Interactions. Journal of Molecular Biology *346*, 557–564.

Lee, V.D., Finstad, S.L., and Huang, B. (1997). Cloning and characterization of a gene encoding an actin-related protein in Chlamydomonas. Gene *197*, 153–159.

Lehman, W., Craig, R., and Vibert, P. (1994). Ca(2+)-induced tropomyosin movement in Limulus thin filaments revealed by three-dimensional reconstruction. Nature *368*, 65–67.

Leung, D.W., and Rosen, M.K. (2005). The nucleotide switch in Cdc42 modulates coupling between the GTPase-binding and allosteric equilibria of Wiskott-Aldrich syndrome protein. Proc Natl Acad Sci USA *102*, 5685–5690.

Li, Y., Christensen, J.R., Homa, K.E., Hocky, G.M., Fok, A., Sees, J.A., Voth, G.A., and Kovar, D.R. (2016). The F-actin bundler α-actinin Ain1 is tailored for ring assembly and constriction during cytokinesis in fission yeast. Molecular Biology of the Cell *27*, 1821–1833.

Loisel, T.P., Boujemaa, R., Pantaloni, D., and Carlier, M.F. (1999). Reconstitution of actin-based motility of Listeria and Shigella using pure proteins. Nature *401*, 613–616.

Lomakin, A.J., Lee, K.-C., Han, S.J., Bui, D.A., Davidson, M., Mogilner, A., and Danuser, G. (2015). Competition for actin between two distinct F-actin networks defines a bistable switch for cell polarization. Nat. Cell Biol. *17*, 1435–1445.

Loong, C.K.P., Zhou, H.-X., and Chase, P.B. (2012). Persistence Length of Human Cardiac α-Tropomyosin Measured by Single Molecule Direct Probe Microscopy. PLoS ONE *7*, e39676–11.

Lu, J., and Pollard, T.D. (2001). Profilin binding to poly-L-proline and actin monomers along with ability to catalyze actin nucleotide exchange is required for viability of fission yeast. Molecular Biology of the Cell *12*, 1161–1175.

Marchand, J.B., Kaiser, D.A., Pollard, T.D., and Higgs, H.N. (2001). Interaction of WASP/Scar proteins with actin and vertebrate Arp2/3 complex. Nat. Cell Biol. *3*, 76–82.

Martin, S.G., Rincón, S.A., Basu, R., Pérez, P., Chang, F. (2007). Regulation of the Formin for3p by cdc42p and bud6p. Molecular Biology of the Cell. *18,* 4155-4167.

McCullough, B.R., Blanchoin, L., Martiel, J.L., and la Cruz, De, E.M. (2008). Cofilin increases the bending flexibility of actin filaments: implications for severing and cell mechanics. Journal of Molecular Biology *381*, 550–558.

McGough, A., Pope, B., Chiu, W., and Weeds, A. (1997). Cofilin changes the twist of F-actin: implications for actin filament dynamics and cellular function. The Journal of Cell Biology *138*, 771–781.

McGough, A., Way, M., and DeRosier, D. (1994). Determination of the α-Actinin-binding Site on Actin Filaments by Cryoelectron Microscopy and Image Analysis. The Journal of Cell Biology *126*, 433–443.

Meijering, E., Dzyubachyk, O., and Smal, I. (2012). Methods for cell and particle tracking. Meth. Enzymol. *504*, 183–200.

Miao, Y., Han, X., Zheng, L., Xie, Y., Mu, Y., Yates, J.R., and Drubin, D.G. (2016). Fimbrin phosphorylation by metaphase Cdk1 regulates actin cable dynamics in budding yeast. Nat Commun *7*, 11265.

Miao, Y., Wong, C.C.L., Mennella, V., Michelot, A., Agard, D.A., Holt, L.J., Yates, J.R., and Drubin, D.G. (2013). Cell-cycle regulation of formin-mediated actin cable assembly. Proceedings of the National Academy of Sciences of the United States of America *110*, E4446–E4455.

Michelot, A., Berro, J., Guerin, C., Boujemaa-Paterski, R., Staiger, C.J., Martiel, J.L., and Blanchoin, L. (2007). Actin-filament stochastic dynamics mediated by ADF/cofilin. Current Biology : CB *17*, 825–833.

Michelot, A., Costanzo, M., Sarkeshik, A., Boone, C., Yates, J.R.3., and Drubin, D.G. (2010). Reconstitution and protein composition analysis of endocytic actin patches. Current Biology : CB *20*, 1890–1899.

Michelot, A., and Drubin, D.G. (2011). Building Distinct Actin Filament Networks in a Common Cytoplasm. Current Biology *21*, R560–R569.

Milligan, R.A., Whittaker, M., and Safer, D. (1990). Molecular structure of F-actin and location of surface binding sites. Nature *348*, 217–221.

Misteli, T. (2001). The concept of self-organization in cellular architecture. The Journal of Cell Biology *155*, 181–186.

Mockrin, S.C., and Korn, E.D. (1980). Acanthamoeba profilin interacts with G-actin to increase the rate of exchange of actin-bound adenosine 5'-triphosphate. Biochemistry *19*, 5359–5362.

Monteiro, P.B., Lataro, R.C., Ferro, J.A., and Reinach, F. de C. (1994). Functional alpha-tropomyosin produced in Escherichia coli. A dipeptide extension can substitute the amino-terminal acetyl group. J. Biol. Chem. *269*, 10461–10466.

Mouneimne, G., Hansen, S.D., Selfors, L.M., Petrak, L., Hickey, M.M., Gallegos, L.L., Simpson, K.J., Lim, J., Gertler, F.B., Hartwig, J.H., et al. (2012). Differential remodeling of actin cytoskeleton architecture by profilin isoforms leads to distinct effects on cell migration and invasion. Cancer Cell *22*, 615–630.

Mullins, R.D., Kelleher, J.F., Xu, J., and Pollard, T.D. (1998). Arp2/3 complex from Acanthamoeba binds profilin and cross-links actin filaments. Mol. Biol. Cell *9*, 841–852.

Nadkarni, A.V., and Brieher, W.M. (2014). Aip1 Destabilizes Cofilin-Saturated Actin Filaments by Severing and Accelerating Monomer Dissociation from Ends. Current Biology *24*, 2749–2757.

Nakano, K., and Mabuchi, I. (2006a). Actin-capping protein is involved in controlling organization of actin cytoskeleton together with ADF/cofilin, profilin and F-actin crosslinking proteins in fission yeast. Genes Cells *11*, 893–905.

Nakano, K., Satoh, K., Morimatsu, A., Ohnuma, M., and Mabuchi, I. (2001). Interactions among a fimbrin, a capping protein, and an actin-depolymerizing factor in organization of the fission yeast actin cytoskeleton. Mol. Biol. Cell *12*, 3515–3526.

Nakano, K., and Mabuchi, I. (2006b). Actin-depolymerizing protein Adf1 is required for formation and maintenance of the contractile ring during cytokinesis in fission yeast. Molecular Biology of the Cell *17*, 1933–1945.

Namba, Y., Ito, M., Zu, Y., Shigesada, K., and Maruyama, K. (1992). Human T cell L-plastin bundles actin filaments in a calcium-dependent manner. J. Biochem. *112*, 503–507.

Neidt, E.M., Scott, B.J., and Kovar, D.R. (2009). Formin differentially utilizes profilin isoforms to rapidly assemble actin filaments. J. Biol. Chem. *284*, 673–684.

Newman, M.E.J., and Barkema, G.T. (1999). Monte Carlo Methods in Statistical Physics (New York, NY: Oxford University Press).

Nolen, B.J., Tomasevic, N., Russell, A., Pierce, D.W., Jia, Z., McCormick, C.D., Hartman, J., Sakowicz, R., and Pollard, T.D. (2009). Characterization of two classes of small molecule inhibitors of Arp2/3 complex. Nature *460*, 1031–1035.

Onishi, M., Pringle, J.R., and Cross, F.R. (2015). Evidence That an Unconventional Actin Can Provide Essential F-Actin Function and That a Surveillance System Monitors F-Actin Integrity in Chlamydomonas. Genetics 1–62.

Ono, S., and Ono, K. (2002). Tropomyosin inhibits ADF/cofilin-dependent actin filament dynamics. The Journal of Cell Biology *156*, 1065–1076.

Otomo, T., Otomo, C., Tomchick, D.R., Machius, M., and Rosen, M.K. (2005). Structural Basis of Rho GTPase-Mediated Activation of the Formin mDia1. Molecular Cell *18*, 273–281.

Papp, G., Bugyi, B., Ujfalusi, Z., Barko, S., Hild, G., Somogyi, B., and Nyitrai, M. (2006). Conformational changes in actin filaments induced by formin binding to the barbed end. Biophysical Journal *91*, 2564–2572.

Paul, A.S., and Pollard, T.D. (2008). The role of the FH1 domain and profilin in formin-mediated actin-filament elongation and nucleation. Current Biology : CB *18*, 9–19.

Pelham, R.J., and Chang, F. (2001). Role of actin polymerization and actin cables in actin-patch movement in Schizosaccharomyces pombe. Nat. Cell Biol. *3*, 235–244.

Perelroizen, I., Didry, D., Christensen, H., Chua, N.H., and Carlier, M.F. (1996). Role of nucleotide exchange and hydrolysis in the function of profilin in action assembly. J. Biol. Chem. *271*, 12302–12309.

Perelroizen, I., Marchand, J.B., Blanchoin, L., Didry, D., and Carlier, M.F. (1994). Interaction of profilin with G-actin and poly(L-proline). Biochemistry *33*, 8472–8478.

Petrella, E.C., Machesky, L.M., Kaiser, D.A., and Pollard, T.D. (1996). Structural requirements and thermodynamics of the interaction of proline peptides with profilin. Biochemistry *35*, 16535–16543.

Pollard, T.D. (1986). Rate constants for the reactions of ATP- and ADP-actin with the ends of actin filaments. The Journal of Cell Biology *103*, 2747–2754.

Pollard, T.D., and Cooper, J.A. (1984). Quantitative analysis of the effect of Acanthamoeba profilin on actin filament nucleation and elongation. Biochemistry *23*, 6631–6641.

Pollard, T.D. (2016). Actin and Actin-Binding Proteins. Cold Spring Harbor Perspectives in Biology *8*, a018226–18.

Pring, M., Weber, A., and Bubb, M.R. (1992). Profilin-actin complexes directly elongate actin filaments at the barbed end. Biochemistry *31*, 1827–1836.

Ranjan, A., Townsley, B.T., Ichihashi, Y., Sinha, N.R., and Chitwood, D.H. (2015). An

Intracellular Transcriptomic Atlas of the Giant Coenocyte Caulerpa taxifolia. PLoS Genet *11*, e1004900–e1004910.

Razin, S. (1996). Chapter 37: Mycoplasmas. In Medical Microbiology. 4th Edition, S. Baron, ed. (Galveston, TX).

Romero, S., Le Clainche, C., Didry, D., Egile, C., Pantaloni, D., and Carlier, M.F. (2004). Formin is a processive motor that requires profilin to accelerate actin assembly and associated ATP hydrolysis. Cell *119*, 419–429.

Rotty, J.D., Wu, C., Haynes, E.M., Suarez, C., Winkelman, J.D., Johnson, H.E., Haugh, J.M., Kovar, D.R., and Bear, J.E. (2015). Profilin-1 Serves as a Gatekeeper for Actin Assembly by Arp2/3-Dependent and -Independent Pathways. Developmental Cell *32*, 54–67.

Schmidt, W.M., Lehman, W., and Moore, J.R. (2015). Direct observation of tropomyosin binding to actin filaments. Cytoskeleton (Hoboken) *72*, 292–303.

Scott, B.J., Neidt, E.M., and Kovar, D.R. (2011). The functionally distinct fission yeast formins have specific actin-assembly properties. Mol. Biol. Cell *22*, 3826–3839.

Shao, H., Wu, C., and Wells, A. (2010). Phosphorylation of α-actinin 4 upon epidermal growth factor exposure regulates its interaction with actin. J. Biol. Chem. *285*, 2591–2600.

Sirotkin, V., Berro, J., Macmillan, K., Zhao, L., and Pollard, T.D. (2010). Quantitative analysis of the mechanism of endocytic actin patch assembly and disassembly in fission yeast. Mol. Biol. Cell *21*, 2894–2904.

Skau, C.T., Courson, D.S., Bestul, A.J., Winkelman, J.D., Rock, R.S., Sirotkin, V., and Kovar, D.R. (2011). Actin Filament Bundling by Fimbrin Is Important for Endocytosis, Cytokinesis, and Polarization in Fission Yeast. J. Biol. Chem. *286*, 26964–26977.

Skau, C.T., and Kovar, D.R. (2010). Fimbrin and Tropomyosin Competition Regulates Endocytosis and Cytokinesis Kinetics in Fission Yeast. Current Biology *20*, 1415–1422.

Skau, C.T., Neidt, E.M., and Kovar, D.R. (2009). Role of tropomyosin in formin-mediated contractile ring assembly in fission yeast. Mol. Biol. Cell *20*, 2160–2173.

Skoumpla, K., Coulton, A.T., Lehman, W., Geeves, M.A., and Mulvihill, D.P. (2007). Acetylation regulates tropomyosin function in the fission yeast Schizosaccharomyces pombe. J. Cell. Sci. *120*, 1635–1645.

Skórzewski, R., Śliwińska, M., Borys, D., Sobieszek, A., and Moraczewska, J. (2009). Effect of actin C-terminal modification on tropomyosin isoforms binding and thin filament regulation. BBA - Proteins and Proteomics *1794*, 237–243.

Small, J.V., Stradal, T., Vignal, E., and Rottner, K. (2002). The lamellipodium: where motility begins. Trends in Cell Biology *12*, 112–120.

Sousa, A.D., and Farah, C.S. (2002). Quantitative analysis of tropomyosin linear polymerization equilibrium as a function of ionic strength. J. Biol. Chem. *277*, 2081–2088.

Soza, A., Norambuena, A., Cancino, J., la Fuente, de, E., Henklein, P., and Gonzalez, A. (2004). Sorting Competition with Membrane-permeable Peptides in Intact Epithelial Cells Revealed Discrimination of Transmembrane Proteins Not Only at the trans-Golgi Network but Also at Pre-Golgi Stages. J. Biol. Chem. *279*, 17376–17383.

Spudich, J.A., and Watt, S. (1971). The regulation of rabbit skeletal muscle contraction. I. Biochemical studies of the interaction of the tropomyosin-troponin complex with actin and the proteolytic fragments of myosin. J. Biol. Chem. *246*, 4866–4871.

Spudich, J.A., Huxley, H.E., and Finch, J.T. (1972). Regulation of skeletal muscle contraction. II. Structural studies of the interaction of the tropomyosin-troponin complex with actin. Journal of Molecular Biology *72*, 619–632.

Stark, C., Breitkreutz, B.-J., Reguly, T., Boucher, L., Breitkreutz, A., and Tyers, M. (2006). BioGRID: a general repository for interaction datasets. Nucleic Acids Res. *34*, D535–D539.

Strand, J., Nili, M., Homsher, E., and Tobacman, L.S. (2001). Modulation of Myosin Function by Isoform-specific Properties ofSaccharomyces cerevisiae and Muscle Tropomyosins. J. Biol. Chem. *276*, 34832–34839.

Straub, F.B., and Feuer, G. (1950). Adenosinetriphosphate. The functional group of actin. Biochim. Biophys. Acta *4*, 455–470.

Suarez, C., and Kovar, D.R. (2016). Internetwork competition for monomers governs actin cytoskeleton organization. Nat Rev Mol Cell Biol 1–12.

Suarez, C., Carroll, R.T., Burke, T.A., Christensen, J.R., Bestul, A.J., Sees, J.A., James, M.L., Sirotkin, V., and Kovar, D.R. (2015). Profilin Regulates F-Actin Network Homeostasis by Favoring Formin over Arp2/3 Complex. Developmental Cell *32*, 43–53.

Suarez, C., Roland, J., Boujemaa-Paterski, R., Kang, H., McCullough, B.R., Reymann, A.-C., Guérin, C., Martiel, J.-L., La Cruz, De, E.M., and Blanchoin, L. (2011). Cofilin Tunes the Nucleotide State of Actin Filaments and Severs at Bare and Decorated Segment Boundaries. Current Biology *21*, 862–868.

Svitkina, T.M., and Borisy, G.G. (1999). Arp2/3 complex and actin depolymerizing factor/cofilin in dendritic organization and treadmilling of actin filament array in lamellipodia. The Journal of Cell Biology *145*, 1009–1026.

Symons, M., Derry, J.M., Karlak, B., Jiang, S., Lemahieu, V., McCormick, F., Francke, U., and Abo, A. (1996). Wiskott-Aldrich syndrome protein, a novel effector for the GTPase CDC42Hs, is implicated in actin polymerization. Cell *84*, 723–734.

Takaine, M., Numata, O., and Nakano, K. (2009). Fission yeast IQGAP arranges actin filaments into the cytokinetic contractile ring. The EMBO Journal *28*, 3117–3131.

Theriot, J.A. (1997). Accelerating on a treadmill: ADF/cofilin promotes rapid actin filament turnover in the dynamic cytoskeleton. The Journal of Cell Biology *136*, 1165–1168.

Tilney, L.G., and Portnoy, D.A. (1989). Actin filaments and the growth, movement, and spread of the intracellular bacterial parasite, Listeria monocytogenes. The Journal of Cell Biology *109*, 1597–1608.

Tobacman, L.S. (2008). Chapter 7. In Tropomyosin, P.W. Gunning, ed. pp. 85–94.

Tojkander, S., Gateva, G., Schevzov, G., Hotulainen, P., Naumanen, P., Martin, C., Gunning, P.W., and Lappalainen, P. (2011). A Molecular Pathway for Myosin II Recruitment to Stress Fibers. Current Biology *21*, 539–550.

Tsuchiya, T., and Szabo, A. (1982). Cooperative binding of n-mers with steric hindrance to finite and infinite one-dimensional lattices. Biopolymers *21*, 979–984.

Wagner, E., and Glotzer, M. (2016). Local RhoA activation induces cytokinetic furrows independent of spindle position and cell cycle stage. The Journal of Cell Biology *213*, 641-649.

Washington, R.W., and Knecht, D.A. (2008). Actin binding domains direct actin-binding proteins to different cytoskeletal locations. BMC Cell Biol *9*, 10–16.

Watanabe, N., Madaule, P., Reid, T., Ishizaki, T., Watanabe, G., Kakizuka, A., Saito, Y., Nakao, K., Jockusch, B.M., and Narumiya, S. (1997). p140mDia, a mammalain homolog of Drosophila diaphanous, is a target for Rho small GTPase and is a ligand for profilin. Embo J. *16*, 3044–3056.

Welch, M.D., Rosenblatt, J., Skoble, J., Portnoy, D.A., and Mitchison, T.J. (1998). Interaction of human Arp2/3 complex and the Listeria monocytogenes ActA protein in actin filament nucleation. Science *281*, 105–108.

Wilson, N.F., Foglesong, M.J., and Snell, W.J. (1997). The Chlamydomonas mating type plus fertilization tubule, a prototypic cell fusion organelle: isolation, characterization, and in vitro adhesion to mating type minus gametes. The Journal of Cell Biology *137*, 1537–1553.

Winkelman, J.D., Bilancia, C.G., Peifer, M., and Kovar, D.R. (2014). Ena/VASP Enabled is a highly processive actin polymerase tailored to self-assemble parallel-bundled F-actin networks with Fascin. Proceedings of the National Academy of Sciences of the United States of America.

Winkelman, J.D., Suarez, C., Hocky, G.M., Harker, A.J., Morganthaler, A.N., Christensen, J.R., Voth, G.A., Bartles, J.R., and Kovar, D.R. (2016). Fascin- and α-Actinin-Bundled Networks Contain Intrinsic Structural Features that Drive Protein Sorting. Current Biology 1–11.

Winter, D., Lechler, T., and Li, R. (1999). Activation of the yeast Arp2/3 complex by Bee1p, a WASP-family protein. Current Biology : CB *9*, 501–504.

Wu, J.Q., Bahler, J., and Pringle, J.R. (2001). Roles of a fimbrin and an alpha-actinin-like protein in fission yeast cell polarization and cytokinesis. Molecular Biology of the Cell *12*, 1061–1077.

Wu, J.-Q., and Pollard, T.D. (2005). Counting cytokinesis proteins globally and locally in fission yeast. Science *310*, 310–314.

Young, M.E., Cooper, J.A, Bridgman, P.C. (2004). Yeast actin patches are networks of branched actin filaments. The Journal of Cell Biology *166*, 629–735.

Zimmermann, D., Morganthaler, A.N., Kovar, D.R., and Suarez, C. (2015). In vitro biochemical characterization of cytokinesis actin-binding proteins. In Yeast Cytokinesis, A. Sanchez-Diaz, and P. Perez, eds. (Humana Press).